AMRL-TR-67-132

MODELS OF NEUROELECTRIC INTERACTIONS

EDWIN R. LEWIS, PhD

FOREWORD

This report covers work done by the Librascope Group of General Precision Systems, Inc., 808 Western Avenue, Glendale, California under Contract No. AF 33 (615) - 2464 and in support of Project 7233, "Biological Information Handling Systems and Their Functional Analogs," and Task 723305, "Theory of Information Handling," for the Aerospace Medical Research Laboratories, Wright-Patterson Air Force Base, Ohio 45433.

The Air Force project engineer for this contract was Dr. Hans L. Oestreicher, Mathematics and Analysis Branch, Biodynamics and Bionics Division, Biomedical Laboratory. The Librascope principal investigator was Dr. Edwin R. Lewis. The work was begun 15 April 1965, and was completed 15 July 1967.

This technical report has been reviewed and is approved.

WAYNE H. McCANDLESS
Technical Director
Biomedical Laboratory
Aerospace Medical Research
Laboratories

ABSTRACT

The Hodgkin-Huxley descriptions of electrically excitable conductances are combined with Eccles descriptions of synaptic conductances to provide the basis of an electronic analog of nerve cell membrane. A neural simulation facility is constructed, comprising ten pairs of these analogs with associated input and output equipment. A detailed description of the simulation facility is presented, including design philosophy, circuit, system and mechanical details. The simulation facility is used to model spatially distributed neuroelectric phenomena. Significant results include resetting of potentials in integrative regions by spikes generated at a remote site, stable spike synchrony in independently driven, mutually inhibiting distributed neural models, burst formation in mutually exciting neural models, and various nonuniformities of wave shape and velocity in conduction along a distributed axon. In addition, the facility is used in a simulation study of the lobster cardiac ganglion. As results of this study, mechanisms are proposed for ganglion operation and specific neuronal connectivities are predicted.

CONTENTS

LIST OF ILLUSTRATIONS

TABLES

SECTION I

INTRODUCTION

In a program supported by the Air Force Office of Scientific Research under contract AF 49(638)-1232, members of the Systems Research Department, Librascope Group, General Precision Inc., developed elaborate electronic circuits to simulate the signal processing properties of single nerve cells. These circuits were based on the properties of electrically excitable neuronal membranes, as specified by Hodgkin and Huxley combined with the properties of subsynaptic membranes as specified by Eccles and others. Using these circuits, we were able to show that those membrane properties could be extrapolated to account for many of the previously unexplained graded electrical phenomena observed in neuronal dendrites and somata.

The purpose of our work under the present contract, AF 33(615)-2464, was to extend these studies to include signal processing in small nerve networks and ganglia. Specifically, we constructed a neural simulation facility with ten neural models, and we used that facility to simulate the nine-neuron cardiac ganglion of the lobster. Each neural model in the facility comprised two circuits, a SOMA MODEL and a SPIKE INITIATOR MODEL. The SOMA MODEL represented an integrative region of a neuron, complete with synaptic inputs. The SPIKE INITIATOR MODEL, on the other hand, represented a trigger region of a neuron, capable of generating spikes - but little else.

The neural analog facility is described in Sections II and III. Section II provides a general description of the facility along with its physiological basis. Section III provides descriptions of the electronic circuits and their operation.

In preliminary studies with the facility, we examined the signal processing properties of single neurons. These are discussed in Section IV. We also examined the properties of a lumped approximation to a distributed axon, which are described in Section V. Finally, we carried out a reasonably large portion of our proposed program of simulation of the lobster cardiac ganglion. Our results are described in considerable detail in Section VI. Our references are listed in Section VII.

The simulation study has led to specific predictions of the connectivity among cells in the ganglion and to specific proposals of mechanisms of operation of the ganglion. These results are described in the last part of Section VI and should serve as a starting point for a project combining simulation with the facility and direct experimentation on the ganglion.

SECTION II

GENERAL DESCRIPTIONS

THE NEURAL ANALOG FACILITY

The Librascope neural analog facility consists of ten electronic neural models housed together in a double, desk-cabinet rack, with associated input-signal generating equipment and output-signal monitoring equipment housed in two additional racks. Each of the ten neural models consists of two separate networks, and each of these networks itself may be considered a complete neural model. One network, comprising most of the electronic circuitry in any of the ten models, provides a detailed and faithful simulation of the electrical properties of a single patch of nerve-cell membrane. This network is essentially a two-terminal system with one terminal representing the conducting medium inside the nerve cell and the other terminal representing the conducting medium outside the cell. The electronic equivalents of seven elements are connected in parallel between the two terminals (see figure 1). Four of these elements together represent the components of electrically excitable membrane as determined by Hodgkin and Huxley (1952a, b, c, d). The remaining three elements represent the components of synaptic membrane as determined by Eccles and others (Eccles, 1964). The combination of these seven components in parallel represents a wide range of topographies within a single membrane patch. It may represent, for example, a patch of subsynaptic membrane with a contiguous patch of electrically excitable membrane, or it equally well may represent a

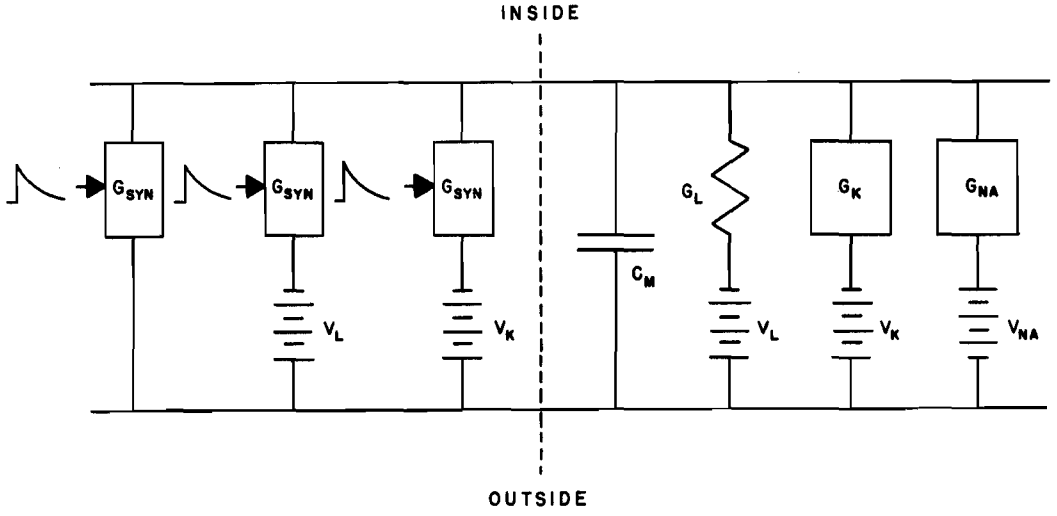

Figure 1. Circuit Equivalent of the SOMA MODEL in the Neural Analog Facility.

homogeneous distribution of the two types of membrane. The important features of the electronic simulations of these seven components are their detailed consistency with their physiological counterparts and their high degree of flexibility. The network incorporating these simulations has eighteen different parameters under the direct control of the experimenter.

The second basic network in each of the ten neural models is much simpler than the first. It consists of two parts: A rather inflexible approximation of a patch of electrically excitable membrane without synaptic components (the Spike Initiator) and a circuit that imposes a variable delay on voltage pulses (the Axon Delay Circuit). This combination is used to simulate the initiation and propagation of spikes in an axon. It has only two controllable parameters, the spike threshold and the simulated propagation time. Like the more flexible membrane model described in the previous paragraph, the spike initiator is a two-terminal network. One terminal represents the inside of the nerve cell; the other terminal represents the outside. The network was designed to be a reasonable approximation to the Hodgkin-Huxley model for spike activity (Hodgkin and Huxley, 1952d).

The combination of the two networks in each neural model provides the capability of a two-lump approximation to a spatially distributed neuron (see figure 2). The detailed, flexible model can be modified easily to provide the various electrical characteristics and diverse forms of behavior found in integrative regions of nerve cells; and the Spike Initiator can be coupled to it to represent a trigger region. The two-terminal nature of each network makes this type of coupling extremely easy.

THE HODGKIN-HUXLEY MODEL

The networks representing electrically excitable membrane were designed to simulate the system of ionic conductances described by Hodgkin and Huxley for the squid-axon membrane. This system is basically one of dynamic opposition of ionic fluxes across the membrane. The membrane itself forms the boundary between two liquid phases - the intracellular fluid and the extracellular fluid. The intracellular fluid is rich in potassium ions and immobile organic anions, while the extracellular fluid contains an abundance of sodium ions and chloride ions. The membrane is slightly permeable to the potassium, sodium, and chloride ions, so these ions tend to diffuse across the membrane. When the axon is inactive (not propagating a spike), the membrane is much more permeable to chloride and potassium ions than it is to sodium ions. In this state, in fact, sodium ions are actively transported from the inside of the membrane to the outside at a rate just sufficient to balance the inward leakage. The relative sodium ion concentrations on both sides of the membrane are thus fixed by the active transport rate, and the net sodium flux across the membrane is effectively zero. The potassium ions, on the other hand, tend to move out of the cell; while chloride ions tend to move into it. The inside of the cell thus becomes negative with respect to the outside. When the potential across the membrane is

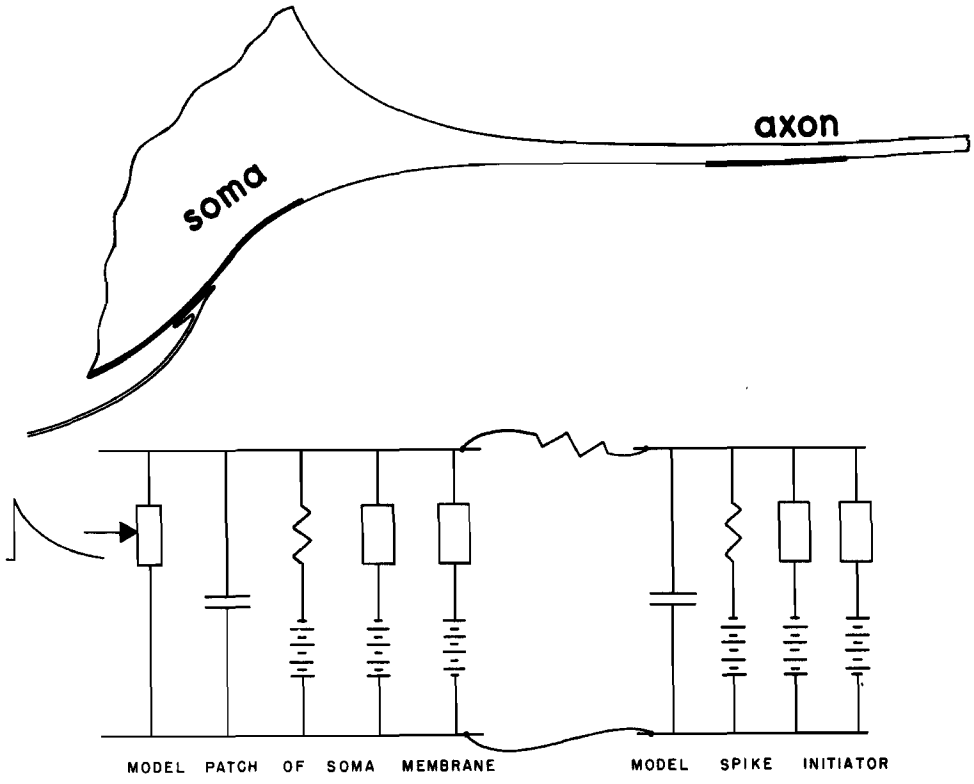

Figure 2. A Two-Patch Representation of a Neuron.

sufficient to balance the inward diffusion of chloride with an equal outward drift, and the outward diffusion of potassium with an inward drift (and possibly an inward active exchange), equilibrium is established. The equilibrium potential is normally in the range of 60 to 65 millivolts.

The resting neural membrane is thus polarized, with the inside approximately 60 millivolts negative with respect to the outsdie. Most of the Hodgkin-Huxley data is based on measurements of the transmembrane current in response to an imposed stepwise reduction (depolarization) of membrane potential. By varying the external ion concentrations, Hodgkin and Huxley were able to resolve the transmembrane current into two "active" components, the potassium-ion current and the sodium-ion current. They found that while the membrane permeabilities to chloride and most other inorganic ions were relatively constant, the permeabilities to both potassium and sodium were strongly dependent on membrane potential. In response to a suddenly applied (step) depolarization, the sodium permeability rises rapidly to a peak and then declines exponentially to a steady value. The potassium permeability, on the other hand, rises with considerable delay to a value which is maintained as long as the membrane remains depolarized. The magnitudes of both

the potassium and the sodium permeabilities increase monotonically with increasing depolarization. A small imposed depolarization will result in an immediately increased sodium permeability. The resulting increased influx of sodium ions results in further depolarization; and the process becomes regenerative, producing the all-or-none action potential. At the peak of the action potential, the sodium conductance begins to decline, while the delayed potassium conductance is increasing. Recovery is brought about by an efflux of potassium ions, and both ionic permeabilities fall rapidly as the membrane is repolarized. The potassium permeability, however, falls less rapidly than that of sodium. This is basically the explanation of the all-or-none spike according to the Modern Ionic Hypothesis.

By defining the net driving force on any given ion species as the difference between the membrane potential and the equilibrium potential for that species and describing permeability changes in terms of equivalent electrical conductance changes, Hodgkin and Huxley reduced the Ionic Hypothesis to the equivalent electrical circuit shown in figure 3. The important dynamic variables in this equivalent network are the sodium conductance (G_{Na}) and the potassium conductance (G_K). The change in the sodium conductance in response to a step depolarization is shown in figure 4. This change can be characterized by seven voltage dependent parameters:

1. Delay time (generally much less than 1 msec)

2. Rise time (1 msec or less)

3. Magnitude of peak conductance (increases monotonically with increasing depolarization)

4. Inactivation time constant (decreases monotonically with increasing depolarization)

5. Time constant of recovery from inactivation (incomplete data)

6. Magnitude of steady-state conductance (increases monotonically with increasing depolarization)

7. Fall time on sudden repolarization (less than 1 msec.)

Figure 4 also shows the potassium conductance change in response to an imposed step depolarization. Four parameters are sufficient to characterize this response:

1. Delay time (decreases monotonically with increasing depolarization)

2. Rise time (decreases monotonically with increasing depolarization)

3. Magnitude of steady-state conductance (increases monotonically with increasing depolarization)

4. Fall time on sudden repolarization (20 msec or more, decreases slightly with increasing depolarization)

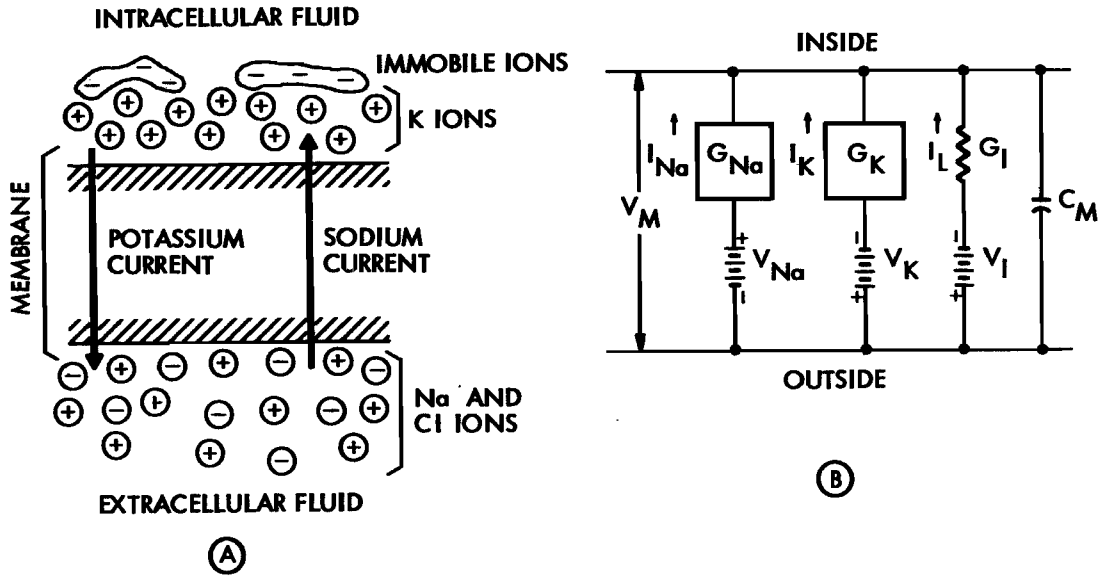

Figure 3. The Hodgkin-Huxley Electrical Equivalent of a Patch of Squid-Axon Membrane.
3A shows the distributions of ionic species across the axon membrane. 3B shows the equivalent electrical circuit proposed by Hodgkin and Huxley.

The remaining elements in the Hodgkin-Huxley model are constant and are listed below:

1. Potassium potential - 80 to 85 mv (inside negative)
2. Sodium potential - 45 to 50 mv (inside positive)
3. Leakage potential - 45 to 67 mv (inside negative)
4. Leakage conductance - approximately 0.23 millimhos/cm^2
5. Membrane capacitance - approximately 1 μf/cm^2
6. Resting potential - 60 to 65 mv
7. Spike amplitude - approximately 100 mv

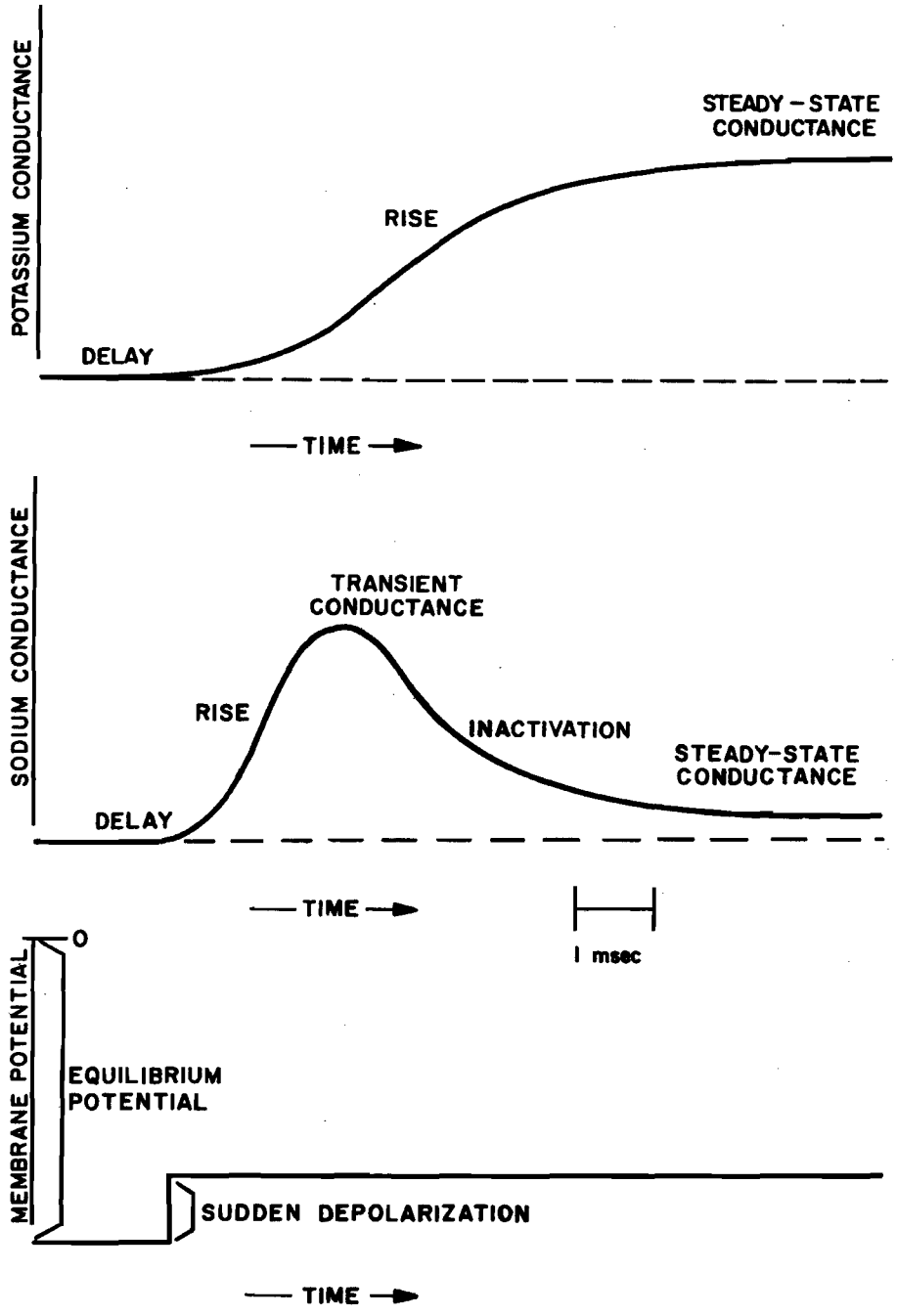

Figure 4. Generalized Plots of the Changes of Potassium and Sodium Conductances in Response to a Step Depolarization of the Axon Membrane.

THE ECCLES MODEL OF SUBSYNAPTIC MEMBRANE

It has been established that many if not almost all nerve cells communicate with one another by means of chemical synapses. It has been postulated by Eccles (1964) and others that a spike, reaching the termination of one nerve cell on another, induces emission of a chemical

transmitter substance into the extracellular space between the two cells. This transmitter substance apparently induces an increase in one or more ionic permeabilities in the subsynaptic membrane of the receiving cell.

Eccles has described these permeability changes in terms of equivalent electrical conductances. It is assumed generally that the equivalent synaptic conductance is directly proportional to the concentration of transmitter present in the space between the sending cell and the receiving cell. This concentration rises abruptly during a presynaptic spike, then falls again toward zero as the transmitter is dissipated or inactivated. If the transmitter is dissipated by a simple diffusion process or inactivated by a first-order chemical process, its concentration following a spike will decay exponentially with time. The synaptically induced equivalent conductances will thus have the forms of decaying exponentials.

The current associated with excitatory synapses goes to zero when the potential across the membrane is zero; so the equivalent conductance associated with these synapses is apparently a nonspecific shunt to all ions. Inhibitory synapses, on the other hand, appear to be associated with specific ions - potassium and chloride. Some inhibitory synapses operate by means of a transient increase of the equivalent potassium conductance, others by a transient increase of the equivalent chloride (or leakage ion) conductance, and others by means of a combination of chloride and potassium conductance.

METHODS OF SIMULATION

Nonlinear, active filters in each model generate the time- and voltage-dependent potassium and sodium conductances specified by Hodgkin and Huxley. The input to each of these filters is the simulated transmembrane potential. The output is a voltage or current representing the appropriate Hodgkin-Huxley conductance. Since the current through a conductor is proportional to the product of the conductance itself and the voltage across it, electronic multipliers are required in order to convert the filter outputs to equivalent conductances. The remaining two elements (G_l and C_M) of the Hodgkin-Huxley model are fixed and linear. These are simulated by simple electrical components.

The time course of synaptic conductance is simulated by a simple resistor-capacitor network. The output of this network is transformed to an equivalent conductance by means of electronic multipliers.

FUNCTIONAL DESCRIPTION OF THE NEURAL MODELS

The ten neural models that make up the main part of the facility are identical in every respect but one: the right side of the front panel of each model contains thirteen tip jacks whose color is unique. The

models are thus differentiable by means of their individual colors. Color is the only difference among the models, and the following description applies equally well to any of them. Henceforth, each of the ten models will be called a MODULE.

Functionally, each MODULE is composed of two basic parts: (1) a flexible, detailed simulation of a patch of neuronal membrane according to the Hodgkin-Huxley Model, with a contiguous patch of synaptic membrane according to the models of Eccles and others, and (2) a second, more rigid, less detailed simulation of a patch of neuronal membrane based on the Hodgkin-Huxley Model. Because of its flexibility and its simulated synaptic inputs, the first model can be adapted to simulate the characteristics of neuronal receptive and integrative regions, such as those often observed in the soma or cell body of a nerve cell. For that reason this model henceforth will be called the SOMA MODEL. The second model was designed specifically to represent a region with minimal integrative properties, but with the capability of generating the classical all-or-none spike. This model henceforth will be called the SPIKE INITIATOR MODEL.

The Soma Model

The SOMA MODEL comprises most of the circuitry in a MODULE, and its controls and tip jack terminals occupy almost the entire center of the MODULE'S front panel (shown in figure 5). The SOMA MODEL can be divided functionally into eight parts, each of which is reflected by a set of controls or terminals or both on the front panel:

1. Synaptic Circuits
2. Synaptic Conductance Input Terminals
3. Simulated Sodium Conductance (G_{Na})
4. Simulated Shunt Conductance
5. Simulated Potassium Conductance (G_K)
6. Simulated Fixed Component of the Chloride or Leakage Conductance (G_l)
7. Simulated Synaptic Component of the Chloride or Leakage Conductance
8. Simulated Transmembrane Capacitance (C_M)

The function of each of these parts is described very briefly in the following paragraphs:

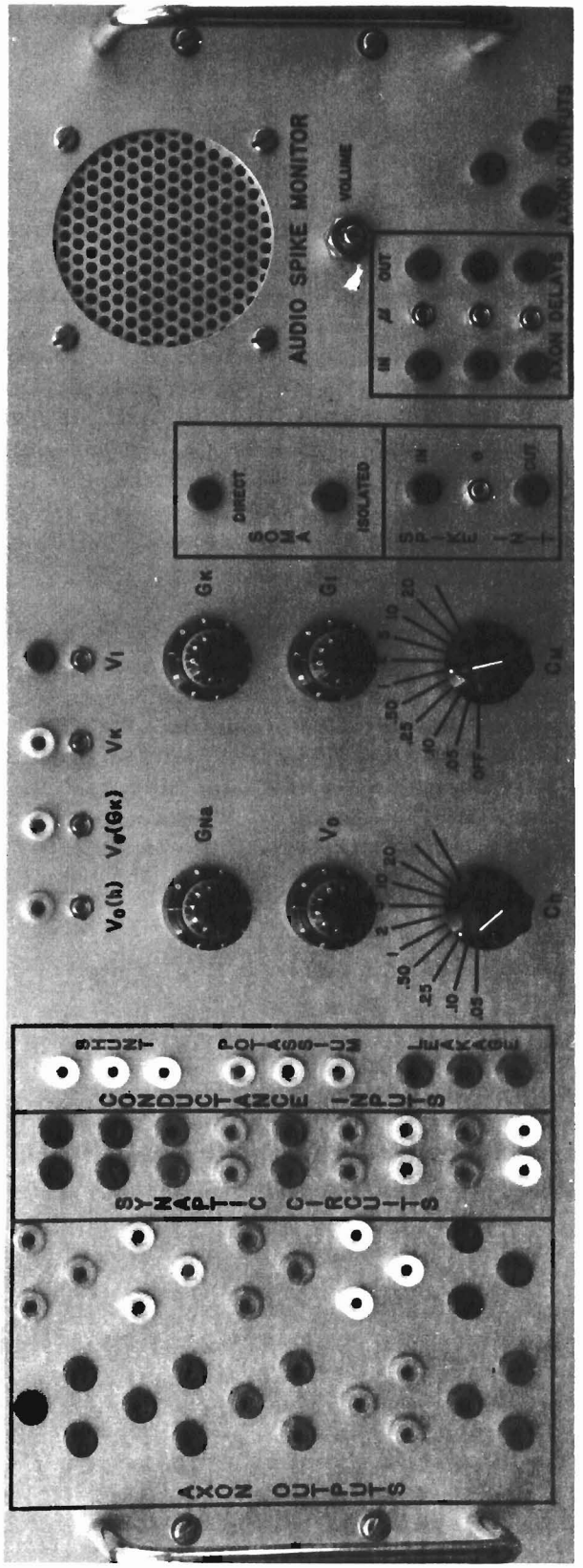

Figure 5. Front Panel of Module

Synaptic Circuits

The synaptic circuits are designed to accept as inputs the positive, 2-msec voltage pulses available from the Axon Delay Lines. The synaptic circuits convert these pulses into decaying exponential current waveforms simulating the time courses of synaptic conductances in nerve cells. These current waveforms are applied to the appropriate conductance inputs where they are summed and subsequently converted into equivalent conductances.

Associated with each synaptic circuit are two variable resistors representing two synaptic parameters. One resistor controls the magnitude of the incremental conductance increase in response to a simulated presynaptic spike or, equivalently, the simulated quantity of synaptic transmitter substance emitted for each presynaptic spike. The other resistor controls the rate of inactivation of the simulated transmitter substance.

Synaptic Conductance Input Terminals

The synaptic conductance input terminals are summing points for the output currents of the synaptic circuits. These terminals are divided into three groups representing the three known types of synaptic conductance: nonspecific shunt, potassium, and chloride or leakage. The total current input to each of these terminals is directed to a circuit that converts it into the appropriate equivalent conductance across the simulated membrane of the SOMA MODEL.

Simulated Sodium Conductance

The simulated sodium conductance in the SOMA MODEL is an approximation to a true time and voltage dependent conductance. Over the range of membrane potentials normally encountered in the soma, changes in the net driving force on sodium ions are small in comparison with the driving force itself. In this range of potentials, therefore, the voltage across the sodium conductance in the Hodgkin-Huxley Model reasonably can be considered constant, and the sodium current can be taken to be directly proportional to the sodium conductance. Under this approximation, the circuit that simulates the sodium conductance simply transforms the membrane potential into a current proportional to that specified by Hodgkin and Huxley for sodium ions. Then, rather than being applied to an electronic multiplier and converted into a true equivalent conductance, this current is applied directly across the simulated soma membrane.

Five controllable parameters are associated with the simulated sodium conductance, and each of these is related to a parameter of the Hodgkin-Huxley Model (Hodgkin and Huxley, 1952c, d). Three of the controllable parameters are related to the sodium inactivation variable, h. The simulated voltage-dependent rate of decline of h can be scaled by

means of a switch to any one of nine ranges. The simulated rate of rise of h can be varied continuously by means of a variable resistor, and the value of h for the simulated resting state of the membrane can be varied continuously by means of another variable resistor. The remaining two parameters are related to the magnitude of the sodium conductance. Both the magnitude itself and its value at the simulated resting state are independently and continuously variable.

Simulated Shunt Conductance

The shunt conductance is approximated under the same assumption as that applied to the sodium conductance (i.e., that the voltage across the equivalent shunt conductance is essentially constant). The circuit simulating the shunt conductance is designed to receive as an input the current directed to it from the synaptic conductance input terminals. The circuit converts this current into an equivalent transmembrane current of the correct polarity to simulate a nonspecific shunt.

Simulated Potassium Conductance

Under normal circumstances, the membrane potential of the soma is close to the equilibrium potential for potassium ions (i.e., V_M is nearly equal to V_K). So the voltage across the equivalent potassium conductance in the Hodgkin-Huxley Model varies considerably relative to its total magnitude. A reasonable simulation of the potassium conductance must include, therefore, a means of forming the product of a time varying voltage and a time varying conductance.

The circuit simulating the potassium conductance was designed to transform the simulated membrane potential into a current which meets the Hodgkin-Huxley specifications for potassium conductance. This current is added to the current directed to the potassium conductance from the synaptic conductance input terminals, and the sum is applied to one input terminal of an electronic multiplier. This multiplier forms the product of the total potassium conductance (i.e., the Hodgkin-Huxley component plus the synaptic component) and the net driving force on potassium ions (i.e., the difference between V_K and V_M) and converts this product to a current across the simulated soma membrane.

Seven parameters of the simulated potassium conductance are variable. Three parameters apply only to the Hodgkin-Huxley component; these are the shape of the inflected rise of potassium conductance (controlled by three variable resistors), the shape of the noninflected fall (controlled by one variable resistor), and the magnitude of the potassium conductance at the resting potential of the simulated soma membrane (controlled by one variable resistor). The four remaining parameters apply to both the Hodgkin-Huxley component and the synaptic component; these are the potassium equilibrium potential, its rate of change with respect to potassium current, its rate to recovery from nonequilibrium

values, and the magnitude of the total potassium conductance. Each of these parameters is controlled by a single variable resistor.

Simulated Fixed Component of Chloride or Leakage Conductance

In the Hodgkin-Huxley model, the chloride or leakage conductance is neither time nor voltage dependent; it is a fixed, linear conductance and is simulated quite accurately by means of an ordinary electrical resistor. Two parameters of the chloride conductance are variable: the magnitude of the conductance itself and the chloride equilibrium potential. Each of these parameters is controlled by a single, variable resistor.

Synaptic Component of Chloride or Leakage Conductance

Under ordinary circumstances the soma membrane potential is very close to the equilibrium potential for chloride ions; in fact the net driving force on chloride ions not only varies considerably in magnitude, but it often reverses its direction. Reasonable simulation of the time-varying synaptic component of chloride conductance requires a multiplier that can accommodate a reversal of the sign of one of its inputs. This is accomplished by the chloride conductance circuit.

The chloride conductance circuit accepts as its input the current directed to it from the synaptic conductance input terminal. This input current is multiplied by the difference between V_1 and V_M (which may be be either a positive or a negative potential); and the product is converted to a current and applied to the simulated soma membrane.

The chloride equilibrium potential is controllable and is identical to that for the fixed component. Control of the magnitude of the synaptic component of chloride conductance is achieved by means of a variable resistor and is independent of the magnitude control of the fixed component.

Simulated Transmembrane Capacitance

The membrane capacitance in the Hodgkin-Huxley model is neither time dependent nor voltage dependent (Hodgkin, Huxley and Katz, 1952). It is simulated quite accurately by an ordinary electrical capacitor. The membrane capacitances measured in neuronal somata are generally larger than that specified by Hodgkin and Huxley. To accommodate these data, the simulated membrane capacitance has been made variable and can be switched to any one of nine magnitudes.

THE SPIKE INITIATOR MODEL

The SPIKE INITIATOR MODEL can be divided functionally into three parts: (1) the Spike Initiator Circuit, (2) the Audio Spike Monitor and (3) the Axon Delay Circuit. The input and output terminals as well as the controls for these parts occupy most of the area on the right-hand side of the front panel of each MODULE (see figure 5).

The Spike Initiator Circuit

The spike initiator circuit is a two-terminal network designed to simulate the Hodgkin-Huxley model for large excursions of membrane potential, such as spikes. It contains approximate simulations of each of the four Hodgkin-Huxley elements (membrane capacitance, leakage conductance, sodium conductance, and potassium conductance), but it does not contain simulated synaptic conductances.

This circuit is intended to be the shunt element in a distributed neuronal system such as that shown in figure 2. Like its squid axon prototype, it possesses all of the classical properties of electrically excitable membrane, including threshold, all-or-none response, absolute and relative refractoriness, chronaxie, and rheobase. It is thus a reasonably complete neural model in itself.

Spike threshold is the only parameter of the spike initiator circuit that is controllable. It can be adjusted to allow the spike initiator to respond to the slowly varying potentials of a soma model (applied to the spike initiator through a resistor), or it can be adjusted to allow the spike initiator to fire spontaneously, producing periodic spikes.

The Audio Spike Monitor

The audio spike monitor amplifies the spikes from the spike initiator circuit and transmits the amplified spikes to the loudspeaker on the right-hand side of each MODULE. Many spike patterns are more easily characterized from audio presentation than from visual presentations on an oscilloscope, especially when more than one MODULE is participating in the pattern. The audio spike monitor has an adjustable loudness control, and the sound may be turned completely off by means of this control.

The Axon Delay Circuit

The Axon Delay Circuit is designed to accept inputs from the spike initiator circuit (not from the SOMA MODEL), or from another axon delay circuit. Each spike from the spike initiator circuit is delayed for a finite time and converted into a form compatible with the synaptic circuit input requirements. The delay imposed by the axon delay circuit is variable and is controlled by a single resistor.

Peripheral Circuits

In addition to a SOMA MODEL and a SPIKE INITIATOR MODEL, each MODULE has power isolation circuitry and a 30-terminal patch board that facilitates connection to circuits in other MODULES.

Power Input

Each MODULE is operated by means of d-c electrical power supplied from one of two central sources. Each source supplies positive twelve volts and negative twelve volts, with the capability of delivering more than enough current to operate all MODULES simultaneously. The central power sources each supply five MODULES, one supplying the MODULES on the right-hand side of the double rack, the other supplying the MODULES on the left.

Each MODULE has two 20,000 microfarad capacitors and two 50 microfarad capacitors to isolate it and make its operation independent of the other MODULES. Power to each MODULE is controlled by means of a switch on the front panel.

Patch Boards

Each MODULE has a group of thirty tip jacks labeled Axon Outputs on the left-hand side of its front panel. These are arrayed in ten triads, each triad consisting of identically colored jacks. The color associated with each triad is the same as the color associated with one of the ten MODULES.

Each MODULE also has a single triad of tip jacks labeled Axon Outputs on the right-hand side of its front panel. These are among the thirteen jacks whose color is unique to that particular MODULE. Each of the three jacks in the right-hand triad is connected to its counterpart in the triads of the same color on the left-hand sides of all ten MODULES.

Triads of a given color thus appear eleven times in the entire system, once on the left-hand side of each of the ten MODULES and once on the right-hand side of one MODULE. A voltage applied to a member of a triad appears at the corresponding member of each of the other ten triads of the same color. A total of thirty voltages may be made available, therefore, on the left-hand side of every panel. These voltages may include slowly varying potentials from the SOMA MODELS, spikes from the SPIKE INITIATOR MODELS, and delayed spikes from the Axon Delay Circuits. The thirty-channel capacity should be sufficient to avoid messy and confusing external wiring from one MODULE to another.

SECTION III

CIRCUIT DESCRIPTIONS

INTRODUCTION

Most of the electronic circuitry in each MODULE is mounted on six printed circuit cards (see figure 6). A few variable resistors, two isolation capacitors, two sets of switchable capacitors and one loudspeaker are the only functional circuit elements not mounted on the cards. Each of the six cards is different from the other five and each serves one or more functions of its own as indicated by its name. The Sodium Circuit, for example, is part of the SOMA MODEL and provides an electronic simulation of the Hodgkin-Huxley sodium conductance. The Potassium Circuit, also part of the SOMA MODEL, provides the simulated Hodgkin-Huxley potassium conductance and adds it to a simulated synaptic component. The Chloride Circuit serves two functions in the SOMA MODEL: it provides the simulated synaptic chloride conductance, and it serves as a summing point for the various simulated ionic components of soma membrane current. The Spike Initiator Circuit is part of the SPIKE INITIATOR MODEL and provides an approximate simulation of a patch of axon membrane. It also provides an amplifier to drive the loudspeaker on the front panel. The circuit card labeled Axon Delay provides three variable pulse-delay circuits that simulate axon propagation times. The Synaptic Circuit card provides three circuits that convert pulses into decaying exponentials representing the time courses of synaptic transmitter concentration.

SODIUM CIRCUIT (figure 7)

The sodium circuit converts the time-varying simulated membrane potential (V_M) into a current that in almost all respects is equivalent to the sodium current specified in the Hodgkin-Huxley model. In the Hodgkin-Huxley formulation, the sodium current is the product of three variables and one constant:

$$I_{Na} = \bar{g}_{Na} \quad (m^3)\,(h)\,(V_{Na} - V_M)$$

where m^3 and h are functions of membrane potential and time; $\bar{g}_{Na}$ is a constant, and V_{Na} is the equilibrium potential for sodium ion flux and is also constant. Except during a spike, the factor $(V_{Na} - V_M)$ is large compared to changes in V_M and can be considered constant. During a spike, V_M quickly approaches V_{Na}, passing rapidly through the range of potentials intermediate between the threshold and V_{Na}. The variations in $(V_{Na} - V_m)$ in this range are not important in determining the electrical properties of the Hodgkin-Huxley model; on the other hand, the limiting effect imposed upon the sodium current as V_M approaches V_{Na} is important. In the sodium circuit, $(V_{Na} - V_M)$ is treated as a constant over the entire range of membrane potentials; but the limiting effect of the factor is included, so that the simulated sodium current approaches zero as V_M approaches V_{Na}.

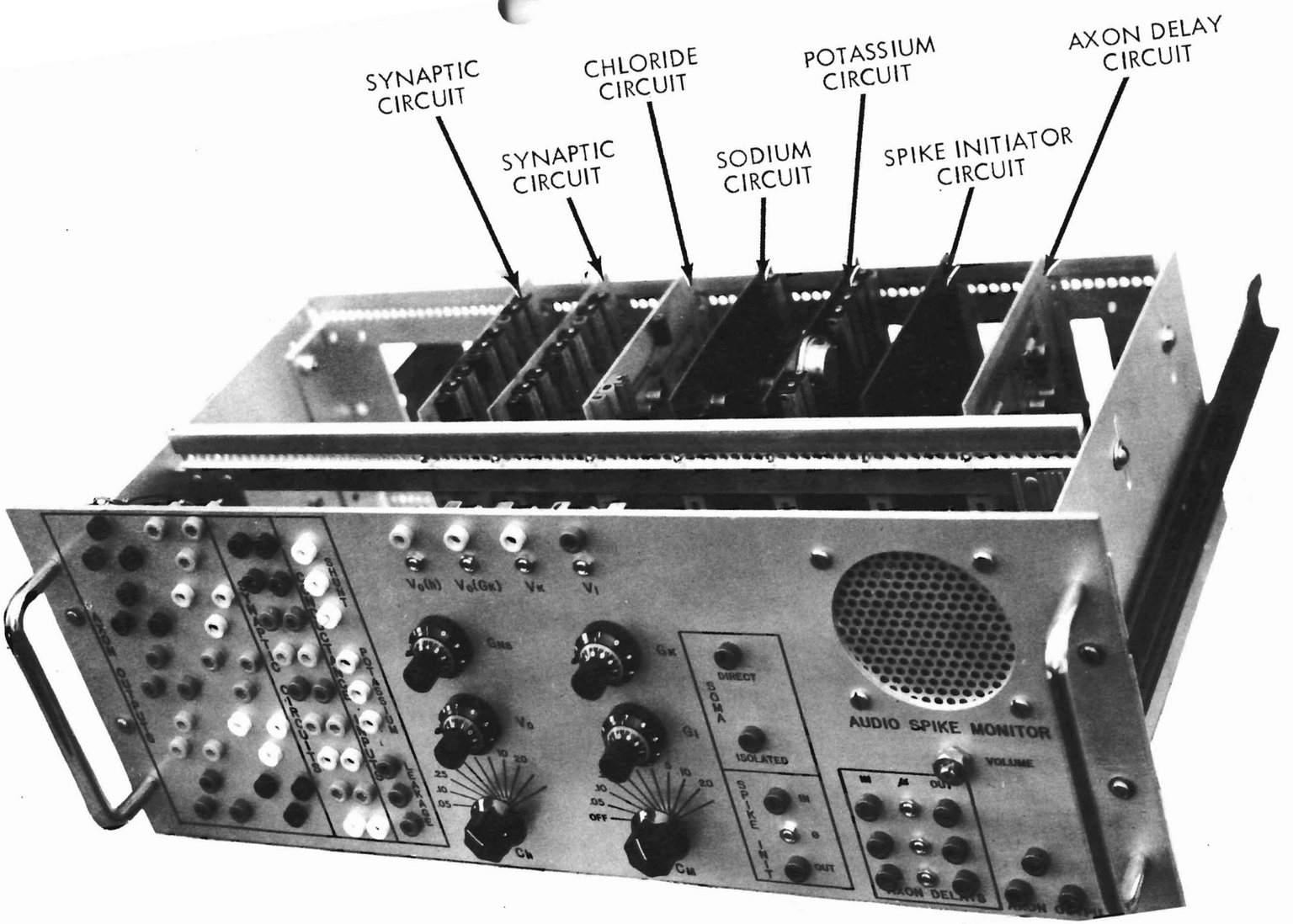

Figure 6. MOUDLE Removed from Rack, Showing Circuit Cards

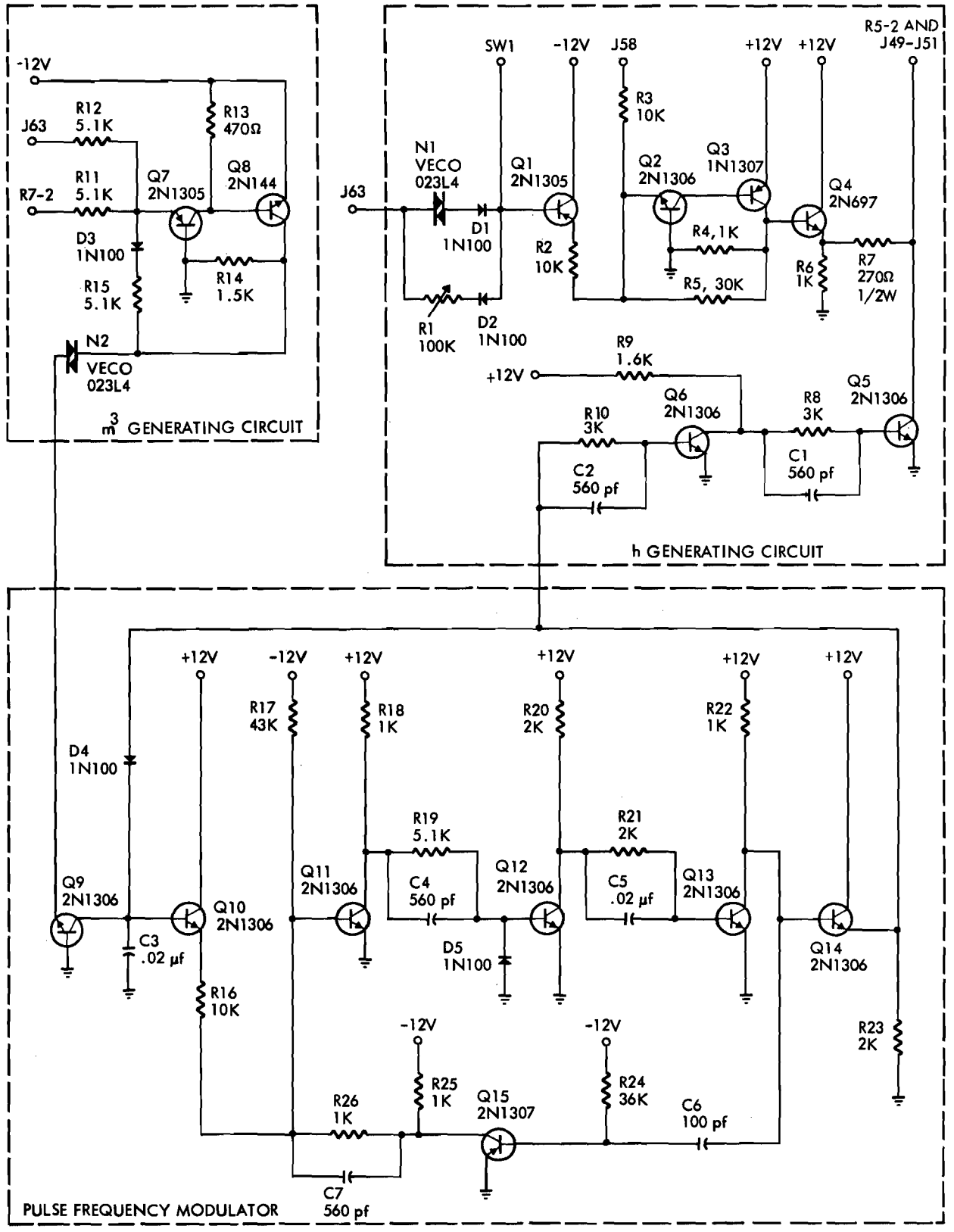

Figure 7. Diagram of Sodium Circuit.

The principal functions of the sodium circuit, therefore, are to generate the time and voltage dependent functions m^3 and h and to generate a current proportional to their product. The membrane potential is applied to the inputs of two subcircuits. One subcircuit (Q1 to Q4) generates a voltage representing h, the other (Q7 to Q9) generates a current representing m^3. The remaining circuit (Q5, Q6, Q10 to Q15) acts as a multiplier, generating a pulsed output voltage whose average over time represents hm^3.

h-Generating Circuit

In the h-generating circuit, V_M is applied through R1, D1, D2, and N1 (a varistor) to a capacitor at SW1, (see figures 7 and 8). The voltage on this capacitor tends to follow V_M, but lagging it in time. The varistor N1 provides an approximation to the voltage-dependent rate of decline of h in response to positive changes in V_M. The variable resistor R1 determines the rate of increase of h in response to negative changes in V_M. Both rate constants can be scaled simultaneously by means of the switched capacitors at SW1. Figure 9 shows for typical settings of R1 and SW1 a family of voltage outputs appearing at the emitter of Q4 in response to square-pulse inputs at J63. The portion of the circuit from Q1 through Q4 is simply an amplifier that provides a piecewise linear approximation of the steady-state magnitude of h as a function of V_M, as shown in figure 10.

Transistor Q1 is an emitter-follower, supplying the voltage at SW1 to R2 without significantly loading the capacitor at SW1. Transistors Q2 and Q3 together act as an inverting amplifier with a gain of 3. The effective input to this amplifier is the sum of the voltages at SW1 and J58. When this sum is positive, the output of the amplifier (i.e., the collector of Q3) is at ground potential. When the input sum is between ground potential and -4 volts, the magnitude of the amplifier output is three times the sum, with positive polarity. When the input sum is more negative than -4V, the amplifier output is +12 volts. The amplifier thus has the response curve shown by the dashed line in figure 10.. This curve can be shifted along the horizontal by adjustment of $V_o(h)$ by means of resistor R1 on the panel (figure 8). Transistor Q4 is an emitter follower supplying the amplifier output to the low resistance load (R7).

m^3 - Generating Circuit

In the m^3 generating circuit, V_M is applied through R12 to the emitter of Q7. Transistors Q7 and Q8 together act as an inverting amplifier with unity gain. The output at the collector of Q8 is positive in polarity and equal in magnitude to the sum of the voltages at J63 (V_M) and R7-2 (V_o). The amplifier output is applied through the varistor N2 to the emitter of Q9. The varistor imposes a nonlinear relationship between $V_M + V_o$ and the collector current of Q9. This relationship is intended to simulate the nonlinear dependence of m^3 on the displacement of the membrane potential from equilibrium, see figure 11.

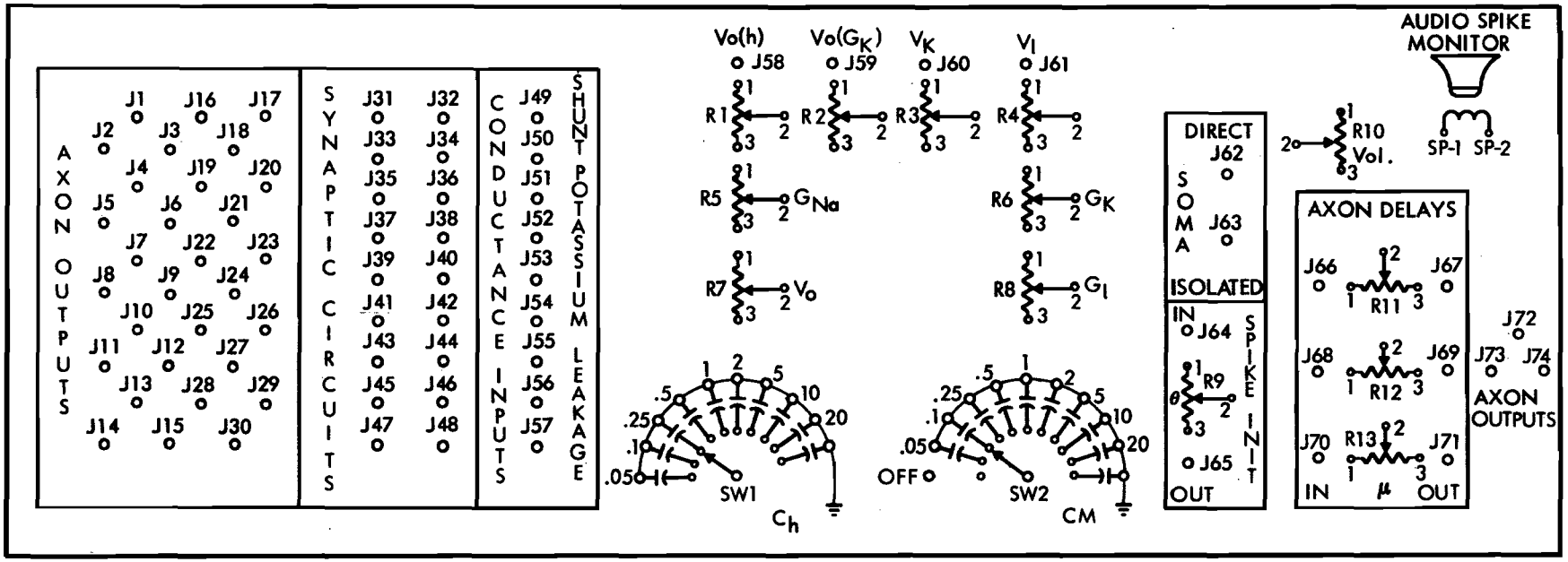

Figure 8. Diagram of the MODULE Front Panel.

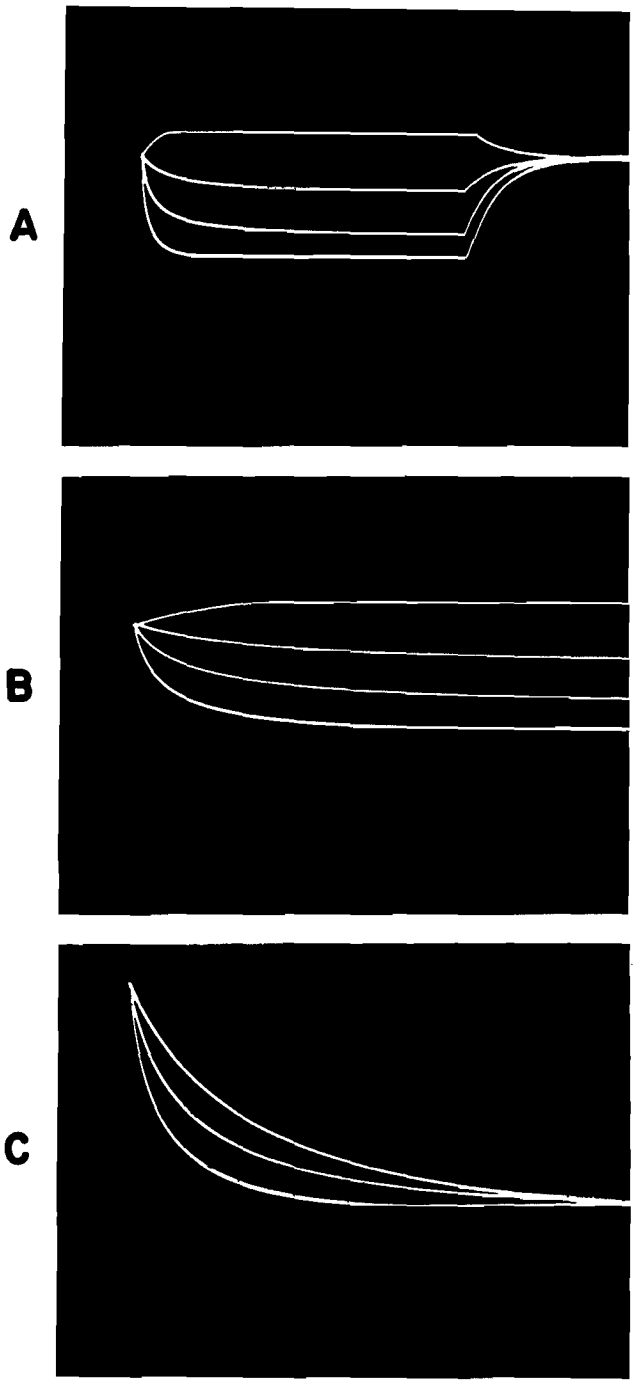

Figure 9. The Time Course of h Simulated in the SOMA MODEL.
9C shows the three negative responses normalized in amplitude to facilitate comparison of rise-times.

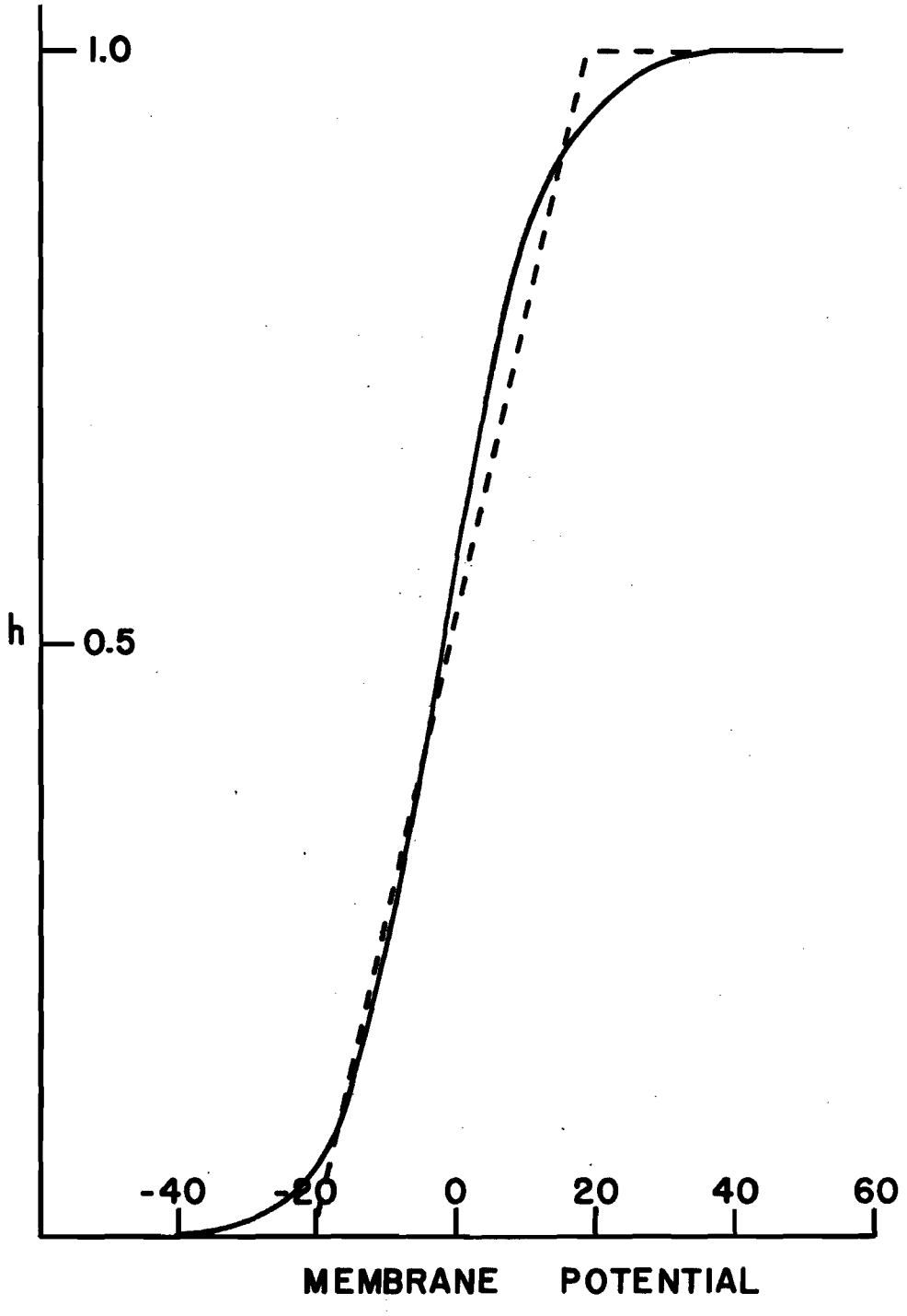

Figure 10. The Voltage-Dependence of the Inactivation Variable, h.

The continous line shows the relationship in the squid axon; the dashed line shows the approximation employed in the simulation.

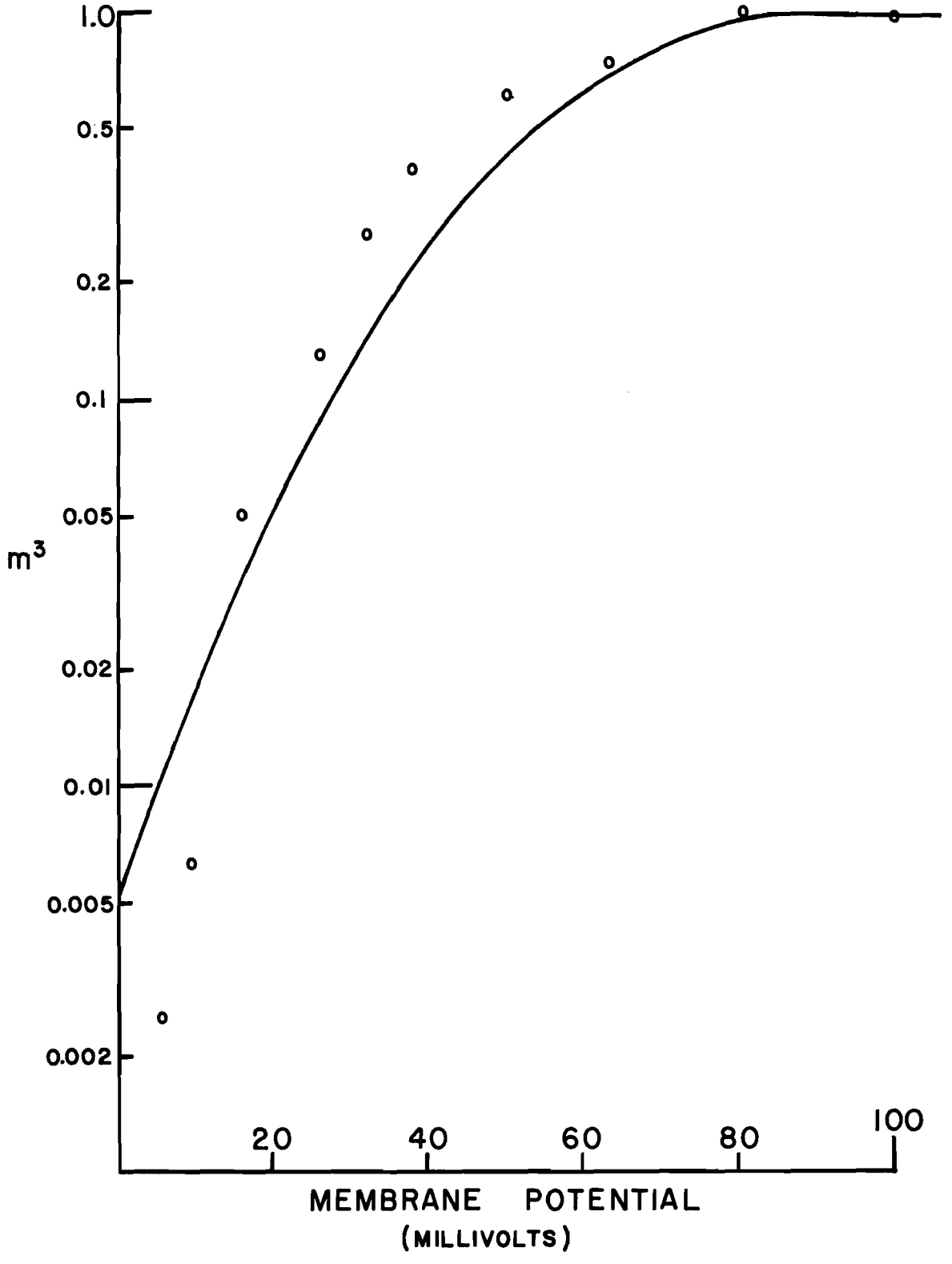

Figure 11. The Voltage-Dependence of the "Activation" Variable, m^3.

Pulse-Frequency Modulator

The subcircuit from transistor Q10 to Q15 generates 1- to 2- microsecond, 12-volt pulses whose frequency is directly proportional to the current into capacitor C3 from the collector of Q9. Immediately after the occurrence of a pulse at the emitter of Q14, capacitor C3 is positively charged and +12 volts appears at the base of Q10. Transistor Q10 is an emitter-follower, supplying the voltage at C3 to R16 without significantly draining the charge on C3. The rate of discharge of C3 is thus almost entirely determined by the collector current of Q9, if this current is constant, the voltage on C3 falls linearly from +12 toward the ground potential. As long as the voltage on C3 is greater than approximately +3V, transistor Q11 remains on, and its collector is at ground potential. While Q11 is on, the following conditions exist: The collector of Q12 is at +6V; the collector of Q13 and the emitter of Q14 are both at ground potential; diode D4 is reverse-biased and therefore not conducting; and transistor Q15 is on, and its collector is at ground potential.

When the voltage of C3 has fallen below +3V, Q11 turns off, and +10V appears at its collector. Transistor Q12 is turned on, driving Q13 off; +12V suddenly appears at the collector of Q13 and the base of Q15. As capacitor C6 is charged through R24, the voltage on the base of Q15 falls from its initial positive value toward -12V. As long as the base voltage of Q15 is positive, its collector is at -12V. During this time, Q11 is held in the nonconducting state and +12V appears at the collector of Q13 and the emitter of Q14. The positive voltage at the emitter of Q14 causes D4 to conduct and recharges C3 to +12V. The duration of the positive emitter voltage at Q14 is determined by the combination of R24 and C6. When the voltage at the base of Q15 reaches the ground potential, Q15 turns on. This causes Q11 to turn on, driving Q12 off and Q13 on. The collector voltage of Q12 and the emitter voltage of Q14 both return to the ground potential, terminating the output voltage pulse. The next pulse occurs after a time determined by the collector current of Q9. The voltage waveform at C3 is a sawtooth, varying between +12V and +3V. Its frequency is directly proportional to the collector current of Q9.

Sodium Circuit Output

Transistors Q5 and Q6 act as pulse amplifiers. The collector voltage of Q6 normally is +12V, while the collector of Q5 is at ground potential. When a positive pulse appears at the emitter of Q14, the collector of Q6 is switched to ground potential and the voltage output of the h-generating circuit suddenly appears at the collector of Q5. The waveform at Q5 is thus a positive, one-to-two-microsecond pulse whose amplitude is proportional to h and whose frequency is proportional to m^3. The average voltage at the collector of Q5 is directly proportional to m^3h.

POTASSIUM CIRCUIT (See figure 12)

The potassium circuit converts the time varying simulated membrane potential (V_M) into a current which in almost all respect is equivalent to the potassium current specified in the Hodgkin-Huxley model.

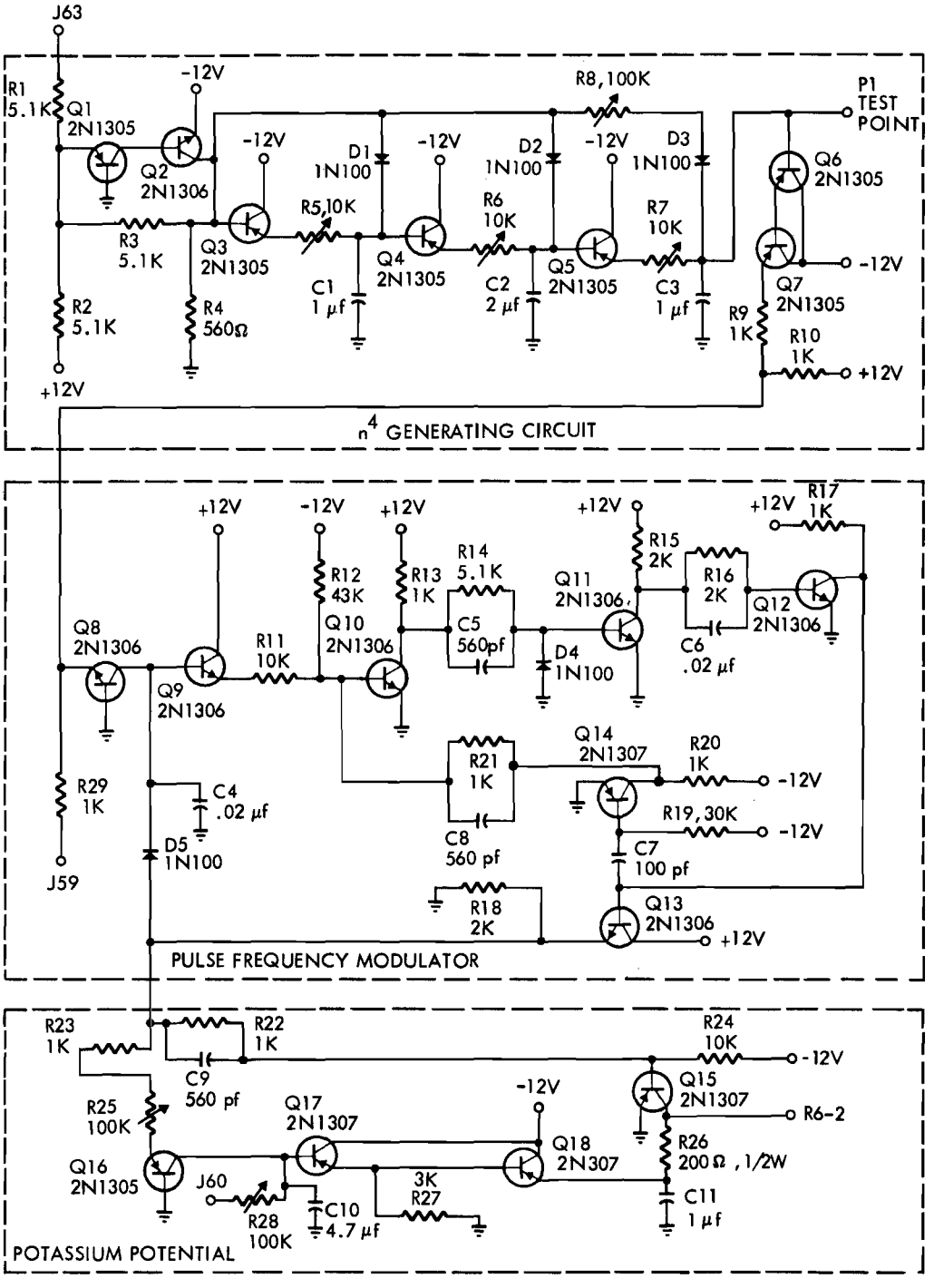

Figure 12. Diagram of the Potassium Circuit.

The potassium circuit also provides for the addition of a simulated synaptic component of potassium current, as specified by Eccles and others. In the Hodgkin-Huxley formulation, the potassium current is the product of two variables and one constant:

$$I_K = \bar{g}_K \ (n^4) \ (V_K - V_M)$$

Where n^4 is a function of membrane potential and time; $\bar{g}_K$ is a constant, and V_K is the equilibrium potential for potassium ion flux and is either constant or very slowly varying. The membrane potential (V_M) is normally close to V_K, and the difference between the two potentials ($V_K - V_M$) may vary considerably, even in the absence of spikes. Realistic simulation of the potassium current thus requires formation of the product of the two variables, n^4 and $(V_K - V_M)$.

The potassium circuit is divided into three subcircuits. One of these generates a current representing n^4; another effectively forms the product of n^4 and $(V_K - V_M)$; and the third provides optional dependence of V_K on the time integral of simulated potassium current.

n^4 - Generating Circuit

In the n^4-generating circuit, V_M is applied through resistor R1 to the emitter of Q1. The combination of Q1 and Q2 is a linear, inverting amplifier whose output is $-(V_M + 12v)$. Since V_M is negative, the amplifier output varies between -12v (for $V_M = 0$) and 0 (for $V_M = -12v$). The principal characteristic of the variable n^4 in the Hodgkin-Huxley model is its response to stepwise changes in V_M. For positive steps in V_M, n^4 falls in a nearly exponential manner. This combination of inflected rise and noninflected fall is simulated by the subcircuit beginning with Q3 and ending with Q7. Under static conditions, the voltage at the collector of Q2 (i.e., $-(V_M + 12v)$) appears at the base and emitter terminals of each of the transistors Q3, Q4, Q5 and Q6. A positive step in V_M produces a negative step at the base of Q3, reverse-biasing the diodes D1, D2 and D3. The step is thus transmitted to the base of Q6 through the ladder network made up of R5-C1, R6-C2, and R7-C3. Measured at the base of Q6, the response to the step is sigmoid, with a degree of inflection determined by the values of the variable resistors R5, R6 and R7.

In response to a negative step in V_M, a positive step appears at the collector of Q2. The diodes D1, D2 and D3 become forward-biased, and the voltage at the collector of Q2 appears immediately at the base terminals of Q4 and Q5. The voltage at the base of Q6 rises exponentially toward the new value of $-(V_M + 12v)$ with a time constant determined by the value of variable resistor R8. The output voltage of this circuit can be monitored at test point P1 on the printed-circuit card. A sample wave-

form showing the inflected rise and noninflected fall of the simulated n^4 is shown in figure 13. Transistors Q6 and Q7 act together as an emitter follower to prevent loading effects on the n^4 generating circuit by the low input resistance of the following circuit (the pulse frequency modulator).

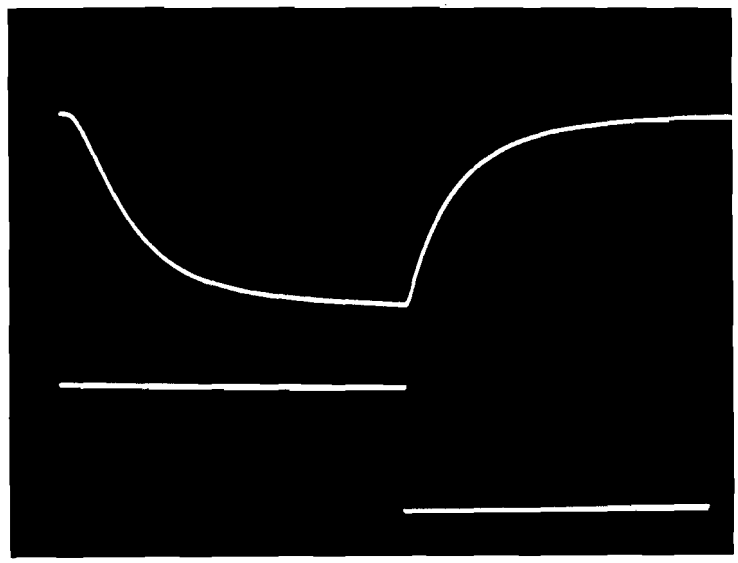

Figure 13. The Time-Course of n^4, Simulated in the SOMA MODEL.

The final output representing n^4 is the sum of the currents through R9, R10, and R29. Under static conditions, the current through R9 is $(V_M + 12v)/1K\Omega$, the current through R29 is $V_o\ (G_K)/1K\Omega$, and the current through R10 is $12v/1K\Omega$. The sum of these currents represents the steady-state value of n^4 and is equal to $-(V_M - V_o(G_K))/1K\Omega$. This linear approximation to n^4 is compared in figure 14 with the Hodgkin-Huxley data. The magnitude of Vo (G_K) is controlled by variable resistor R2 on the panel and monitored at J59.

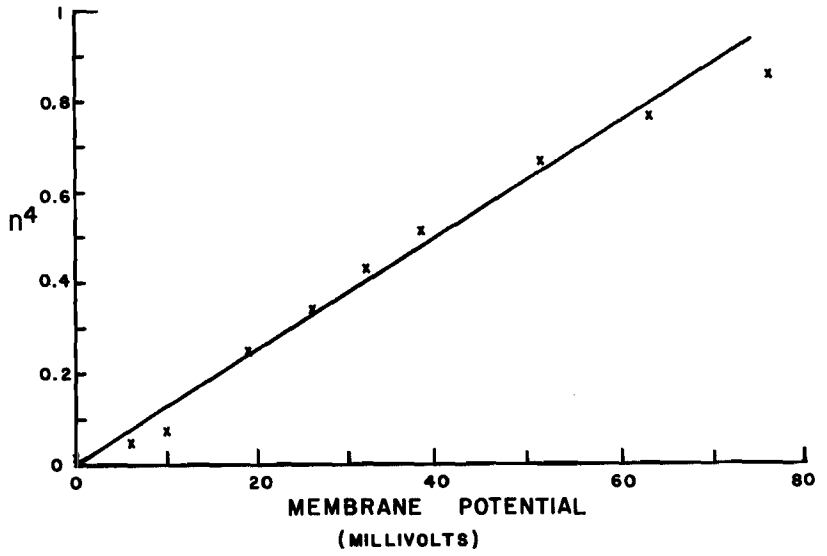

Figure 14. The Voltage Dependence of the Potassium Conductance Variable, n^4.

The solid line is the approximation in the SOMA MODEL; the x's are taken from the Hodgkin-Huxley data (Ref. 6). In this figure, positive voltages represent depolarizations, zero represents the resting potential.

The Pulse-Frequency Modulator

The collector current of Q8 is equal to the sum of the currents representing n^4 (i.e., the currents through R9, R10 and R29) and the current input from T3-6. The latter is equal to the sum of the simulated synaptic currents supplied from the synaptic circuits to terminals J52, J53 and J54 on the front panel (see figure 8).

The pulse-frequency modulator (Q9 through Q14) is identical to that described for the sodium circuit. The frequency of positive 12 volt pulses at the emitter of Q13 is directly proportional to the collector current of Q8.

The Potassium Potential Circuit

The simulated potassium potential in this model is the voltage at the collector of Q18. Under quiescent conditions, this voltage normally will be identical to that appearing at terminal J60 on the panel (figure 8). The latter is controlled by potentiometer R3 on the panel. If variable resistor R25 is set to its maximum value (approximately 100KΩ) and variable resistor R28 is set to its minimum value (approximately zero), the simulated potassium potential will be constant and equal to the voltage at J60. If R25 and R28 are set to other values, the simulated potassium potential will be dependent on the time integral of the potassium current, just as it would in the case of a limited extracellular space (see Frankenhauser and Hodgkin, 1965). The dependence in nerve cells is logarithmic; in the circuit it is approximated by a linear dependence.

Each positive voltage pulse at the emitter of Q13 produces a current pulse at potentiometer terminal R6-2. Each of these current pulses represents an increment of potassium current in this system. In addition to producing an increment of simulated potassium current at R6-2, each voltage pulse at the emitter of Q13 produces an incremental change in the simulated potassium potential at the collector of Q16. This change represents the effects of potassium-ion efflux from the nerve cell. The magnitude of the change is determined by the value of variable resistor R25. Restoration of the potassium potential is brought about by potassium-ion influx, simulated by the current through R28. The rate of restoration is determined by the setting of R28. Transistors Q17 and Q18 act together as an emitter-follower to provide the simulated potassium potential at capacitor C11 and resistor R26 without loading the collector circuit at Q16.

In the absence of a positive pulse at the emitter of Q13, transistor Q15 is on and its collector is at ground potential. During the occurrence of a positive pulse at Q13, transistor Q15 is off and the simulated potassium potential appears at its collector. The voltage waveform at R6-2 is thus a series of negative pulses, each starting at the gound potential and each having an amplitude equal to V_K. These pulses are applied through resistor R6 on the panel to diode D6 on the chloride circuit board. In the absence of a negative voltage pulse at R6-2 diode D6 is off and no current flows through R6. During a pulse, on the other hand, diode D6 is forward biased and a pulse of simulated potassium current flows to the point representing the inside of the membrane. This is illustrated in figure 15. The current (I_K) through R6 is described by the following expressions:

$$I_K = 0 \qquad \text{(in absence of a pulse at Q15)}$$

$$I_K = \frac{V_K - V_M}{R6} \qquad \text{(during a pulse at Q15)}$$

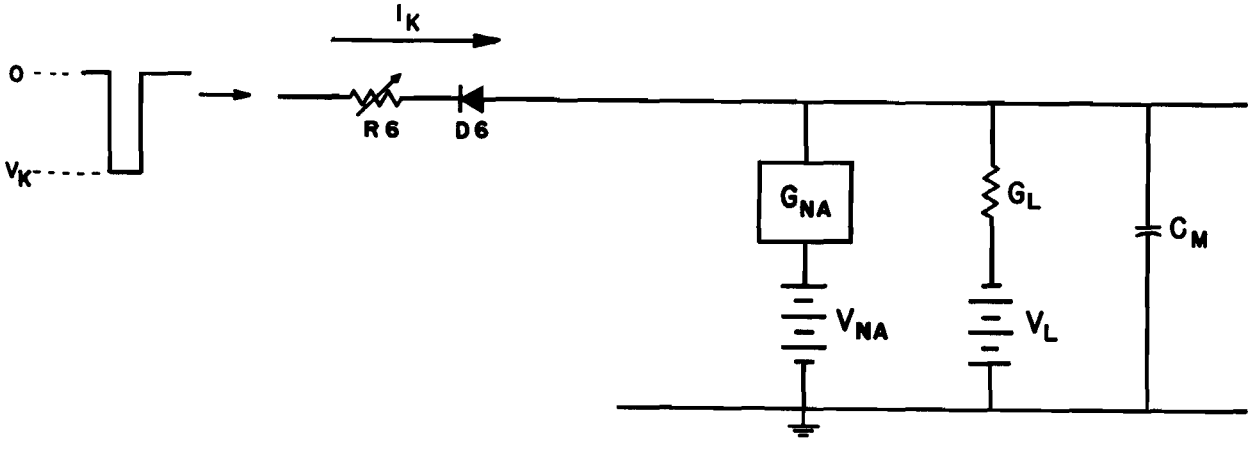

Figure 15. The Use of Frequency-Modulated Pulses to Simulate a Time-Varying Conductance.

The frequency of pulses at Q15 is directly proportional to the sum of the two simulated components of potassium conductance: The electrically excitable component which is proportional to n^4, and the synaptic component. In the case of one-microsecond pulses at Q15, the maximum pulse frequency is 10^6 Hz; and the average current through R6 over several pulse periods is given by

$$(I_K) = \frac{f}{10^6} \frac{V_K - V_M}{R6}$$

Where V_K is the potassium potential; R6 is the resistance of variable resistor R6; and f is the pulse frequency. The equivalent potassium conductance in this system becomes equal to $f/10^6R6$. Resistor R6 thus provides simultaneous control over the magnitudes of both simulated potassium conductance components.

CHLORIDE CIRCUIT (See figure 16)

The chloride circuit serves three functions. It provides the electronic equivalent of synaptically induced chloride (or leakage) conductance, as postulated by Eccles and others; it provides the summing point for the various simulated ionic currents in the model; and finally, it provides impedance transformation in a unity-gain amplifier so that the simulated membrane potential (V_M) can be applied to various external and internal circuits without allowing these circuits to load the simulated membrane and thus change its properties.

The circuit that simulates synaptic chloride conductance is divided functionally into two basic subcircuits - a pulse frequency modulator (Q2 to Q7) and a pulse amplifier and inverter (Q8 to Q11). Transistor Q1 serves as a summing point for currents applied to one or more of three jacks (J55, J56, J57) on the front panel (figure8). The collector current of Q1 is equal to the sum of those currents and is the input to the pulse frequency modulator. The pulse frequency modulator is the exact electrical complement of the circuit employed for the sodium conductance and the potassium conductance. The polarities of diodes and voltages in the chloride pulse frequency modulator are the opposite of those in the pulse frequency modulator of the potassium and sodium circuits, and where a pnp transistor appears in one circuit, an equivalent npn transistor appears in the other. All capacitance and resistance values are identical in the two circuits and the operations are basically the same. The output of the chloride pulse frequency modulator is a series of negative twelve-volt pulses whose frequency is directly proportional to the sum of the currents applied to J55, J56 and J57.

The negative voltage pulses from the pulse frequency modulator are applied simultaneously to two channels in the pulse amplifier-inverter circuit. The simulated chloride equilibrium potential is applied through a third channel. The amplifier inverter converts each pulse from the pulse

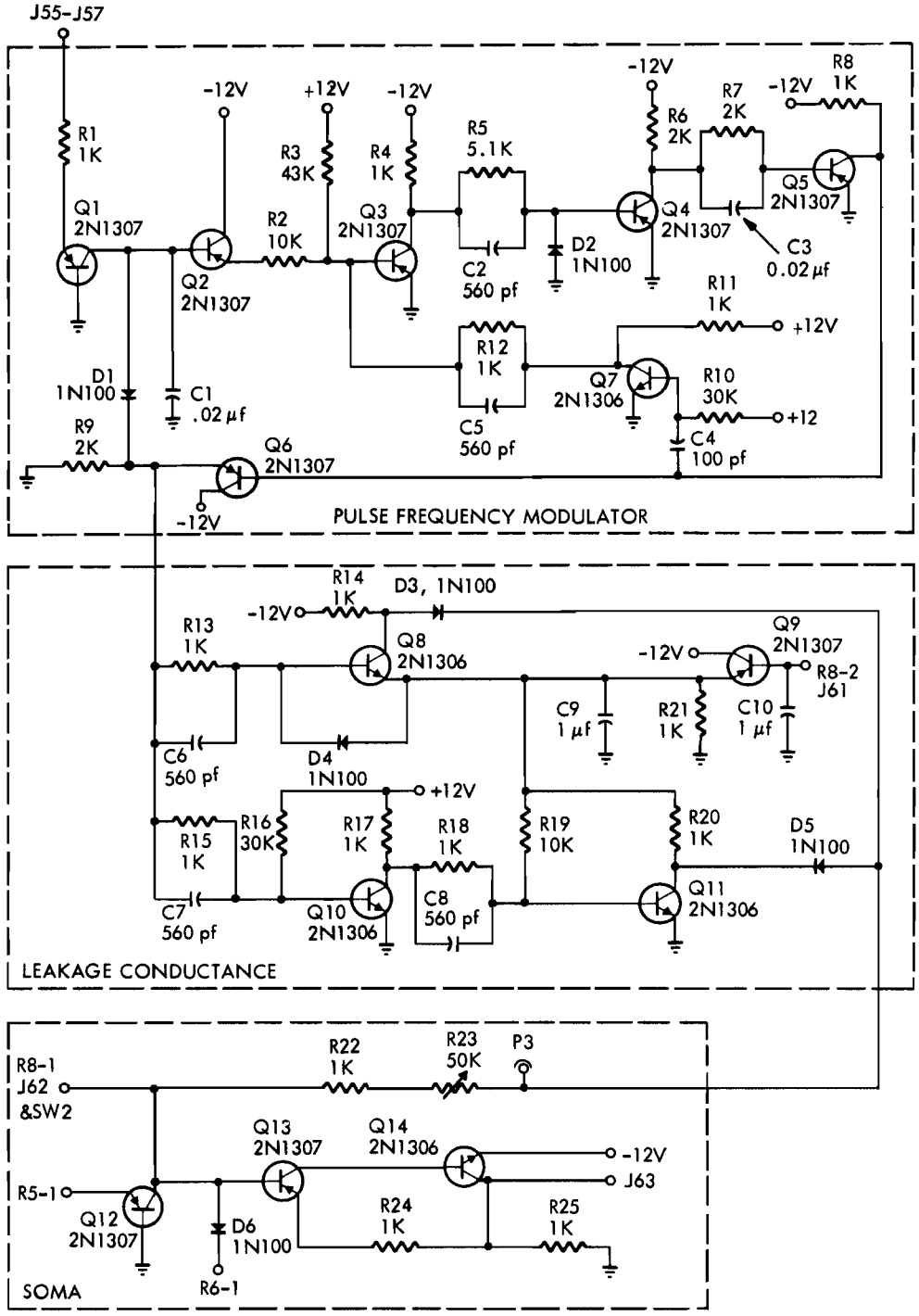

Figure 16. Diagram of the Chloride Circuit.

frequency modulator into two pulses, one going positive from -12 volts to the simulated chloride potential, the other going negative from the ground potential to the simulated chloride potential.

The simulated chloride equilibrium potential (V_1) is determined by the variable resistor R4 on the front panel. It can be monitored at J61. This voltage is applied directly to the fixed chloride conductance, R8 on the front panel, and through an emitter follower (Q9) to the emitter of Q8 and the collector resistor of Q11 of the chloride circuit.

In the absence of a negative pulse at the emitter of Q6, -12v appears at the collector of Q8 and the ground potential appears at the collector of Q11. During the negative pulse, V_1 appears at both collectors. The resistor R22 is connected directly to the inside of the simulated soma membrane at J62. Since the potential at this point is always between -12v and the ground potential, diodes D3 and D5 are reverse-biased except during a pulse. If the simulated internal soma membrane potential is between V_1 and ground potential, D5 conducts during a pulse and D3 does not. If, on the other hand, the soma potential is between V_1 and -12v, D3 conducts during a pulse and D5 does not. The current through R22 and R23 is thus equal to $(V_1 - V_M) / (R22 + R23)$ during a pulse and zero in the absence of a pulse; and the polarity of the current during a pulse is determined by the magnitude of V_M (the soma membrane potential) relative to V_1. If the duration of each pulse is one microsecond, the maximum pulse frequency is one megacyle. The average current through R22 and R23 over several pulses is $f (V_1 - V_M) / 10^6 (R22 + R23)$; where f is the pulse frequency. The equivalent synaptically induced chloride conductance become $f/10^6$ (R22 + R23) and is controlled by the variable resistor R23.

The terminal J62 is the summing point for all of the simulated trans-membrane currents of the SOMA MODEL, and five of these current are summed on the chloride circuit board. The currents from the simulated Hodgkin-Huxley sodium conductance and the synaptic shunt conductance both are delivered through transistor Q12 from potentiometer-terminal R5-1 (figure 8). The Hodgkin-Huxley and synaptic potassium currents are delivered through diode D6 from potentiometer-terminal R6-1. The synaptic chloride current is delivered through R22 and R23. Terminal J62 is connected directly to the simulated membrane capacitance (C_M) and fixed chloride or leakage conductance on the front panel. This terminal represents the internal conducting fluid of the soma membrane. The voltage appearing at this terminal is the simulated soma membrane potential. Any external loads connected to this terminal represent loads on the soma membrane. Currents applied to this terminal represent current applied to the inside of the soma membrane.

The simulated soma membrane potential also appears at the collector of Q14, but Q13 and Q14 act together as a compound emitter follower, so loads connected to J63 do not affect the simulated soma membrane. Terminal J63 is thus isolated from the soma model. The potential from this terminal serves as the input for the potassium circuit and for the sodium circuit.

SPIKE INITIATOR CIRCUIT (see figure 17)

The spike initiator circuit is a two-terminal network that represents a patch of electrically excitable membrane. One terminal (J64-J65) represents the inside of the membrane; the other terminal (circuit ground) represents the outside of the membrane. The three Hodgkin-Huxley conductances (sodium conductance, potassium conductance and chloride or leakage conductance) are represented along with the transmembrane capacitance. The circuit can be divided functionally into five subcircuits: (1) the simulated sodium conductance, (2) the simulated potassium conductance, (3) the simulated passive membrane elements, (4) an isolation amplifier and (5) an audio power amplifier.

The simulated sodium conductance receives as its input the potential at the terminal representing the inside of the membrane (i. e., terminal J64-J65). It receives this potential from an emitter follower, however, so that its input resistor (R7) does not draw current from the simulated membrane. The combination of transistors Q5 and Q6 serves as an inverting amplifier with a gain of four. The effective input to this amplifier is the sum of the positive voltage at R9-2 and the negative simulated membrane potential. When this sum is positive, a negative voltage appears at the collector of Q6. When the sum is negative, the collector of Q6 is at the gound potential. The potential at R9-2 is controlled by the potentiometer labeled θ on the front panel. When a negative potential appears at the emitter of Q6, current flows through two paths to the base of Q7. One of these paths (D1, C3, N1) responds to changes in simulated membrane potential and represents the transient portion of the sodium conductance. The other part (R13) responds to the simulated membrane potential itself and represents the steady-state portion of sodium conductance. The currents in the two paths are summed and amplified by Q7. The output (collector) current of Q7 is applied through a current limiting resistor (R15) to the inside of the simulated membrane (i. e., to J64 - J65). The charging of capacitor C3 represents inactivation of the transient sodium conductance, and the discharge of C3 through R12 represents recovery from inactivation. The nonlinear dependence of sodium current on membrane potential is simulated by varistor N1.

The simulated potassium conductance receives as its input the simulated membrane potential from the emitter follower Q1. This potential is applied to a 2-stage resistor-capacitor filter comprising R16, C4 and R18, R19, C5. Each of the two stages is followed by an emitter follower (Q8 and Q9) . In response to positive voltage steps superimposed on the simulated membrane potential, diode D1 conducts and capacitor C5 is charged through R19. The two stages of the filter thus are effectively identical and the response at C5 will be inflected. In response to a negative step change in the simulated membrane potential, diode D1 is reverse-biased and capacitor C5 is charged through R18. The response at C5 in this case is not inflected. This combination of inflected response to positive steps and noninflected response to negative steps is one important characteristic of the Hodgkin-Huxley potassium conductance.

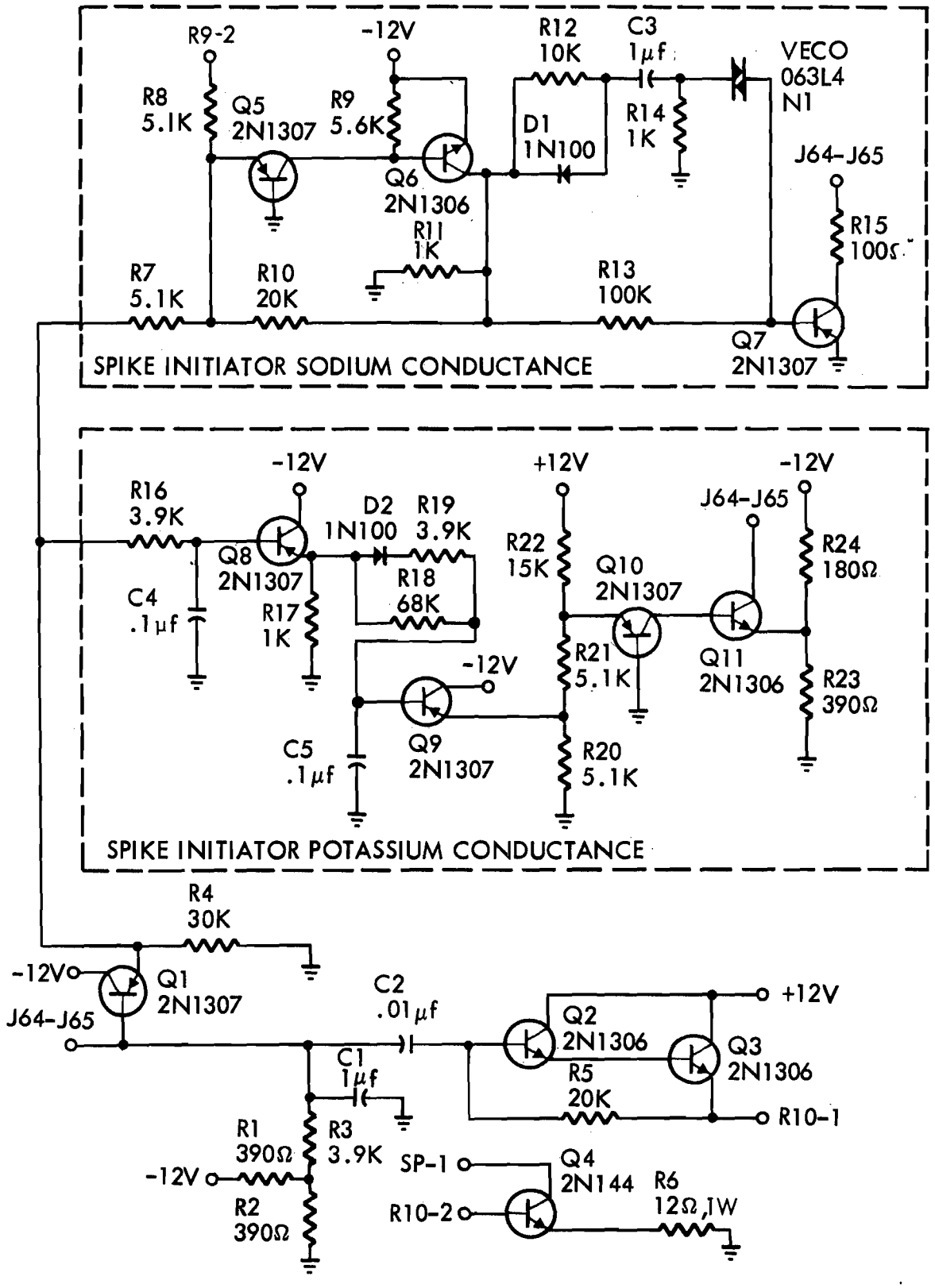

Figure 17. Diagram of the Spike Initiator Circuit.

The potential at C5 appears at the emitter of Q9 where it becomes the input voltage for an amplifier consisting of Q10 and Q11. When the emitter potential of Q9 is greater than 4 volts (negative), transistor Q10 is off and no current flows from J64-J65 through Q11. When the potential is less than 4 volts, on the other hand, Q10 conducts and the current through Q11 tends to increase the simulated membrane potential. The emitter of Q11 is biased to the simulated potassium equilibrium potential (-8v) by the combination of R23 and R24. This potential appears at the base of Q11 and provides the collector bias for Q10. The potential at J64-J65 is always positive with respect to -8v, so the collector of Q11 is reverse biased. Current in Q11 ceases when the potential at J64-J65 reaches -8v.

The passive elements in the Hodgkin-Huxley model are represented by R3 and C1. The simulated chloride or leakage potential (-6v) is developed by the combination of R1 and R2. Resistor R3 represents the chloride conductance and capacitor C1 represents the transmembrane capacitance The emitter follower, Q1, serves as an isolation amplifier to deliver the simulated transmembrane potential to the potassium and sodium conductance circuits without loading the membrane.

Transistors Q2, Q3 and Q4 serve as an audio power amplifier. The combination of Q2 and Q3 is a compound emitter follower. Spikes generated by the spike initiator are applied to this emitter follower through C2. From the emitter of Q3, the spikes are delivered to a 100-ohm, volume-control potentiometer (R10) on the front panel. From the center tap of R10 they are applied to the base of the audio power transistor, Q4, which drives the speaker on the front panel (SP-1).

AXON DELAY (See figure 18)

The axon delay circuit converts a voltage pulse going positive from any d-c level into a delayed voltage pulse going positive from the zero or ground level. This is accomplished by allowing the input pulse to trigger a monostable multivibrator that responds with a prolonged pulse of controllable duration. The trailing edge of the prolonged pulse is differentiated and shaped to produce the output pulse. The delay between the input and output pulses is thus equal to the length of the prolonged pulse.

In the absence of an input pulse, transistors Q1, Q3 and Q4 are conducting, so their collectors are at ground potential. Transistor Q2 is off, so its collector is at -12 volts. A positive pulse applied through C1 to the base of Q1 causes Q1 to turn off momentarily. This turns Q2 on, bringing its collector to ground potential and causing a positive voltage at the base of Q4, which is thus turned off. Q4 remains off until the positive voltage on C3 has been dissipated through the series combination of R8 and R11 (figure 8). While Q4 is off, Q2 remains on and its operation is independent of the voltage at the collector of Q1. The time required for the voltage on the base of Q4 to reach ground potential is determined by the setting of R11 on the panel. When ground potential is reached, Q4 turns on and Q2 turns off. The collector of Q2 swings from ground potential to -12v, causing a negative voltage to appear at the base of Q3, turning it off and causing a positive twelve-volt pulse to appear at the

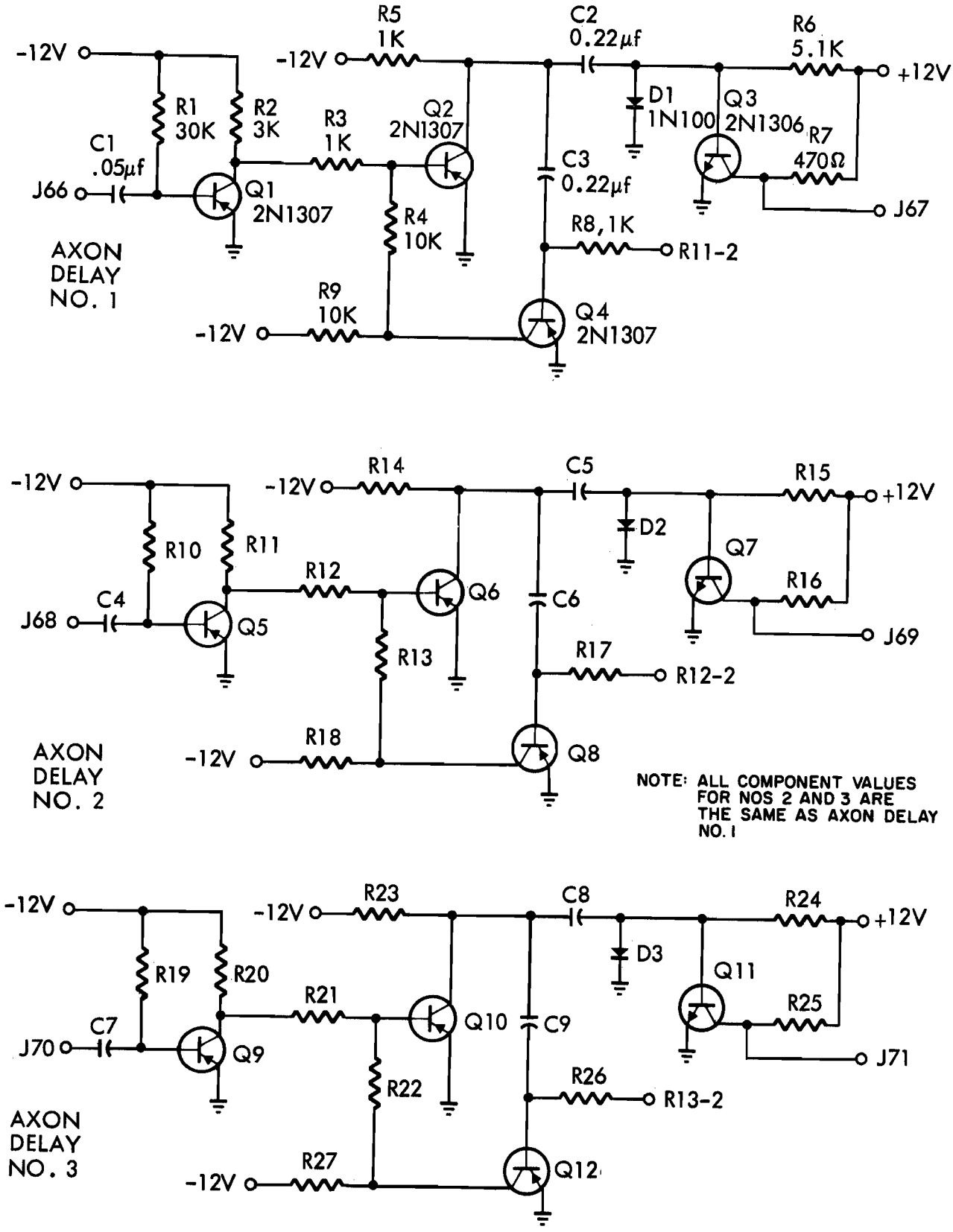

Figure 18. Diagram of the Axon Delay Circuit.

output terminal. As C2 is charged through R6, however, the voltage at the base of Q3 rises toward +12V. When this voltage passes through the ground potential, the output pulse terminates. The output pulse width is thus determined by the values of C2 and R6.

The input impedance of the axon delay circuit is capacitive and equal to 0.05 microfarad. Since the output capacitance of the spike initiator is 1.0 microfarad, the axon delay imposes a 5% load. The axon delay output impedance is 470 ohms, sufficiently low to drive the synaptic circuit inputs.

SYNAPTIC CIRCUIT (See figure 19)

The synaptic circuit is designed to transform the positive voltage pulses from the axon delay circuits into decaying exponential waveforms that simulate the time courses of synaptically induced conductances. The exponential waveforms from the output of the synaptic circuit are connected to various conductance circuits by means of tip jacks (J49 to J57) on the front panel.

During a positive pulse at the input (terminal J31) of the synaptic circuit, the diode D1 conducts and, capacitor C1 is charged through resistor R1. The magnitude of R1 is variable and determines the amount of charge transferred to C1 during a pulse. In the absence of an input pulse, C1 discharges through variable resistor R2; the rate of discharge is determined by the magnitude of R2. The voltage on C1 can be monitored at test jack P1 on the circuit board. This potential is applied to the output terminal J32 through an isolation amplifier (Q1 and Q2) and a resistor, R5.

Three identical synaptic circuits are mounted on each synaptic circuit card. Their operation is identical. They may be distinguished by the colors of their test jacks (P1, P2 and P3) which match the colors of their corresponding input and output terminals (J31-J32, J33-J34 and J35-J36) on the front panel.

A fourth circuit is mounted on the synaptic circuit card. This is an inverting amplifier that has a gain of 0.5 when connected to the output terminal of a synaptic circuit. When the output of a synaptic ciruit is connected to terminals J52, J53 or J54 (i.e., the potassium conductance input terminals) on the front panel, the signal is diverted to this inverting circuit which makes it compatible with the potassium conductance circuitry. The output of the inverter is applied through R21 to the emitter of Q8 of the potassium circuit.

OPERATING PROCEDURES

The Neural Analog Facility is designed to provide real-time simulation of membrane currents and voltages. The simulated transmembrane capacitance and equivalent ionic conductances are designed to be equal in magnitude to those found in the nerve-cell prototpyes. The simulated transmembrane currents and voltages, on the other hand, are increased

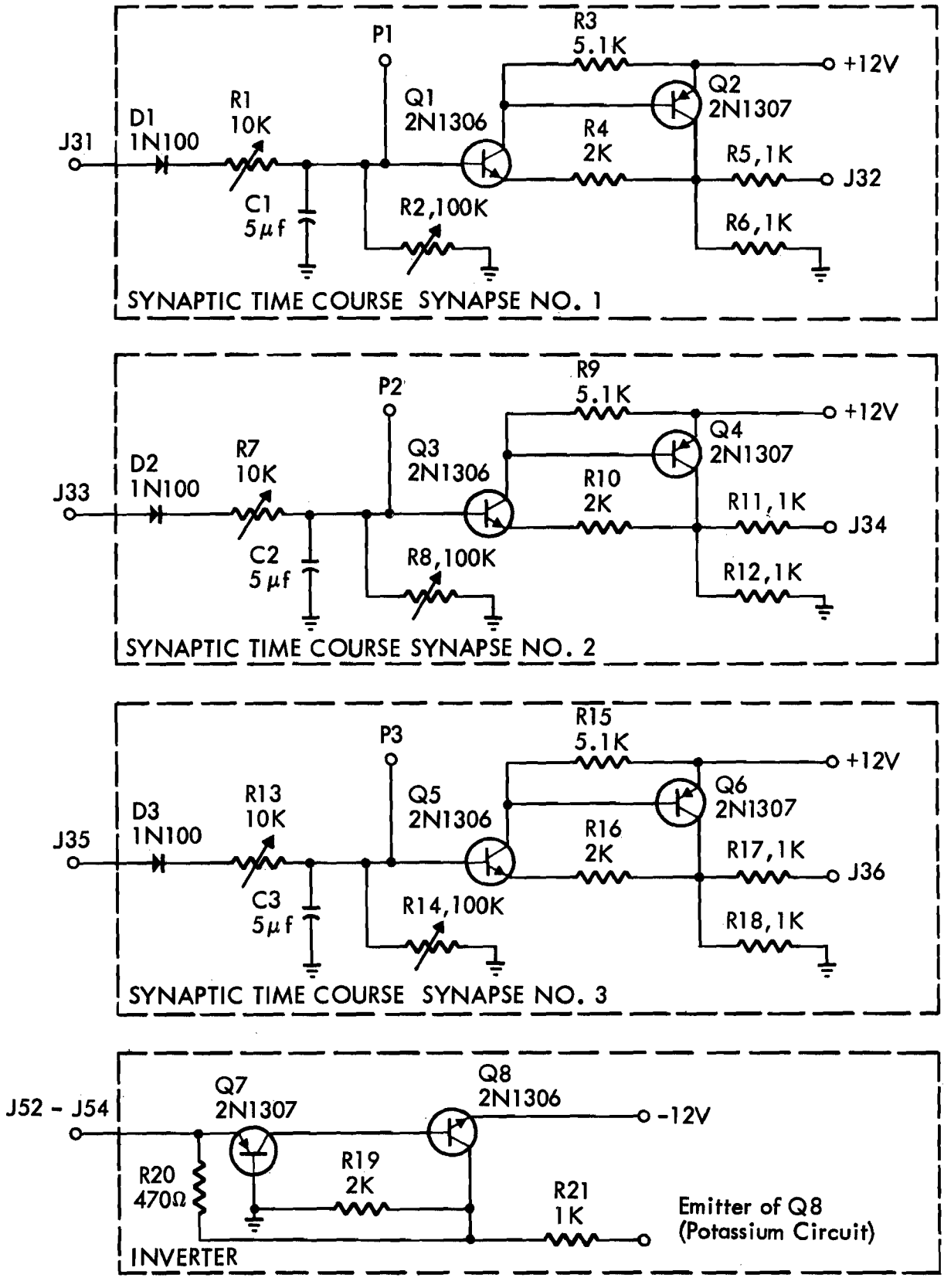

Figure 19. Diagram of the Synaptic Circuit.

by a factor of 100 to make them compatible with the electronic circuits of the models. A potential of ten millivolts in the nerve cell is represented by one volt in the models; ten microamps in the nerve cell is represented by one milliamp in the models.

The simulated intracellular potential of the SOMA MODEL can be monitored at either of two tip jacks on the front panel - SOMA DIRECT (J62) and SOMA ISOLATED (J63), (see figure 8). Functional connections to the node representing the inside of the soma membrane must be made to the SOMA DIRECT tip jack. The simulated intracellular potential of the SPIKE INITIATOR MODEL also can be monitored at either of two tip jacks - IN (J64) and OUT (J65). These tip jacks are connected directly together by a wire, and they both represent the inside of the spike initiator membrane. The nodes representing the outsides of the soma and spike initiator membranes are grounded.

Twenty-four controllable parameters are associated with the SOMA MODEL; seventeen of these are related to electrically excitable membrane and seven are related to subsynaptic membrane. Although this array of parameters is formidable, it is not impossible to manage. One strategy that makes the system tractable, for example, is that under which the parameters of each of the ten MODULES are adjusted to a basic configuration matching the specifications of the Hodgkin-Huxley model (see table 1) and small parameter changes are treated as perturbations of that basic configuration.

When MODULES are interconnected to represent small neural networks, the synaptic parameters become important. Each simulated synapse has only two parameters, however, and the response of the whole network generally is not critically dependent on these. A good strategy for dealing with networks seems to be first to establish and fix the parameters of the electrically excitable portion of each module, then to experiment with the synaptic parameters alone.

SPECIFICATIONS OF THE HODGKIN-HUXLEY MODEL

Most of the membrane conductance data published by Hodgkin and Huxley were inferred from experiments in which the transmembrane potential was suddenly changed and held at a new value, and the time course of the resulting transmembrane current was observed. For that reason the parameters are discussed here in terms of conductance changes in response to a suddenly applied voltage step. The parameters apply to the giant axon of the squid at $6^{o}C$.

Hodgkin and Huxley found that in response to a stepwise change in the membrane potential, the time course of the sodium conductance was described accurately by the following equation:

$$(1) \quad G_{Na} = \overline{g}_{Na} m^3 h$$

where $\bar{g}_{Na}$ is a constant amplitude factor; m(t) is a rising negative exponential; and h(t) is a decaying exponential. They found that the potassium conductance was described accurately by the following equation:

$$(2) \quad G_K = \bar{g}_K \, n^4$$

where $\bar{g}_K$ is a constant, amplitude factor; and n (t) is a rising negative exponential. The membrane capacitance and leakage or chloride conductance were found to be constant (independent of time and voltage).

The time dependent variables are described by the following equations:

$$(3) \quad m(t) = m_\infty - (m_\infty - m_o) \exp(-t/\tau_m)$$

$$(4) \quad h(t) = h_\infty - (h_\infty - h_o) \exp(-t/\tau_h)$$

$$(5) \quad n(t) = n_\infty - (n_\infty - n_o) \exp(-t/\tau_n)$$

where m_o, h_o and n_o depend only on the initial value of membrane potential (before the stepwise change); m_∞, h_∞, n_∞, τ_m, τ_h, and τ_n depend only on the final value of membrane potential (after the stepwise change). The forms of the simulated voltage dependences of n, m, and h are fixed in the model (see figures 10, 11 and 14), but the values at the resting potential are adjustable. In addition, τ_m is generally less than 0.5ms, and changes in m are much more rapid than changes in any other variable in the Hodgkin-Huxley formulation (including membrane potential); so τ_m is taken to be zero in the simulation.

We are thus left with two voltage-dependent time constants from equations 3, 4 and 5: τ_h and τ_n. Hodgkin and Huxley measured the voltage dependences of both of these parameters for stepwise reductions (depolarizations) of membrane potential; but the voltage dependences of these parameters for stepwise increases (polarizations) in membrane potential have not been demonstrated. In the simulation, each of these parameters (τ_h and τ_n) are subdivided into two independent parameters - a time constant for depolarization is called the inactivation time constant τ_i, while the time constant for polarization is called the time constant of recovery from inactivation, τ_r. Figure 20 shows τ_i as a function of membrane potentail for a typical squid giant axon. Hodgkin and Huxley measured τ_r for only one case, repolarization from 44 mv below equilibrium (i.e., a step change from approximately -16 mv to approximately -60 mv). τ_r in this case was 12 ms. The voltage dependence of τ_n for depolarization is shown in figure 21. For polarization, Hodgkin and Huxley observed that in the cases of repolarizations from various potentials to the resting level, the time constant was essentially constant

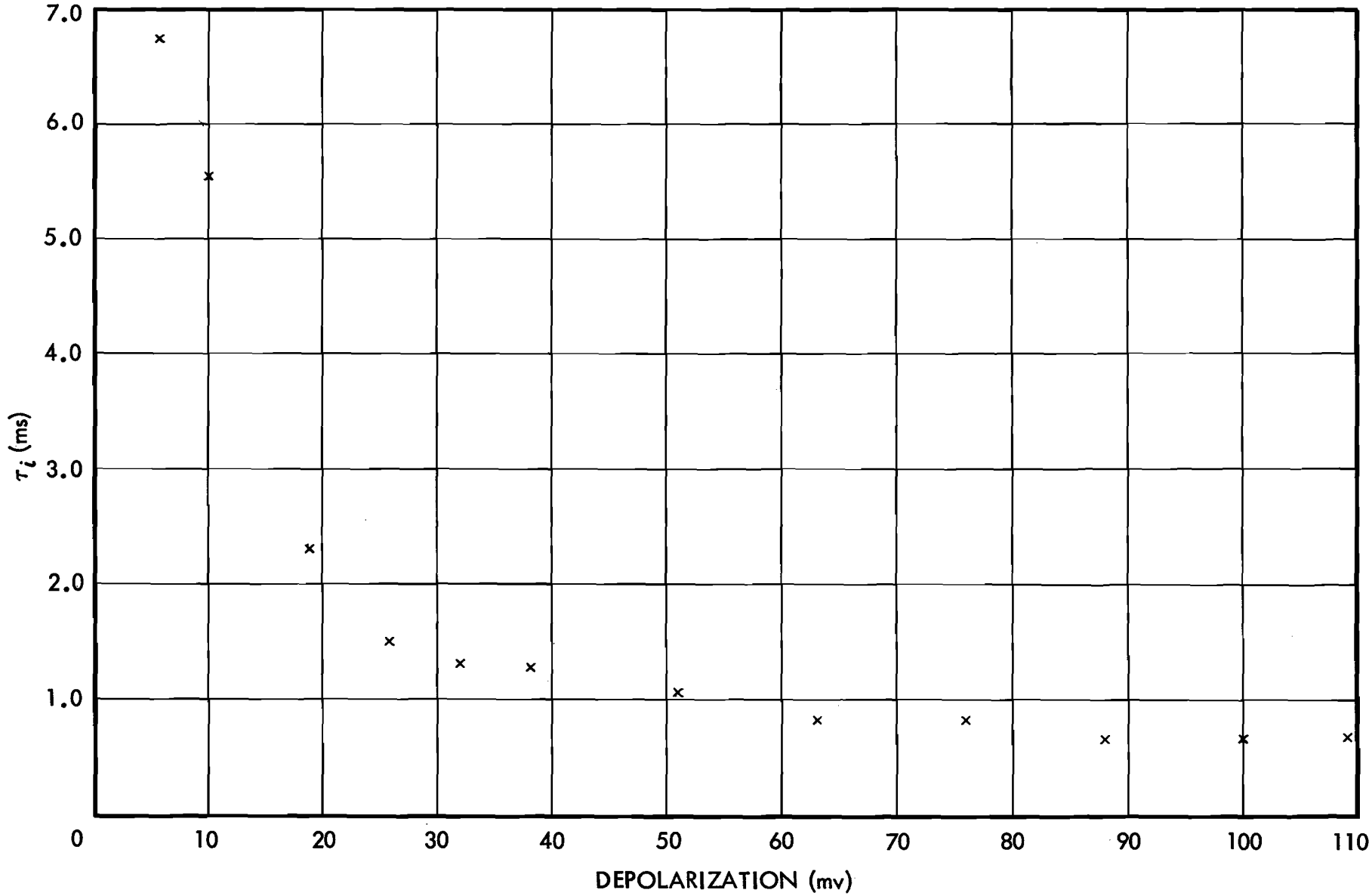

Figure 20. Voltage Dependence of the Time Constant of Sodium Inactivation (taken from Hodgkin and Huxley, 1952d).

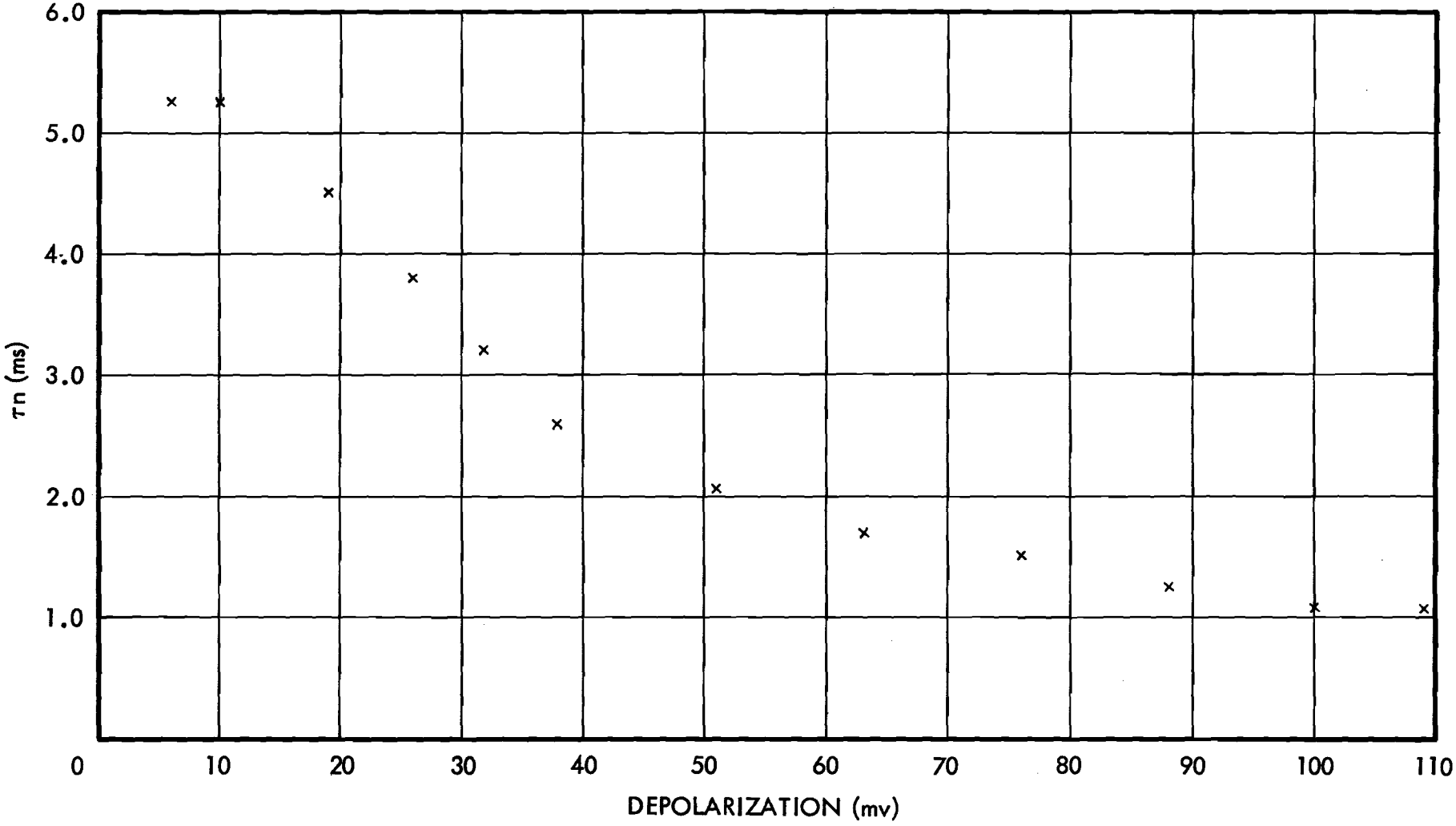

Figure 21. Voltage Dependence of the Time Constant for Increases in the Potassium Conductance Variable, n.

at approximately 5 msec. For polarizations to depolarized states, the time constant was shorter.

In addition to the seven aforementioned parameters from Equations 3, 4 and 5, two parameters from Equations 1 and 2 are adjustable in the SOMA MODEL, $\overline{g_{Na}}$ and $\overline{g_K}$. Finally, the leakage conductance, the membrane capacitance, and the potassium and leakage ion equilibrium potentials are all adjustable. Table 1 is a list of these parameters, their values according to the Hodgkin-Huxley data, and the settings of SOMA MODEL controls that provide those values.

TABLE 1

SOMA MODEL Parameter Setting According to Specifications of the Hodgkin-Huxley Model for 0.25 Sq Cm of Squid Axon Membrane (see figure 8)

Hodgkin-Huxley Parameter		Value Specified by Hodgkin and Huxley	Corresponding Control on front panel	Setting of Control that provides specified value
$\overline{g}_{Na}$	(1)	$10 \times 10^{-3} ohm^{-1}$	G_{Na} (R5)	0Ω
$m(V_o)$ resting value of m	(1)	0.042	V_o (R7)	between 8.5, 9.5 volts at center tap
$h(V_o)$ resting value of h	(1)	0.6	$V_o(h)$	+3v
τ_i inactivation time constant	(1)	voltage dependent 0.67 to 6.7	C_h	1.0 μfd.
τ_r time constant of recovery from inactivation	(2)	12 ms	R1 (Sodium Circuit Card)	$12 \times 10^3 ohm$
$\overline{g}_K$	(3)	2.4×10^{-3} ohm^{-1}	G_K (R6)	0Ω
$n(V_o)$ resting value of n	(3)	0.315	$V_o(G_K)$	-9v
τ_n (for depolarization)	(3)	voltage dependent 1.05 to 5.25 ms	R5, R6, R7 (Potassium Circuit Card)	200Ω, 400Ω, 600Ω

1. The values for sodium conductance variables (not including τ_r) were calculated from Table 2 (p. 514) of Hodgkin and Huxley (1952 d).
2. τ_r was taken from p. 504, Hodgkin and Huxley (1952 c).
3. The values for potassium conductance variables were calculated from Table 1 (p. 509) of Hodgkin and Huxley (1952 d.).

Hodgkin-Huxley Parameter		Value Specified by Hodgkin and Huxley	Corresponding Control on front panel	Setting of Control that provides specified value
τ_n* (for polarization)	(1)	2.5 to 5.0 ms	R8 (potassium circuit card)	5×10^3 ohm
V_K potassium equilibrium potential	(2)	-127 mv referred to the sodium potential	V_K	-10v
$\overline{g_l}$ leakage conductance	(2)	3×10^{-5} ohm^{-1}	G_l (R8)	6.7
V_l	(2)	-105 mv referred to the sodium potential	V_l	-8v
C_M	(2)	0.25 fd	C_M	0.25 µfd
			R23 (chloride circuit card)	100KΩ
			R28 (potassium circuit card)	0Ω
			R25 (potassium circuit card)	100KΩ

1. The value for τ_n* were taken from Hodgkin and Huxley (1952 b; pp 491-492).
2. The values of V_l, g_l, V_K, and C_M were calculated from Table 3, Hodgkin and Huxley (1952 d; p 520).

SECTION IV

THE TWO-PATCH NEURAL MODEL

INTRODUCTION

In Section 1 a two-lump approximation to a spatially distributed neuron was described. This configuration is shown again in figure 22. One lump consists of the SOMA MODEL, which represents the integrative region of the nerve cell; and the other lump consists of the SPIKE INITIATOR MODEL, which represents the trigger region of a nerve cell. The two lumps are separated by a resistor representing the resistance of the intracellular current path from the integrative region to the trigger region. The extracellular resistance is taken to be negligible.

In this section the two-lump, or two-patch neural model is considered again. Throughout the section, the integrative patch (SOMA MODEL) is taken to be capable only of graded response and incapable of producing a spike. All but one of the parameters of the SOMA MODEL were set to the values specified in Table 1, so in every respect but one the model was consistent with the Hodgkin-Huxley data. The single difference was the simulated transmembrane capacitance, which was set

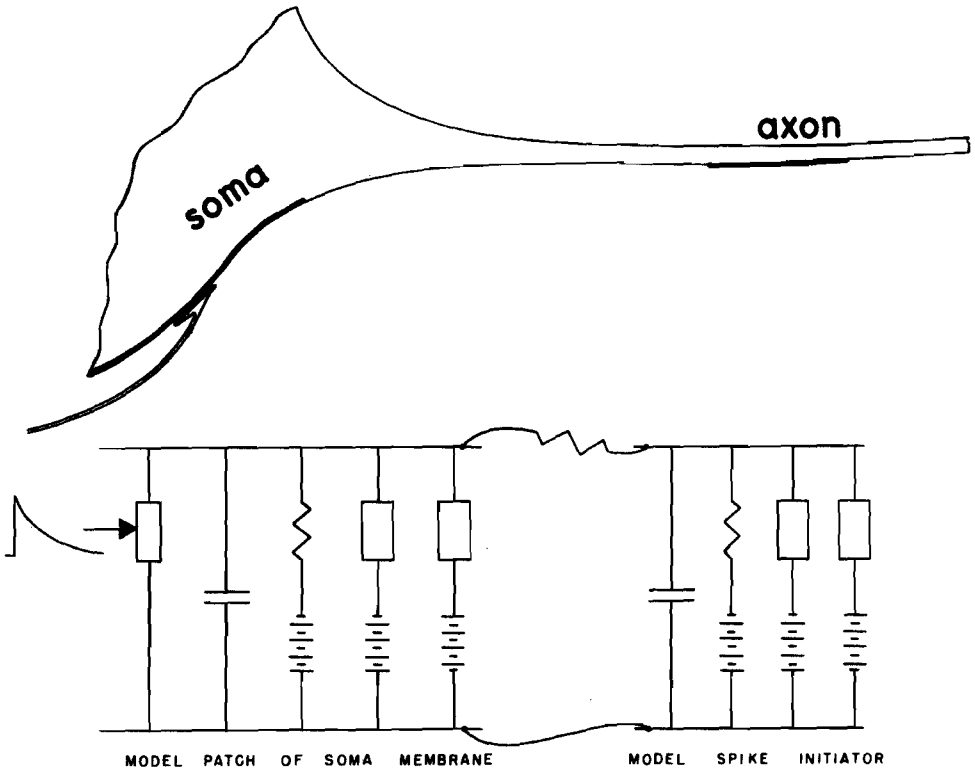

Figure 22. A Two-Patch Representation of a Neuron.

at a magnitude of 2 to 5 microfarads. Since the SOMA MODEL represents 0.25 sq cm of squid axon membrane, the capacitance was eight to twenty times that specified by Hodgkin and Huxley. With the larger values of membrane capacitance, the SOMA MODEL was capable only of completely graded response. Large membrane capacitances have been measured in several integrative neural somata (Hagiwara, 1960, Hagiwara, Watanabe and Saito, 1959), so this seems to be a reasonable parameter adjustment. Figure 23 shows several examples of the effects of the larger capacitance value.

INVASION OF THE SOMA MODEL BY SPIKES

Resetting of Synaptic Potentials

In the system of figure 22, a slow potential such as a prolonged excitatory postsynaptic potential (epsp) at the soma presumably can elicite spikes along the axon, and the occurrence of an axonal spike should have some effect at the soma. Figure 24 shows the effects of invasion of the SOMA MODEL by antidromic spikes. The nonspecific shunt conductance was modulated by a series of three decaying exponentials (lower trace of each pair). The incremental conductance was 0.1×10^{-3} ohm^{-1} and the time constant for the exponential decline of conductance was 50 ms. The transient conductance changes induced simulated epsp's in the SOMA MODEL (upper trace in each pair) and these in turn elicited spikes at the SPIKE INITIATOR MODEL. The reflections of the spikes can be seen superimposed on the epsp's.

From figure 24A to 24E, the resistance between the SOMA MODEL and SPIKE INITIATOR MODEL was progressively reduced from 20K to 1.25K . In 24A, two spikes were elicited by the first epsp and three spikes each by the second and third epsp's. The minature, reflected spikes are barely visible on the epsp's and apparently did not alter their form. In 24B the spike reflections were larger, but do not appear to have altered significantly the epsp's. Three spikes occurred on the first epsp and the spikes on the second and third epsp's occurred earlier than in the case of 24A; the epsp's in 24B thus seem to be more effective in eliciting spikes. In 24C, the invading spikes tended to polarize, or reset the soma potential; so in spite of the fact that the coupling resistance was less than in the case of 24B, the epsp's were less effective in eliciting spikes. This is evident from the fact that only two spikes occurred on the first epsp, and the spikes on the second and third epsp's occurred later than they did in 24B. In 24D and E the resetting of the soma potential was even more pronounced. Figure 24E, in fact, shows only one spike on the first epsp and two each on the second and third epsp's.

Figure 24F shows the resetting of the soma potential by a single spike on the second epsp. The effects of the two epsp's were probably summed at the spike initiator, so the second potential was able to elicite a spike. The time scale has been expanded in this photograph to show the resetting in more detail.

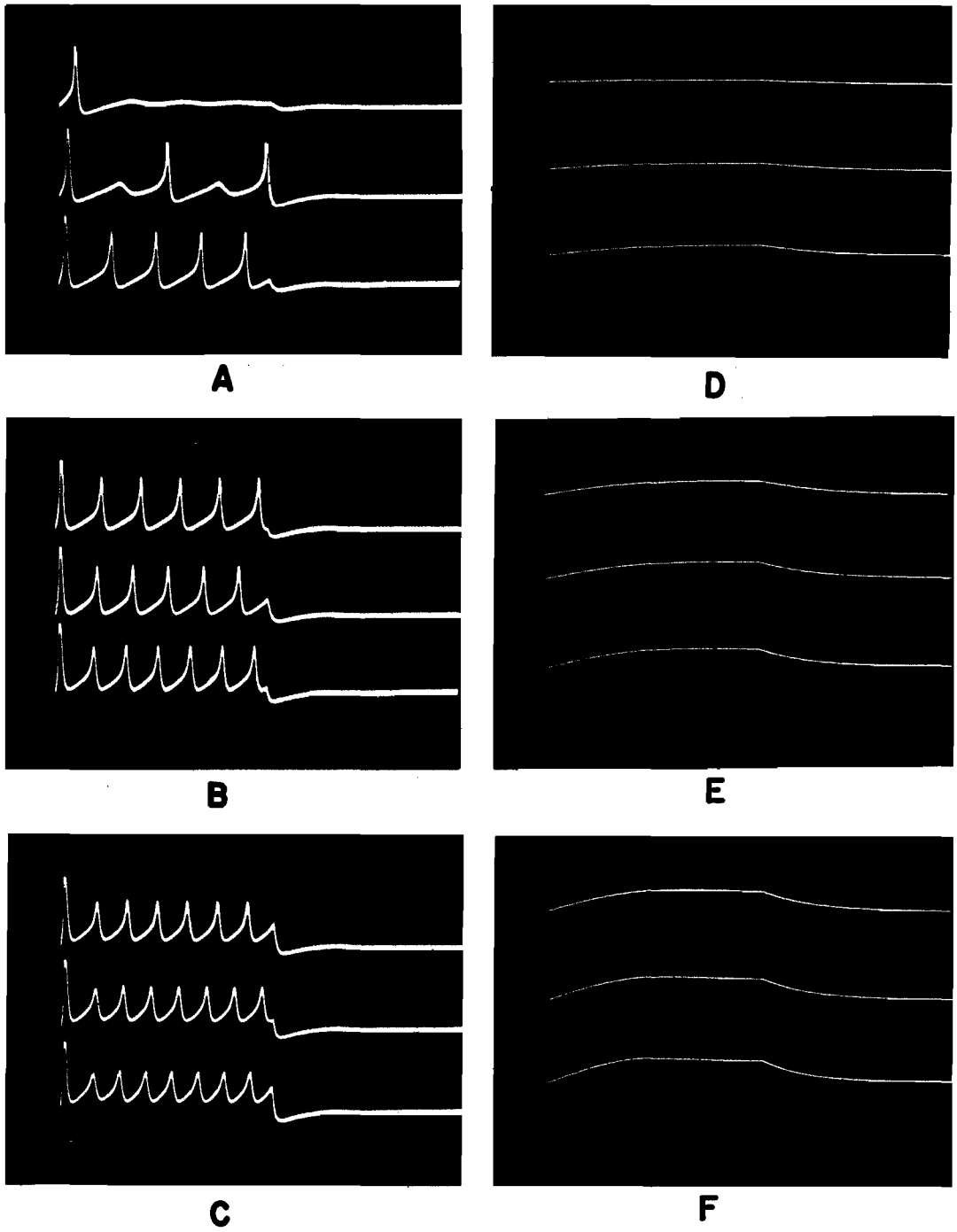

Figure 23. The Effect of Increased Membrane Capacitance in the Hodgkin-Huxley Model.

The three photographs on the left show (from top to bottom) the effects on the membraine potential of progressively larger 100-ms current pulses applied to a SOMA MODEL with the parameter values specified in Table 1. The photographs on the right show responses to the same current pulses after the membrane capacitance was increased by a factor of twenty.

Resetting of Pacemaker Potentials

Spontaneous oscillations of its simulated membrane potential generally can be induced in the isolated SOMA MODEL by a steady depolarizing current. If this current is small, the oscillations are nearly sinusoidal in appearance, if it is larger, the oscillations are more nearly sawtooth. If the simulated membrane capacitance is not too large, spontaneous spikes also may occur. These three types of spontaneous potentials are shown in figure 25. In this case, the simulated transmembrane capacitance was 0.5 microfarads, corresponding to 2 microfarads per sq cm in the squid-axon membrane.

In some cases, local oscillations might occur in regions of a neuron that are effectively isolated and exhibit minimal effects of spatial

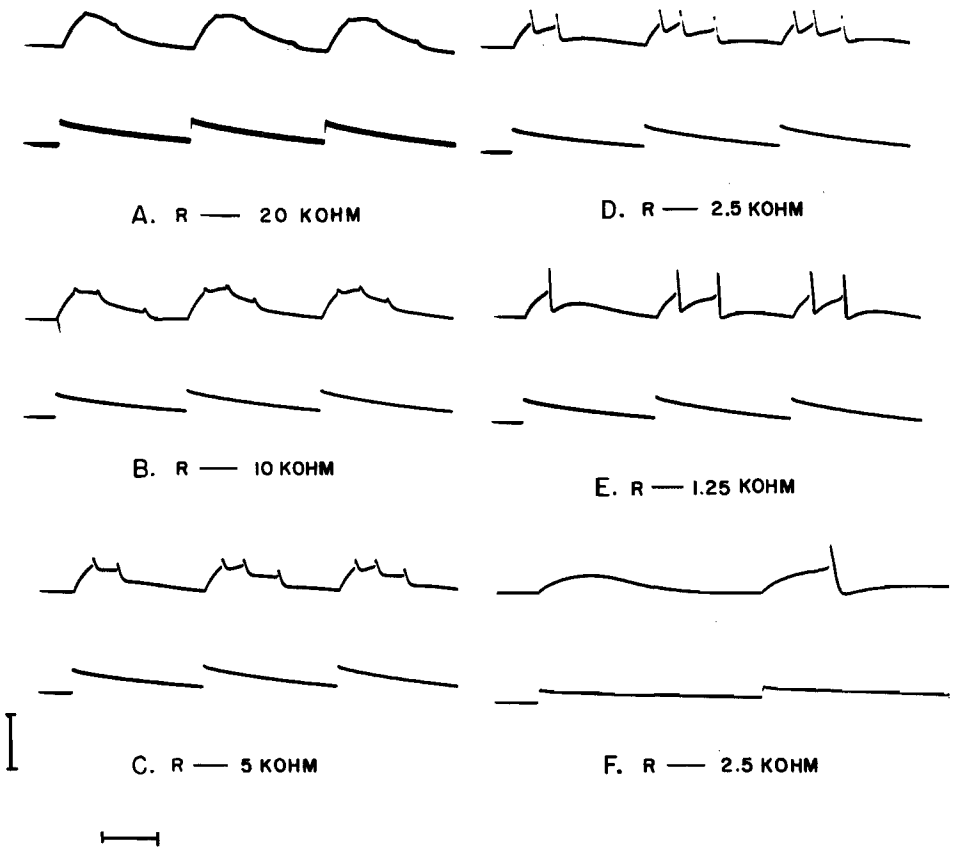

Figure 24. Invasion of the Soma by Spikes

The top trace in each pair shows the internal SOMA potential of a two-patch model receiving simulated excitatory synaptic inputs. The time course of the synaptic shunt conductance is shown in the lower trace. The initial conductance increments were 0.1 mmho. The simulated soma capacitance was 20 μFd per sq cm, and the simulated spike initiator capacitance was 1 μFd per sq cm. The vertical line represents 20mv; the horizontal line represents 50 ms.

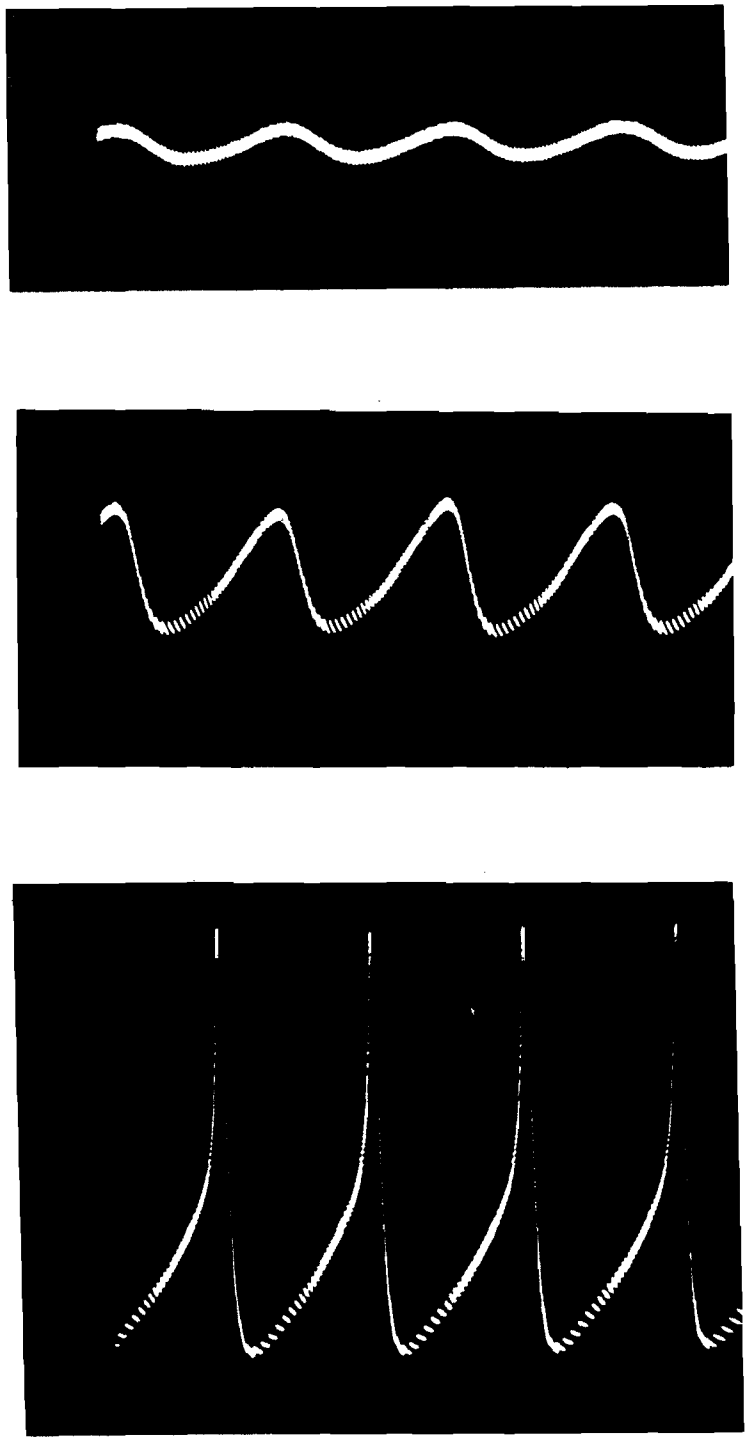

Figure 25. Spontaneous Oscillations in the SOMA MODEL.

The membrane capacitance was equivalent to 2 μFd per sq cm; all other parameters were adjusted to the values specified in Table 1. A steady depolarizing current was applied in order to elicit the oscillations. As this current was increased, the ocillations varied from a nearly sinusoidal from (top trace) to full spikes (bottom trace).

distribution; but in most cases, some interaction of spatially distributed sites probably occurs. One possible interaction is that which may occur between an oscillating site and a trigger region or, in Bullock's terminology between a pacemaker locus and a spike initiator locus (see Bullock 1957, 1958, 1959, 1962). The two-patch neural model is the simplest configuration that will provide this type of interaction.

The SOMA MODEL with a 5-microfarad membrane capacitance was extremely stable and quite resistant to oscillations of any sort. The photographs in figure 26 were taken, therefore, with C_M equal to 2 microfarads in the model. This corresponds to 8 microfarads in the squid axon (eight times the value measured by Hodgkin and Huxley). The SOMA MODEL was connected through a 20KΩ resistor to a SPIKE INITIATOR MODEL to form the two-patch configuration of figure 22. A steady depolarizing current applied to the SOMA MODEL produced the oscillations shown in the top trace. The coupling between soma and spike initiator was too weak to allow these oscillations to elicit spikes. In the case of the second trace, the coupling resistance was halved, allowing spikes to occur on the depolarizing phases of the oscillations. Minature reflections of these spikes can be seen on the oscillations at the soma. The occurrence of these spikes appears to have altered slightly the shape of the oscillations without much affecting their frequency. In the case of the third trace, the coupling resistance was halved again. The amplitude of the oscillations and their frequency were altered noticeably by the antidromic spikes. The fourth, fifth and sixth traces show the effects of further reduction of the coupling resistor. The oscillations that were nearly sinusoidal in the top trace are nearly saw-toothed in the bottom trace. Resetting of the soma potential by the antidromic spike has increased the frequency of oscillation from 15 Hz in the top trace to 44 Hz in the bottom trace.

MUTUAL INHIBITION

Mutual Inhibition in Point Models

The effects of mutual inhibition have been examined in several cases between pairs of models each of which represented a spatially nondistributed neuron or region of a neuron. These nondistributed, or point models did not include representations of axon propagation delay or the spread of subthreshold potentials from one region of a neuron to another. The SOMA MODELS and the SPIKE INITIATOR MODELS individually are point models, since they represent nondistributed patches of membrane.

Reiss (1962) found that a pair of mutually inhibiting point models could respond to a common driving source by producing periodic bursts of spikes. The models alternated, so that while one was generating spikes, the other was quiescent. Reiss included simulated fatigue in his models, and this limited the duration of any single burst, making alternation possible. The simulated synaptic time constants in Reiss' models were quite long, usually being 100 ms or more.

Harmon (1964) studied mutual inhibition in the same pair of models, but without simulated fatigue and with shorter synaptic time constants. He found stable spike patterns that depended on the intensity of the common driving source, but these patterns comprised alternate spikes or small groups of spikes rather than bursts. Harmon also noted hysteresis in the transitions between these patterns. In a similar study Wilson (1966) found stable alternate production of single spikes by mutually inhibiting point models. This alternation of single spikes occurred over a wide range of input intensity, and principal effect of increased intensity was increased frequency of the same pattern.

In all of these studies, the occurrence of a spike in one member of the mutually inhibiting pair almost immediately excluded the possi-

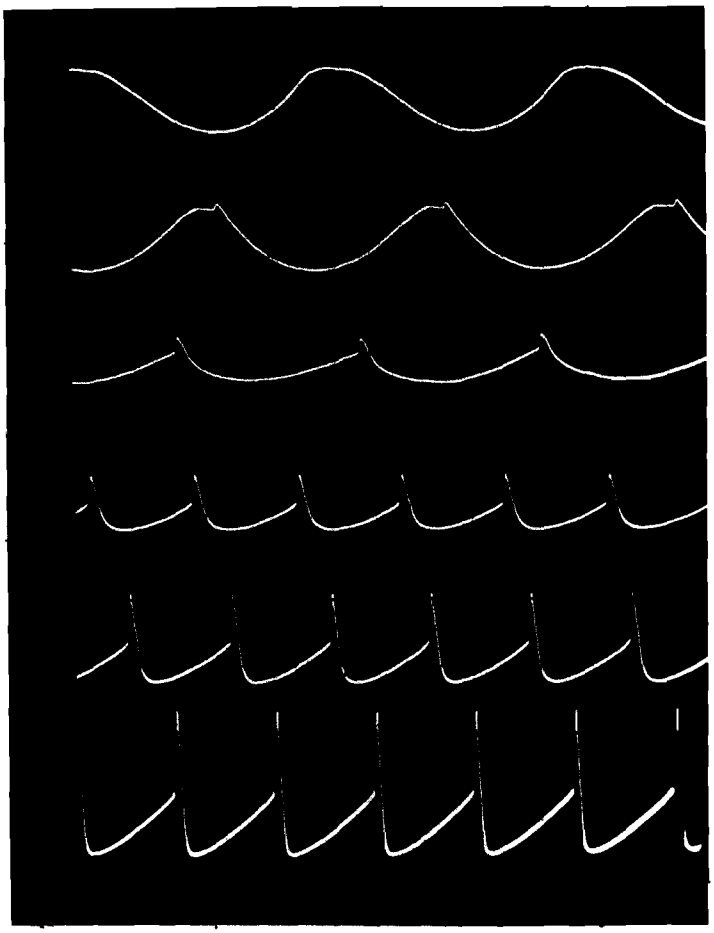

Figure 26. Antidromic Spikes Resetting Spontaneous Potentials in the Soma of a Two-Patch Model.

bility of a spike in the other member. The simultaneous occurrence of spikes in both members generally is possible only when both are driven by a common, pulsed source. In the two-patch models, stable patterns with synchronous spike production are quite common in mutually inhibiting pairs, even when both units are independently driven by nonpulsatile sources. This is perhaps the major distinction between point models and distributed or quasi-distributed models.

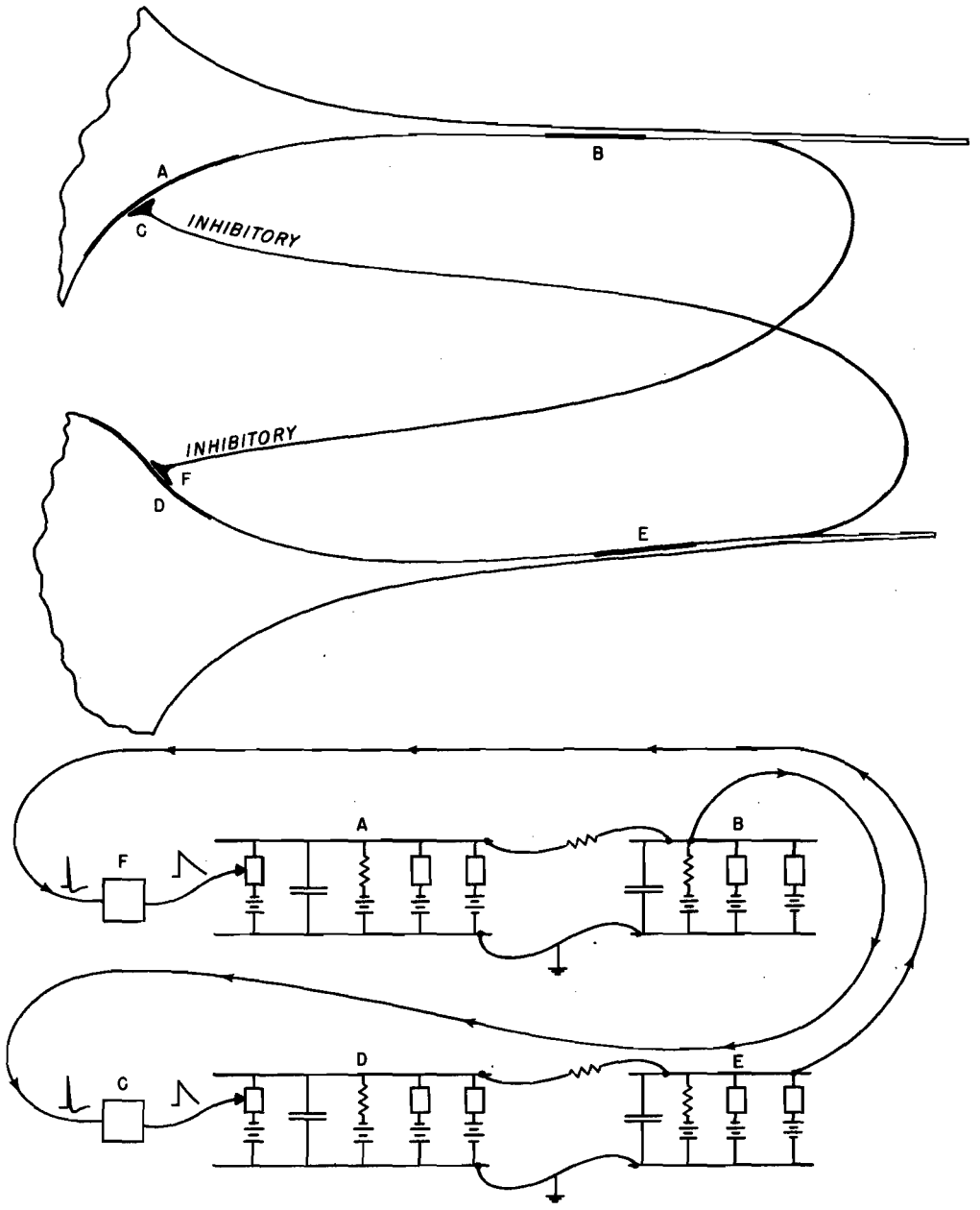

Figure 27. Model of a Mutually Inhibiting Pair of Neurons.

Mutual Inhibition in the Two-Patch Models

A pair of two-patch models were connected in the configuration shown in figure 27; the soma capacitances both were 2 microfarads. The spikes from each spike-initiator were converted to decaying exponentials that modulated the synaptic component of potassium conductance at the soma of the other two-patch model. By means of the modulated potassium conductance, each spike produced a simulated inhibitory post-synaptic potential (ipsp) at the soma of the receiving model. Propagation delay was not simulated in these experiments so the effect of the spike on the conductance was almost immediate.

Before the inhibitory connections were made, a steady depolarizing current was applied to the simulated soma of each two-patch model, producing subthreshold oscillations at the somata and periodic spikes at the spike initiators. When the connections were made, the patterns changed from period spikes to periodic groups of spikes, such as pairs or unevenly spaced triplets. Some of these patterns are shown in figure 28. The asymmetry between the top and bottom traces are due partly to

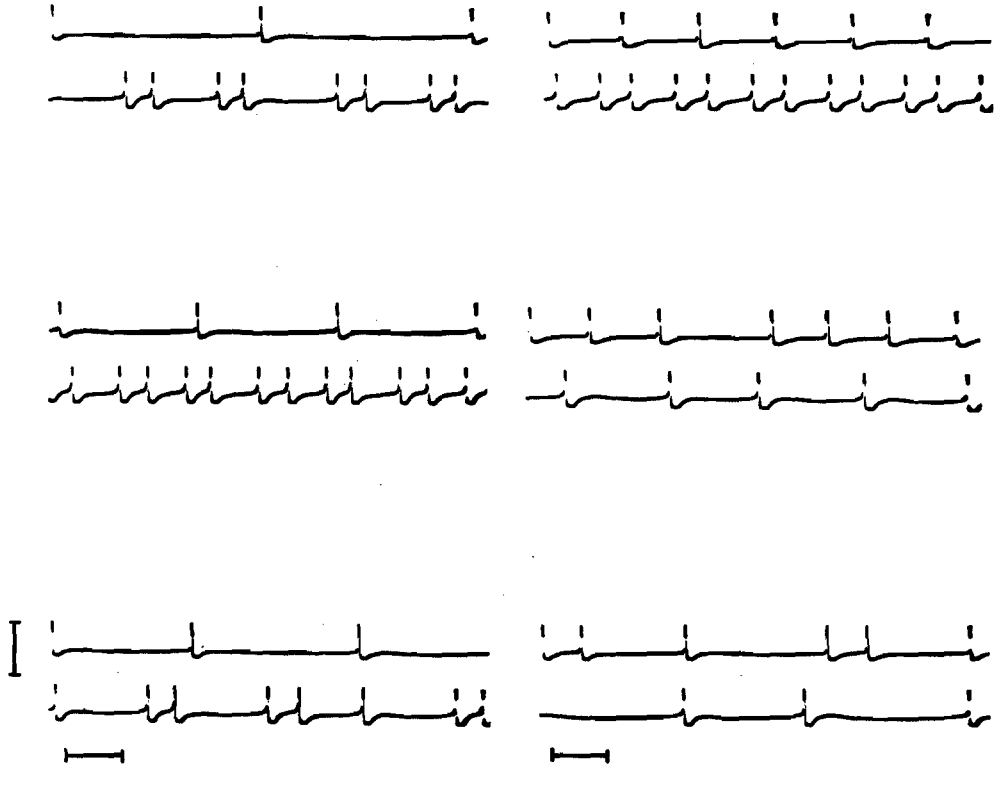

Figure 28. Spikes from a Pair of Mutually Inhibiting Neuron Models.

The vertical line represents 100 mv; the horizontal line represents 200 ms.

differences in synaptic time constants. The time constant of the exponential synaptic conductance was 60 ms in the model represented by the top trace of each pair; the time constant for the other model was 40 ms. This meant that the ipsp's were longer and thus more effective in the model represented by the top trace. In addition, the depolarizing currents were varied at the somata of the two-patch models, accounting for the pattern variation.

The patterns shown in figure 28 were extremely stable, and at least one period of each pattern is shown. The longest pattern shown is in the lower left-hand pair of traces. One unit produced three non-uniformly spaced spikes while the other unit produced two single spikes and two pairs of spikes. Most of the patterns in figure 28 exhibit non-synchronous generation of spikes by the two models, but the pattern on the lower left and that on the lower right both exhibit spike synchrony. Synchrony actually was very common with the mutually inhibiting two patch models. Figure 29 shows two more examples from the same test configuration. Synchrony in these cases was essentially complete; when spikes occurred in both two-patch models, they occurred in synchrony.

The integrative nature of the SOMA MODEL and the fact that simulated synaptic coupling was mediated by a conductance change rather than an abrupt change in membrane potential both tended to delay and inhibitory effects of the spikes. The occurrence of a spike in one model did not immediately preclude the occurrence of a spike in the other, so stable patterns with spike synchrony were possible.

MUTUAL EXCITATION

Burst Formation in a Mutually Exciting Pair of Two Patch Models

The soma capacitance of each member of a pair of two-patch models was set to 2 microfarads, representing 8 microfarads per sq cm in the

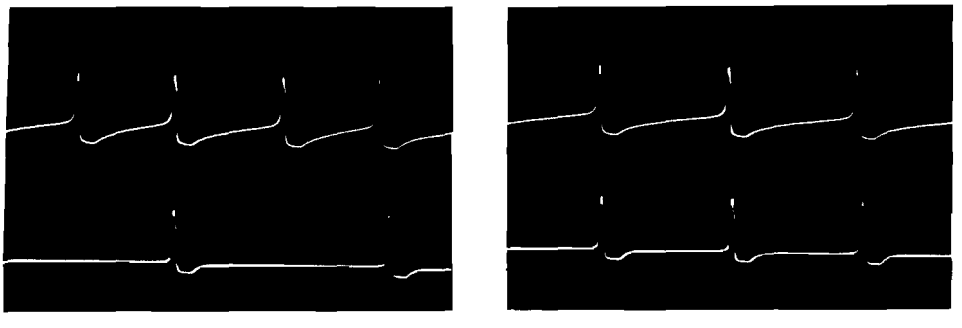

Figure 29. Synchronous Spikes from a Pair of Mutually Inhibiting Neuron Models.

squid giant axon (each soma representing 0.25 sq cm). The synaptic time constant in each model was 50 ms, but the modulated conductance was the nonspecific shunt rather than the potassium conductance, so the simulated synaptic potentials were excitatory rather than inhibitory. When the models were connected to each other in this manner, they represented the configuration of figure 30.

The oscilloscope traces in figure 31 show the simulated intracellular potential of the spike initiator of both models. The pair of traces in 31A were photographed before the synaptic connections were made. A steady depolarizing current was applied to the soma of one model, causing its spike initiator to produce periodic spikes at a

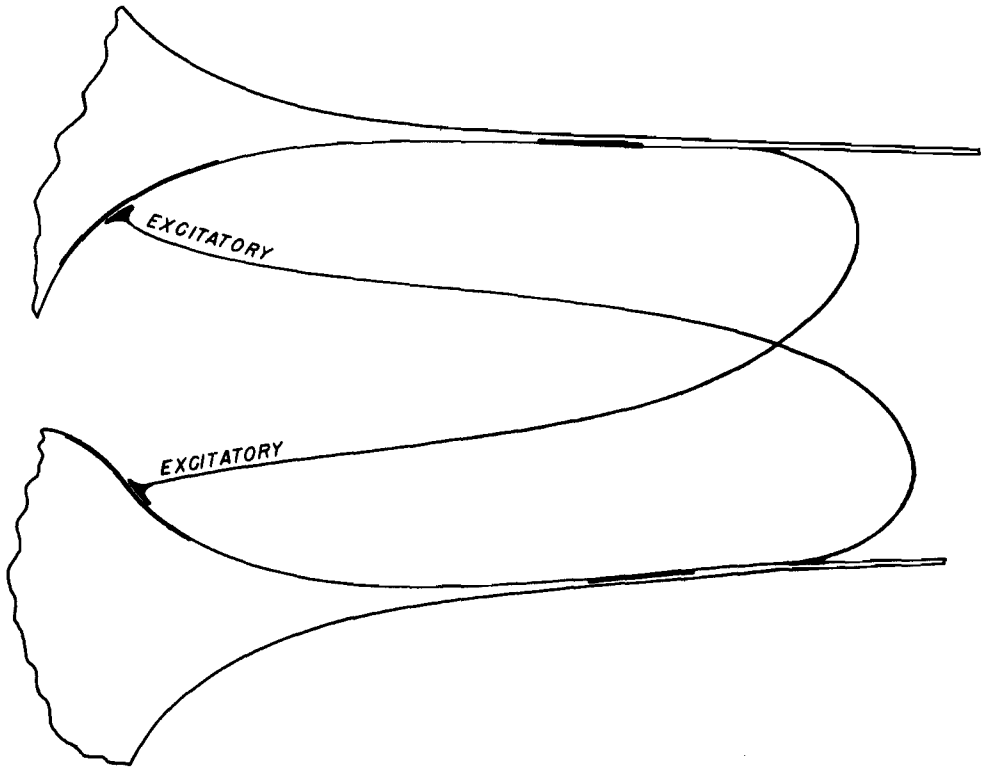

Figure 30. Model of a Pair of Mutually Exciting Neurons.

frequency of approximately 18 spikes per sec (top trace). The model producing the periodic spikes was coupled to the quiescent unit by means of the simulated excitatory synaptic connection. The amplitude of the synaptic conductance increment at the driven model (represented by the lower trace) was adjusted to a magnitude that was barely sufficient to allow the driven model to produce one spike for each spike from the driving unit (upper trace), as shown in 31B. The synaptic conductance increment of the driving model was adjusted to approximately the same magnitude as that in the driven model, and the driven model was coupled back to the driving model through a simulated excitatory synapse. The loop with mutual excitation was now complete.

The spike outputs of the two mutually exciting models are shown in 31C. The models produced spikes in periodic bursts. The maximum spike frequency during a burst was approximately 50 spikes per sec, which represented a considerable acceleration of the frequency of 18 spikes per sec that existed before the excitation loop was closed. The frequency of bursts was about 2 per sec, and the interburst interval (i.e., the period of quiesence between bursts) was approximately 400 ms, considerably longer than the interspike interval before the excitatory loop was closed.

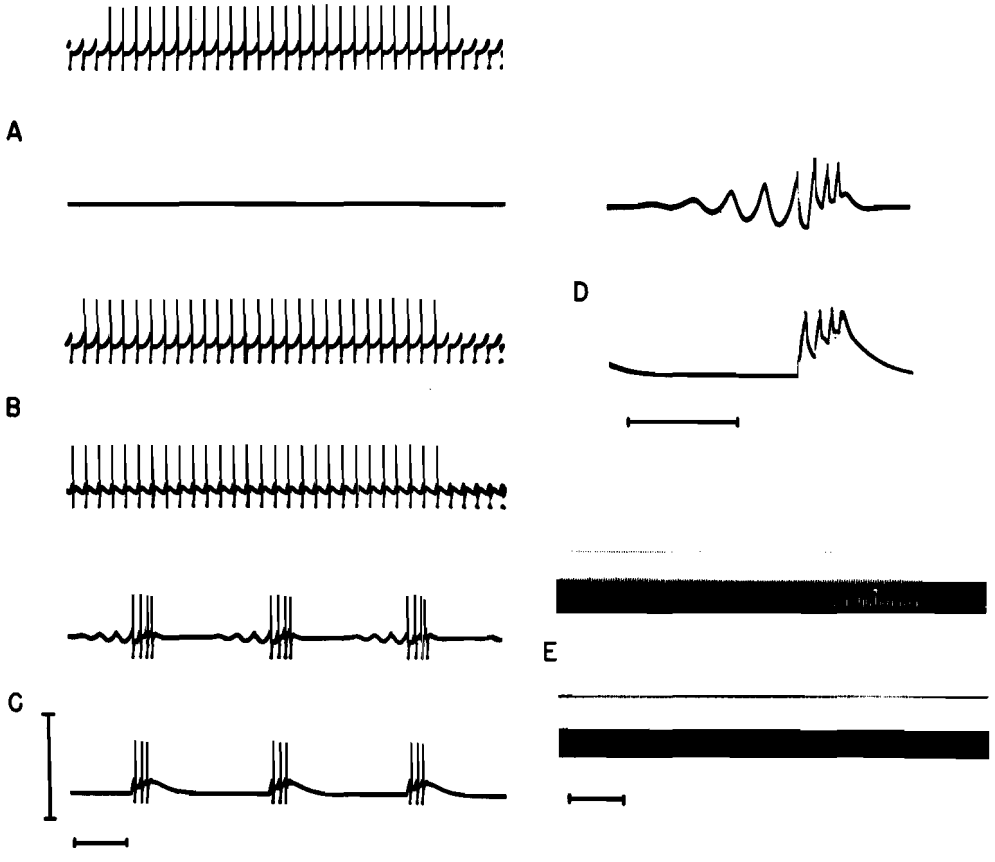

Figure 31. Spike Initiator Potentials from a Pair of Mutually Exciting Neuron Models.

The vertical line represents 100 mv; the horizontal line represents 20 ms.

The simulated intracellular potentials at the two SOMA MODELS during a burst are shown in 31D. The growth of subthreshold oscillations during the interburst interval in the driving unit can be seen in the top trace. The first spike at the spike initiator of the driving unit resets its soma potential, originating a burst and terminating the oscillation. The soma potentials in both models during the burst are combined epsp's and antidromic spikes.

The effect of increased synaptic efficiency in this system can be seen in 31E. The synaptic conductance increment per presynaptic spike was increased in each model. Rather than burst production, the mutually exciting pair now exhibited complete runaway, both models producing spikes at a rate of approximately 100 per sec.

With the mutually exciting pair of models adjusted to produce bursts of spikes, the depolarizing current at the soma of the driving model was varied. The results are shown in figure 32. The frequency of bursts increased and the number of spikes per burst decreased as the depolarizing current was increased. The pair of traces on the upper left show the spike initiator of the driving model (upper trace) producing five spikes per burst, while that of the driven model produced three. The burst rate was approximately 1.6 per sec. In the pair of traces on the lower left, the burst rate was approximately two per sec, and the two models together produced seven spikes per burst. In the trace on the upper right, the burst rate was approximately 2.4 per sec with five spikes per burst from both units. In the final pair of traces, the burst rate was approximately 4.5 per sec with three spikes per burst.

Mechanisms of Burst Formation

Two types of process were required to convert the periodic spike trains of figures 31A and B to the periodic burst of figures 31C and 32: an accelerating process and a quenching process. During the bursts, spike production was accelerated from 18 spikes per sec to nearly 50 spikes per sec. These bursts were terminated or quenched, however, and the spike initiators were quiescent for an interval during which several spikes would have occurred under normal conditions (i.e., if the models were producing periodic spike trains rather than bursts). The accelerating process in the mutually excitatory configuration is obvious. The mutually excitatory synaptic coupling provides positive feedback in the system. When the driven model is coupled back to the driving model, the addition of epsp's to the steady depolarizing current at the soma of the driving model accelerates its spike production. The accelerated spike production at the driving model increases the spike production at the driven model, which in turn further accelerates the driving model. If this process were not arrested, complete runaway such as that shown in figure 31E would occur. Complete runaway is prevented, however, by the quenching process.

It is obvious from the upper trace of figure 31D that the first spike in the driving model invades its soma and resets the oscillatory

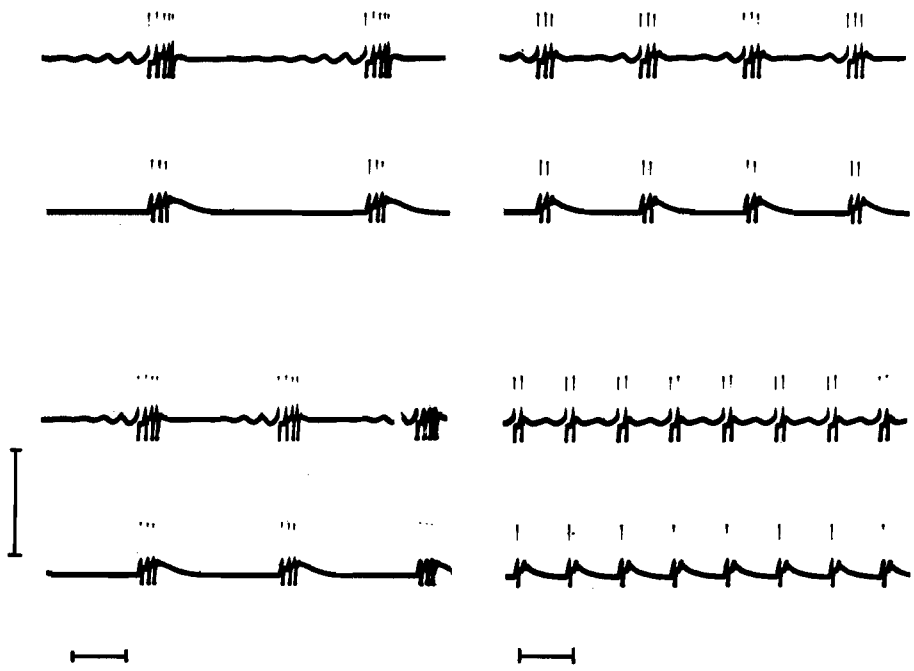

Figure 32. Bursts of Spikes from a Pair of Mutually Exciting Neurons.

The vertical line represents 100 mv; the horizontal line represents 200 ms.

potential there. While this resetting of the soma potential may be part of the quenching process, it cannot be all of it, since the spike generation continues to accelerate after the soma potential has been reset. As a test of the necessity of invasion of the soma by antidromic spikes for quenching, the soma potential was applied through an isolation amplifier to the spike initiator. Thus, while the soma potential was conducted to the spike initiator just as before, the spike initiator and its spikes had absolutely no effect on the soma potential. The models continued to produce bursts with very little difference from those produced in the original configuration. Invasion of the soma by spikes therefore was not an essential part of the quenching process. Although antidromic spikes were blocked, the soma potential nonetheless was reset, but by epsp's rather than spikes. Resetting of the soma potential by one means or another was probably an essential part of quenching.

Another essential part of the quenching apparently was refractoriness in the spike initiator models. Because of the rapid succession of spikes, the variables that produce refractoriness had accumulated sufficiently to prevent the last epsp from eliciting a spike. In 31D, the spike failed on the fourth epsp of the lower trace. Two variables in the Hodgkin-Huxley Model account for refractoriness, there are the potassium conductance variable n, and the sodium inactivation variable, h. The ability of the system to produce spikes declines as the magnitude of n increases and as the magnitude of h decreases. The increase of n and the decrease of h are cumulative with recurrent spikes or with sustained depolarizations.

The quenching mechanisms in this case were inherent in the Hodgkin-Huxley Model. The accelerating mechanisms, on the other hand, were in the excitatory interconnections.

EXCITATION AND INHIBITION

Another set of simple connections between two neurons is the combination of excitation and inhibition. In the configuration discussed here, spikes from the driving model excited the driven model, while spikes from the driven model inhibited the driving model. As in the previously discussed configurations, a steady depolarizing current was applied to the soma of the driving model, inducing oscillations of the soma potential and periodic spikes at the spike initiator (lower trace of each pair in figure 33). The spike from the driving unit elicited a short burst of spikes from the driven unit (upper trace in each pair). This burst in turn inhibited the driving unit. The depolarizing current at the soma of the driving model was gradually increased, and the results of this increased current are shown in figure 33A through 33F, respectively.

If one were to look only at the driving model, he would see an interesting sequence of patterns as he increased the depolarizing current. At low current levels he would see single, periodic spikes whose frequency increased with increasing current. As the current was increased further, he would see alternating spikes and spike pairs, then periodic spike pairs, then alternating spikes and spike pairs again, and finally, periodic spike triplets. The same patterns are reflected in the upper traces, but with short bursts replacing single spikes.

DISCUSSION

The spike patterns described in Section IV are rather complex and diverse, yet they are the results of very simple connections between two very simple neural models. Each experiment described in Section IV included systematic variation of only one parameter; yet the two-patch pair has many parameters, so one should expect much more diversity and perhaps much more complexity in the patterns actually available from these configurations.

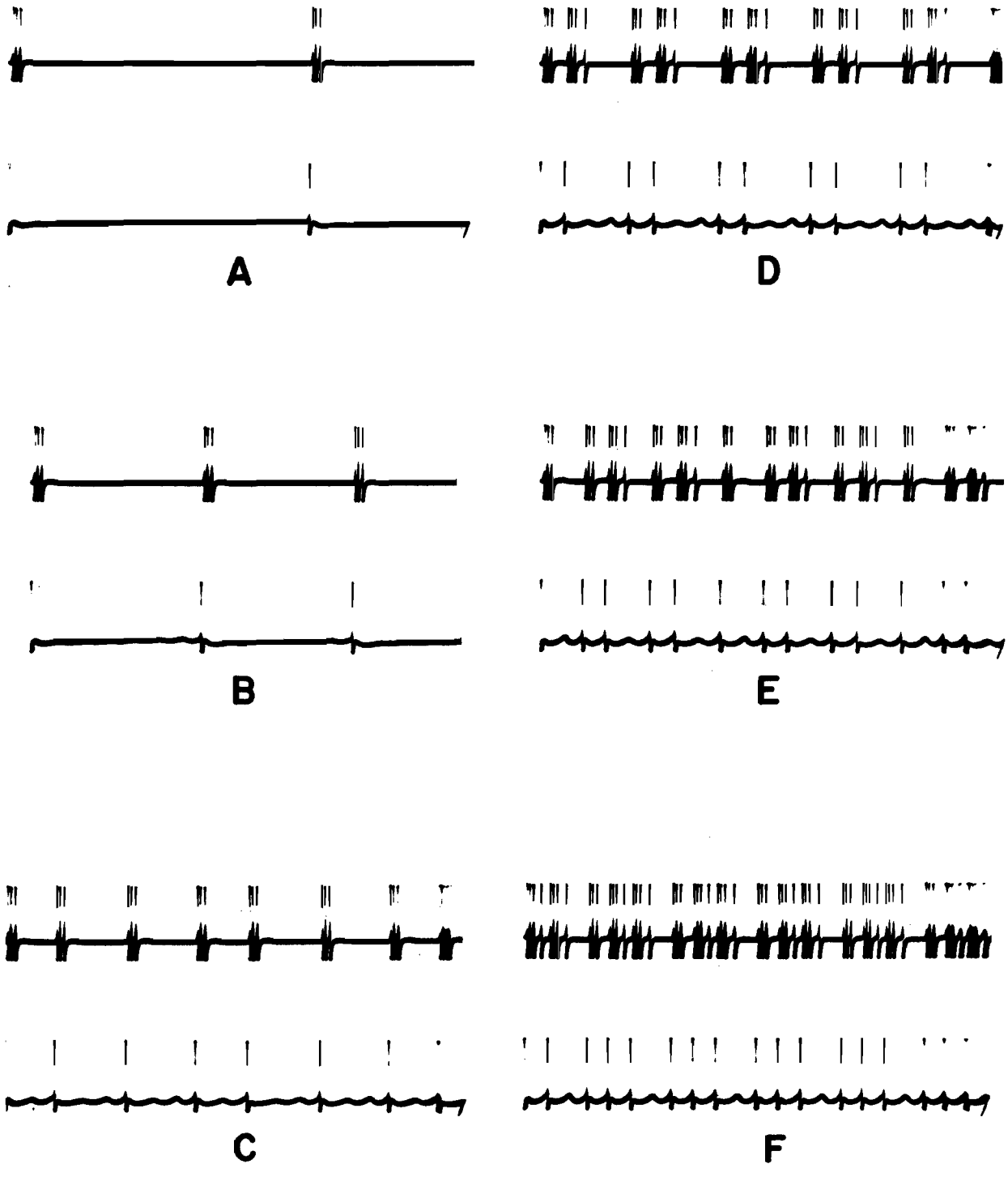

Figure 33. Spike Patterns from a Pair of Neuron Models.

SECTION V

THE MULTIPATCH AXON MODEL

INTRODUCTION

Most models dealing with its distributed properties treat the axon as a lossy cable, or core-conductor, with active electrical properties. These active properties account for the attenuationless propagation of the spike. According to the Hodgkin-Huxley Model, the active electrical properties, at least in the squid giant axon, are the result of the voltage dependent potassium and sodium conductances. The distributed form of the Hodgkin-Huxley Model has the same four shunt elements as the lumped form: membrane capacitance, leakage conductance, sodium conductance and potassium conductance. In the lumped form, the element values were specified as magnitudes per unit area. In the distributed model they must be specified as magnitudes per unit length. This transformation is a simple one, but requires knowledge of the ratio of axon-membrane area to axon length. In addition to the four shunt elements, the distributed representation of the Hodgkin-Huxley Model includes a series resistive element, representing the resistance of the axoplasm to currents flowing from one region of axon membrane to another.

Hodgkin and Huxley described the distributed form of their model by means of a partial differential equation:

$$(6)\quad \frac{\alpha}{2R}\,\frac{\partial^2 V_M}{\partial x^2} = C_M \frac{\partial V_M}{\partial t} + G_K(V_M - V_K) + G_{Na}(V_M - V_{Na}) + G_l\,(V_M - V_l)$$

where α is the axon radius, R is the axoplasm resistance per unit length, V_M is the membrane deplorization, and x is the distance along the axon: the other symbols are defined in Sections II and III. Assuming that the propagated spike travels with a constant velocity, θ, and without changing shape, Hodgkin and Huxley reduced this partial differential equation to the following ordinary differential equation:

$$(7)\quad \frac{\alpha}{2R\theta^2}\,\frac{d^2 V_M}{dt^2} = C_M \frac{dV_M}{dt} + G_K\,(V_M - V_K) + G_{Na}(V_M - V_{Na}) + G_l\,(V_M - V_l)$$

This equation, or its equivalents, has been examined by Cooley and Dodge (1966), Fitzhugh and Antosiewicz (1959), Huxley (1959), and Lieberstein (1967). The equation, when coupled with the Hodgkin-Huxley equations for G_K, and G_{Na}, has inherent instability. This instability is apparently a result of the formulation itself, and not a quality of the membrane system that it describes. Lieberstein (1967) has shown an alternative formulation without inherent instability.

Equation 6 and its equivalents are difficult to solve, but they apparently can be solved by modern numerical methods (see Cooley and Dodge, 1966, Lieberstein, 1967). An alternative to solving Equation 6 might be to simulate the distributed Hodgkin-Huxley system with a lumped approximation using the SOMA MODELS in the neural analog facility. If one ignores its active properties, the distributed Hodgkin-Huxley Model is very similar to a lossy electrical transmission line, with series and shunt resistance and shunt capacitance. It is often said that the response of a lumped series resistance-shunt capacitance filter with five or more stages is essentially identical to the response of a continuous series resistance - shunt capacitance transmission line (see Smith, 1958, p. 312). This is true for most types of input. For very high frequency sine waves, however, the attenuation of the lumped line increases at a rate of 6n db per octave and the maximum phase shift is 90n degrees (where n is the number of stages); the rate of increase of attenuation and the phase shift in the distributed line, on the other hand, increase without limit as the input frequency is increased. While this distinction is subtle, it may be sufficient to differentiate between lumped and distributed processes. A similar limitation is imposed upon the lumped approximation to the distributed Hodgkin-Huxley Model: the spike propagation delay represented by a single lump cannot be much longer than the duration of the spike's phase of depolarization. If the phase of depolarization is two milliseconds, the total obtainable propagation delay from an n-lump approximation cannot be much more than 2 (n-1) milliseconds. As long as the series resistors in this n-lump line are sufficiently small to provide a total delay of considerably less than 2 (n-1) milliseconds, the line should be a reasonably good representation of the distributed Hodgkin-Huxley Model.

This Section describes several experiments in which the SOMA MODELS were adjusted to simulate the Hodgkin-Huxley Model (see Table 1) and then connected as the shunt elements of the lumped approximation of a squid axon, shown in figure 34.

CONDUCTION FROM A POINT STIMULUS

A six-lump axon model was driven by repetitive current pulses of four milliseconds duration. Each of the shunt elements in the model represented 0.25 sq cm of squid axon membrane at 6°C; these were separated by 4000 ohm resistors. The test configuration is illustrated in figure 35. Since the current pulses were applied only to the first of the six shunt elements, the configuration is equivalent to an axon driven from a point adjacent to a long, insulated region (such as the regions

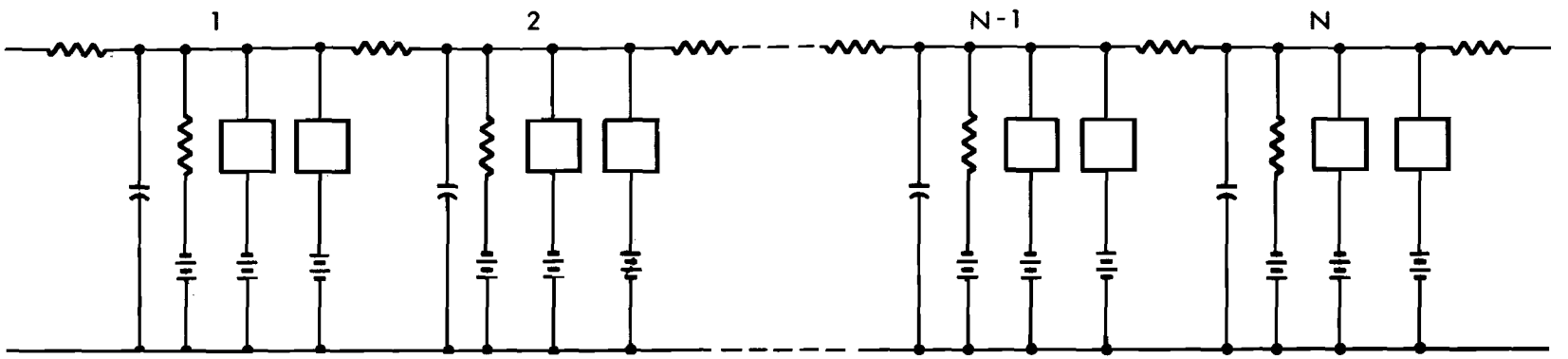

Figure 34. Lumped Representation of an Axon.

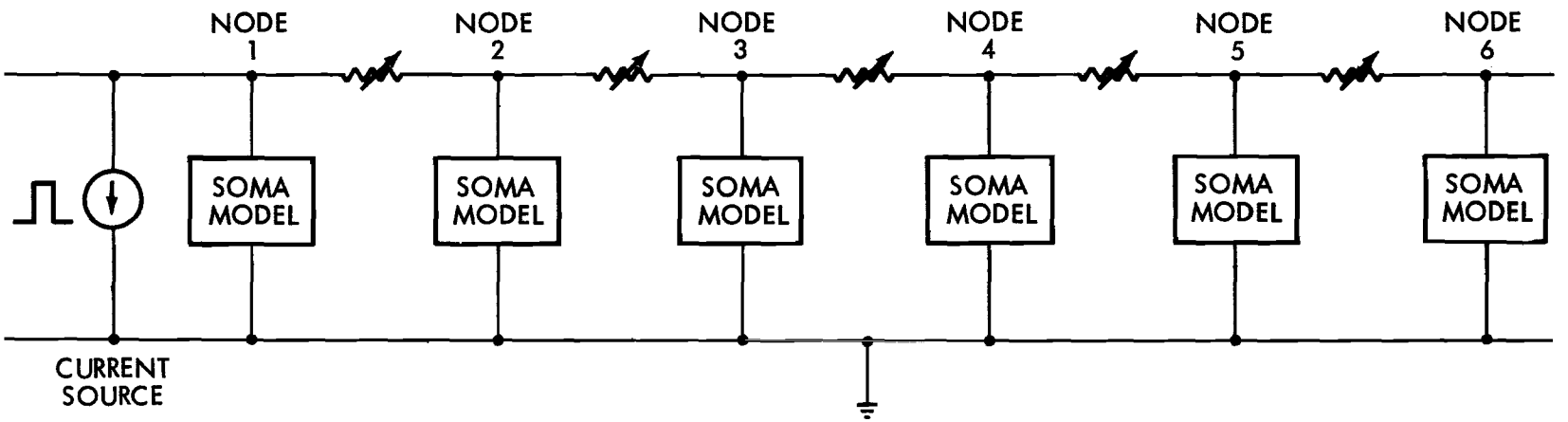

Figure 35. Test Configuration for the Six-Lump Axon Model.

adjacent to the patch of voltage-clamped membrane in the Hodgkin-Huxley experiments).

Decremental Conduction

The oscilloscope traces in the two photographs of figure 36 show the responses of the model axon to subthreshold stimuli. The conduction in these cases is decremental (i. e., the waveform is attenuated as it progresses along the model axon). The traces from top to bottom show the simulated intracellular potentials taken at nodes 1 through 6 repsectively (see figure 35). The top trace therefore shows the potential at the point of stimulus application, and the remaining traces going from top to bottom represent nodes progressively more remote from the point of stimulation. If the conduction time is taken to be the interval between the time of maximum depolarization at node 1 and the time of maximum depolarization at node 6, one can see that it is slightly more than four milliseconds in figure 36.

The electrically excitable conductances (i. e., the potassium and sodium conductances) were removed from each of the six shunt elements, leaving a completely passive system. Figure 37 shows the response of this system to a stimulus of the same intensity and duration as that applied in the case of figure 36B. The axon model without electrically excitable conductances exhibited considerably more attenuation than its counterpart with excitable conductances; so the responses in figure 36A and 36B are due largely to the regenerative action of the excitable conductances. In addition, the response at the sixth node of the purely passive system is more prolonged than that at the same node of the excitable system. This is especially apparent in figure 37B, where the intensity of the input pulse was increased and only the responses at nodes 1 and 6 are shown. The conduction time is also apparent in this figure, and can be seen to be nearly five milliseconds, which is not significantly different from the conduction time in the excitable system.

Subthreshold potentials in the axon model, with its excitable conductances, thus exhibit nearly the same conduction time as potentials in the purely passive model. The potentials in the excitable axon model exhibit less attenuation and less tendency to prolongation or spreading as they are conducted. The reduced attenuation is almost certainly the result of the regenerative action of the simulated sodium conductance; the reduced spreading is probably the result of sharpening of the leading edge by the sodium conductance and sharpening of the trailing edge by the increasing potassium conductance and decreasing sodium conductance.

Decrementless Conduction

The oscilloscope traces in the photographs of figure 38 show the responses of the model axon to suprathreshold stimuli. In the case of

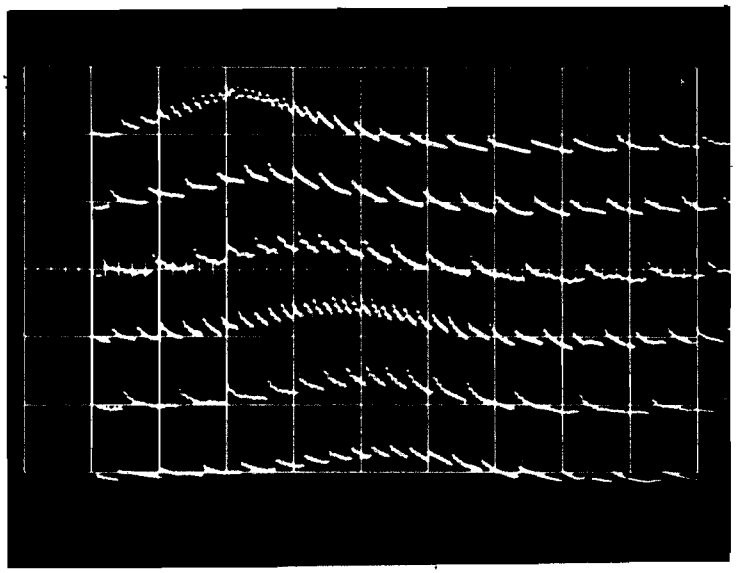

A

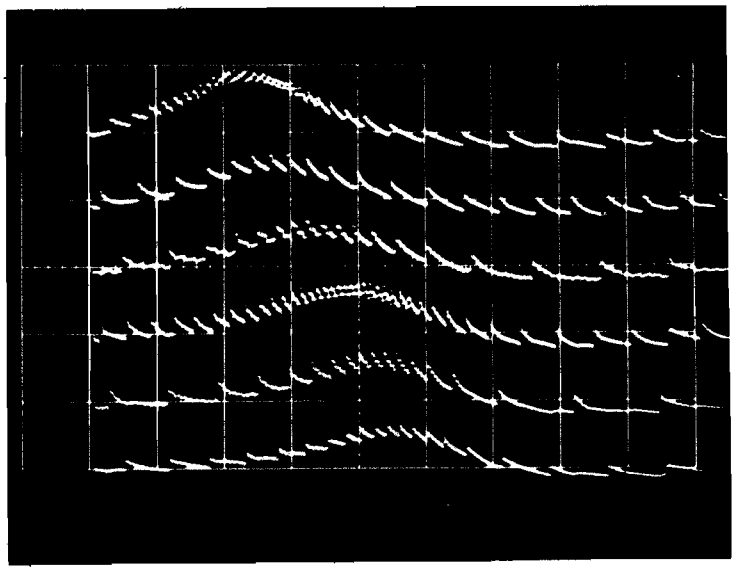

B

Figure 36. Conduction of Subthreshold Potentials in the Six-Lump Axon Model.

Vertically, the major divisions represent 20 mv, horizontally they represent 2 ms. From top to bottom the traces show the potentials at nodes 1 through 6 respectively.

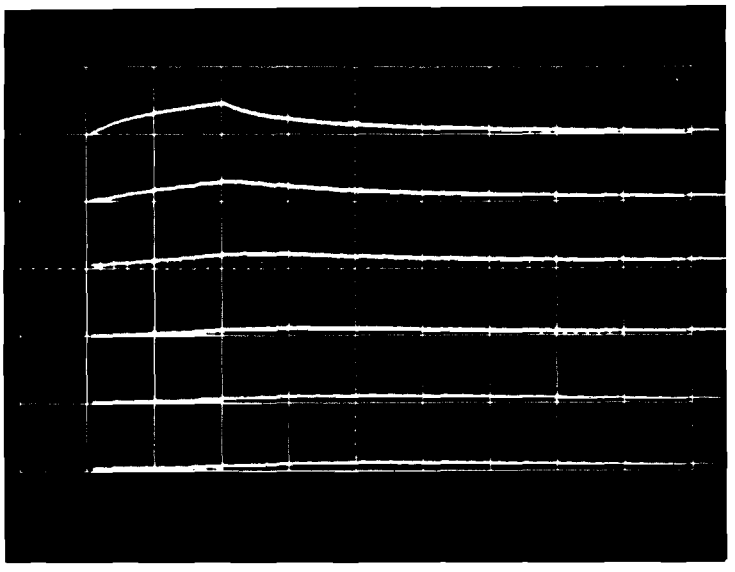

A

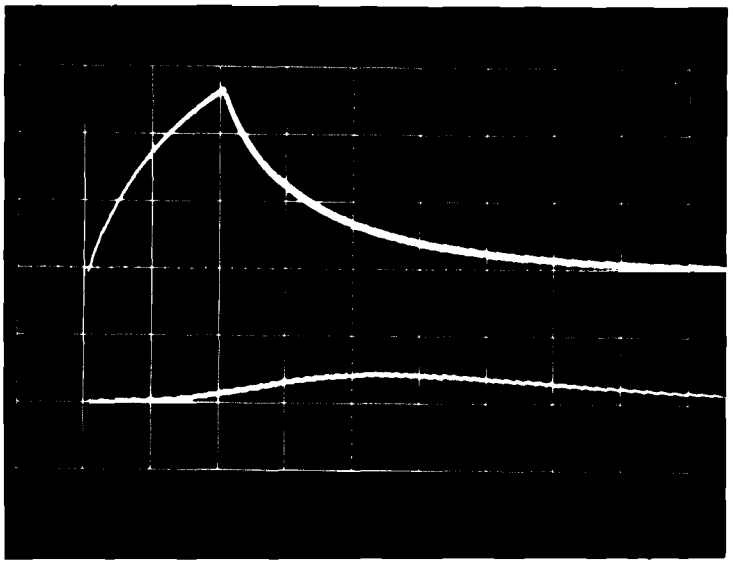

B

Figure 37. Conduction of a Pulse in the Six-Lump Axon Model without Electrically Excitable Potassium and Sodium Conductances.

The vertical scale represents 10 mv per major division; the horizontal is 2 ms per major division. The bottom photographs shows the potentials at nodes 1 and 6 only.

figure 38A, the stimulus was barely sufficient to initiate a spike. The full spike did not develop until the potential reached node 5, however, and nodes 1 through 4 responded in a graded, but increasingly regenerative manner. The spikelike potentials at the first three nodes occur after the spike at node 4 and probably are merely reflections of its decremental, antidromic conduction. The spike appears to have reached a constant form and amplitude at node 5 (i.e., the potential at node 6 is almost identical to that at node 5).

Figures 38B through 38F show the responses of the axon model to increasingly stronger stimuli. In 38B the spike developed at node 4 and conducted antidromically with decrement to node 1 and orthodromically without decrement to node 6. In 38C the spike developed at node 2 and conducted to node 1 antidromically. In 38D through 38F, the spike at node 1 appears to precede that at node 2, so conduction was completely orthodromic.

The spike conduction time from node 1 to node 6 in figure 38F, is slightly more than two milliseconds, or approximately half the time of decremental conduction between the same two nodes (see figure 36). In figures 38A through 38C the conduction time is obscurred by the antidromic spike. In fact the spikes at node 6 in figures 38A and B appear to precede the antidromic spike reflection at node 1, leading to the possible misinterpretation of the data as indicative of negative conduction times. In figure 38C the spike appears almost simultaneously at nodes 1, 2 and 3, leading to the possible interpretation of the data as indicative of an abnormally short conduction time. If one were to observe the potentials only at the point of stimulus (node 1) and some point remote from it (e.g., node 6), he might well overlook the antidromic spike and thus misinterpret the data.

The photographs of figure 38 make one fact clear: the shape and velocity of the propagated spike are not uniform over the axon model; and the nonuniformities lead to interesting and possibly important consequences. The assumptions of uniform velocity and shape in the Hodgkin-Huxley formulation may be quite adequate for steady-state propagation, but the results shown here indicate that these asumptions are probably completely inadequate for portions of the axon near the point of origin of the spike.

The Membrane Spike and the Propagated Spike

Spikes that occur across an isolated patch of neural membrane with spatially uniform potentials (i.e., spikes that do not propagate, but occur over the entire membrane at one time) are often called membrane spikes. Figures 39A through 39C show simulated membrane spikes across the shunt element from node 1 of the axon model. This element was removed from the axon model to prevent propagation and electrical interaction with the succeeding elements. Figures 39D through 39F show spikes across the same element when it was in place at node 1 of the axon model. These spikes were propagated. The

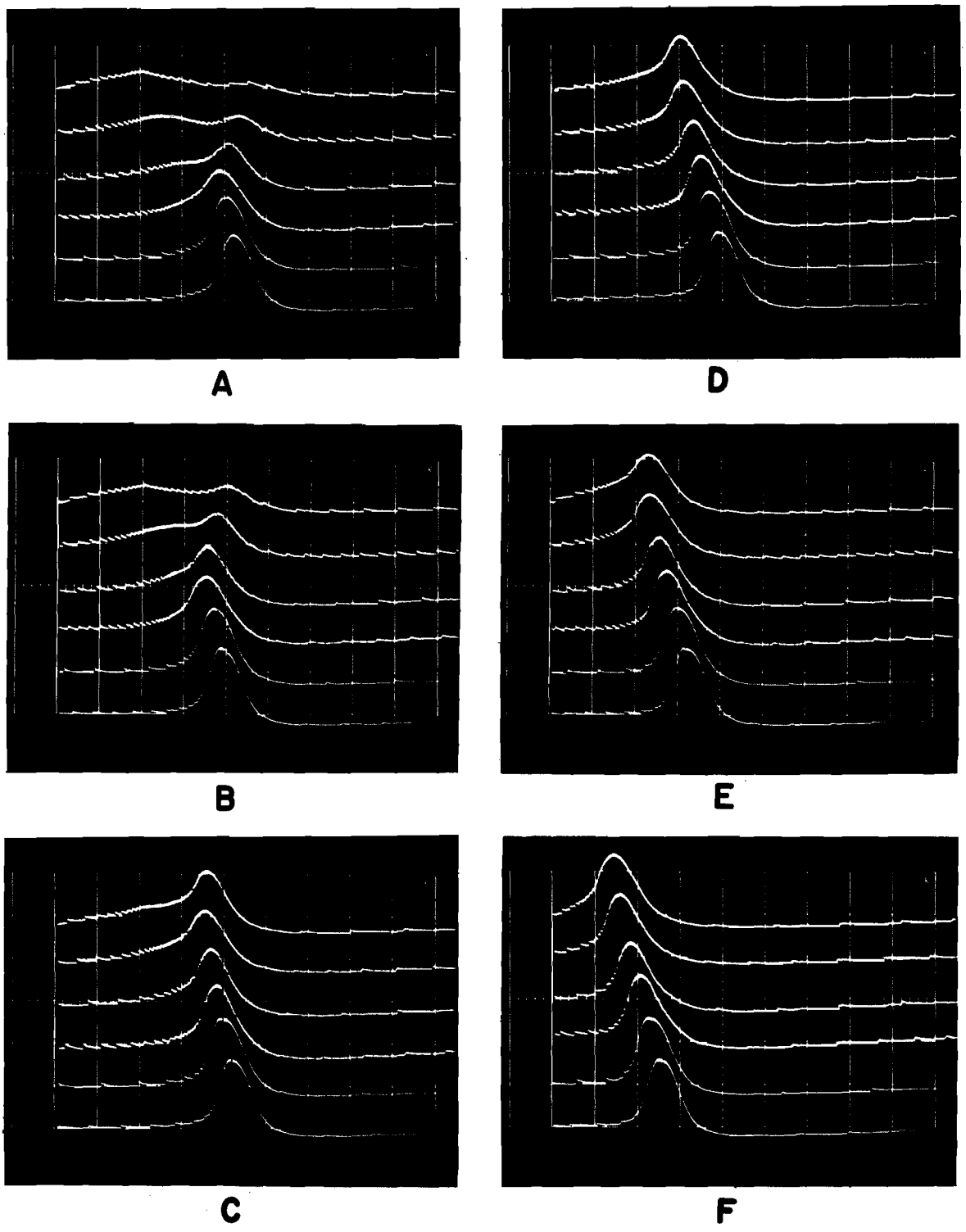

Figure 38. Spikes Propagating in the Six-Lump Axon Model.

Vertical divisions represent 50 mv; horizontal divisions represent 2 ms. From top to bottom the traces show potentials at nodes 1 through 6 respectively.

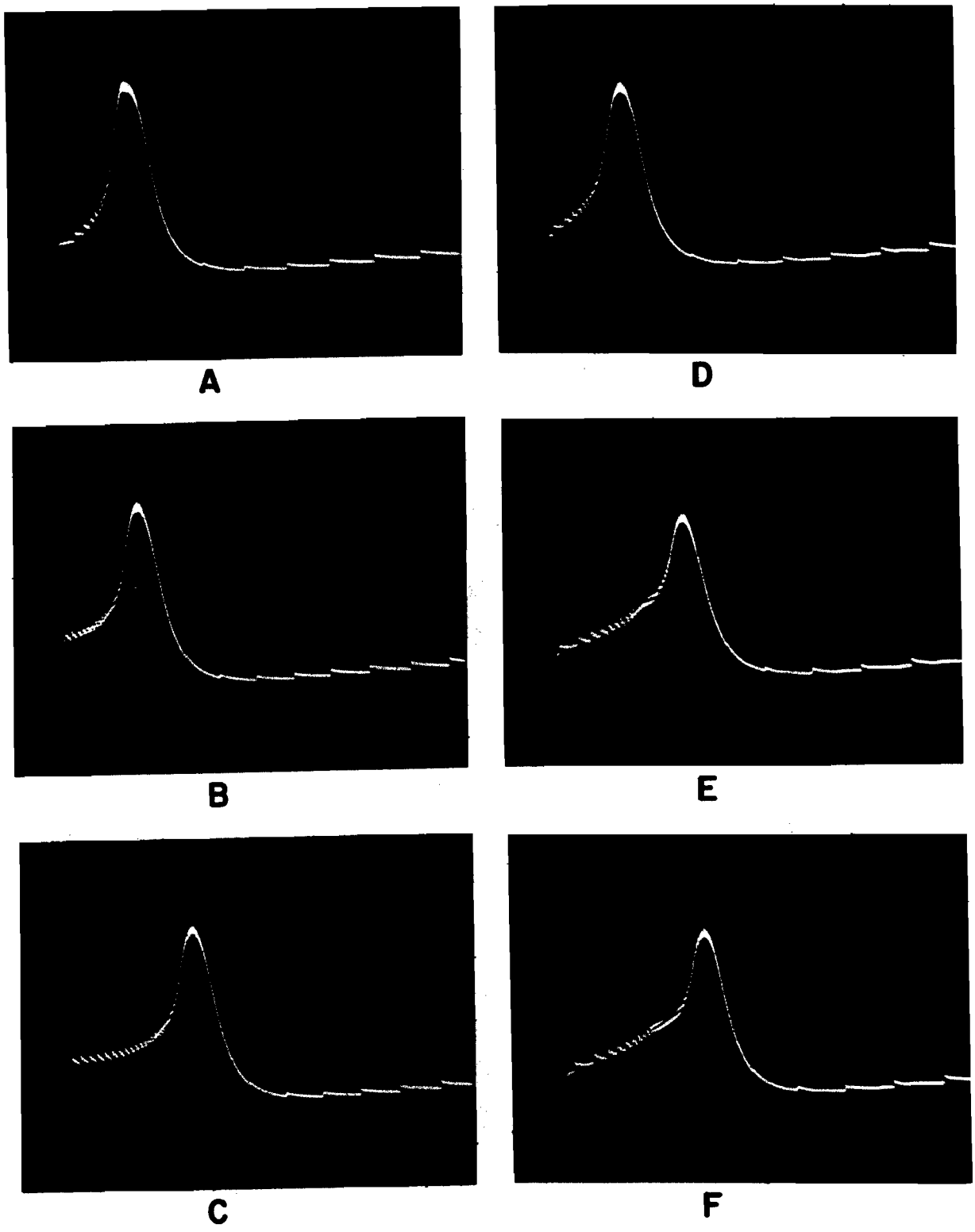

Figure 39. Membrane Spikes Compared with Propagating Spikes.

apparent differences between the propagated spikes and the membrane spikes occur on the rising, or depolarizing phase. The membrane spikes all rise sharply from approximately the same potential, which could be defined as a threshold. The propagated spikes begin the steep portion of their rising phase from different levels and exhibit no clear-cut threshold.

In addition to the differences in shape between the propagated spike and the membrane spike, there was also a marked difference in threshold. The minimum current intensity required to induce a propagated spike was approximately 2.3 times the minimum intensity required to induce a membrane spike. This difference is indicative of the importance of the electrical loading of a region of an axon by neighboring regions.

CONDUCTION FROM A PACEMAKER SITE

When a sufficiently large, steady, depolarizing current was allowed to flow across any of the six shunt elements, the potential across that element exhibited oscillations. When the depolarizing current was small, these oscillations were approximately sinusoidal; when the current was slightly larger, the oscillations were more nearly sawtooth in appearance; when the current was even stronger, spikes occurred.

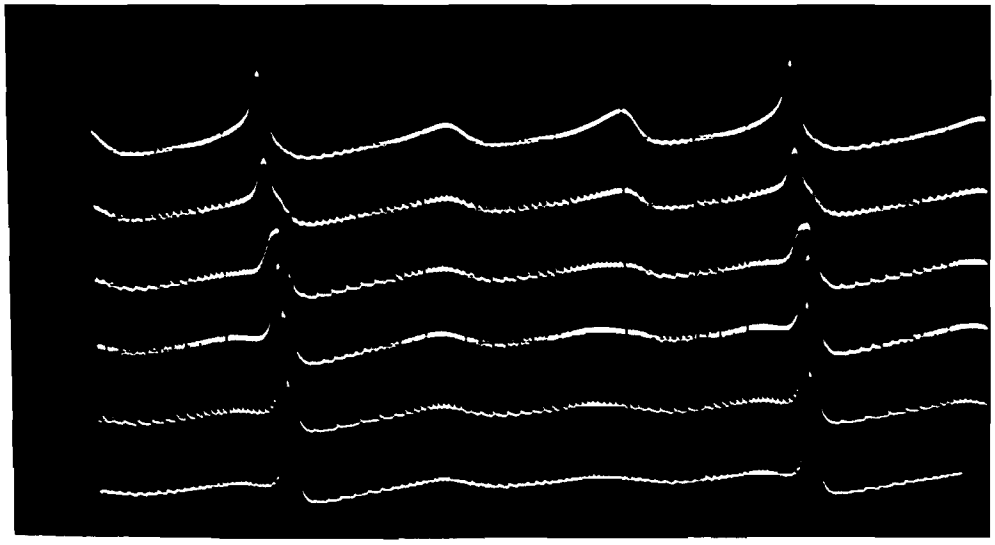

Figure 40. Propagated Spikes and Subthreshold Potentials.

Phase-Lead in Conducted Subthreshold Oscillations

The photograph of figure 40 shows the potentials along the axon model when a steady depolarizing current was applied across node 1 (see figure 35). The resulting oscillations of the potential at node 1 (top trace in figure 40) are conducted to the other five nodes; but the mode of this conduction seems to be quite different from that of decremental conduction from a point stimulus. The subthreshold oscillations (but not the spikes) in figure 40 appear to be conducted with attenuation from node 1 to node 6, but the depolarizing phase at node 6 actually appears to precede that at node 1. The conduction time for those oscillations thus appears to be negative. The spikes, on the other hand, appear to be conducted in a normal manner, without attenuation but with a distinct delay from node 1 to node 6. The conduction of the subthreshold oscillations is shown more clearly in figure 41. In 41A the depolarizing current was applied to node 1 and the resulting oscillations were conducted to node 6; but the peak of the depolarizing phase at node 6 occurs approximately one millisecond before that at node 1. In figure 41B, the configuration was reversed; the depolarizing current was applied to node 6 and the resulting oscillations were conducted to node 1. Once again the peak of the depolarizing phase occurred earlier at the receiving end (node 1) than at the sending end (node 6); so this result did not depend on the direction of conduction. Complete shuffling of the shunt elements did not alter the results, so they did not depend on idiosyncrasies of individual shunt elements.

In figure 42, the subthreshold oscillations occur without the occasional spikes that are present in figures 40 and 41. In 42A the oscillations originate at node 1 and are conducted to node 6. It is difficult to assess the phase relationships in this figure, but the peak of depolarization at node 6 is certainly not delayed with respect to that at node 1. In figure 42B the phase relations are more clear. The oscillations originate at node 6, but the peak of the depolarizing phase at node 4 definitely occurs slightly before that at node 6; while the peak of the depolarizing phase at node 1 occurs almost simultaneously with that at node 6. From its origin at node 6 to its occurrence at node 4, the subthreshold oscillation appears to gain in phase (ie., occur progressively earlier); and from node 4 to node 1, the oscillation seems to lose in phase (occur progressively later).

Discussion of Phase-Lead

All of the photographs in figures 40, 41 and 42 show progressive attenuation of the subthreshold oscillations as they were conducted along the axon model. In several cases, however, a definite increasing phase lead also accompanied conduction (i.e., the oscillations at driven nodes appear to have anticipated those at the driving node). Phase lead is not what one would expect from normal decremental conduction in axons. The decremental conduction from a point stimulus, for example, exhibited progressive phase lag; the peak of depolarizing phase at any node always occurred after the peak at the preceding nodes of the axon model.

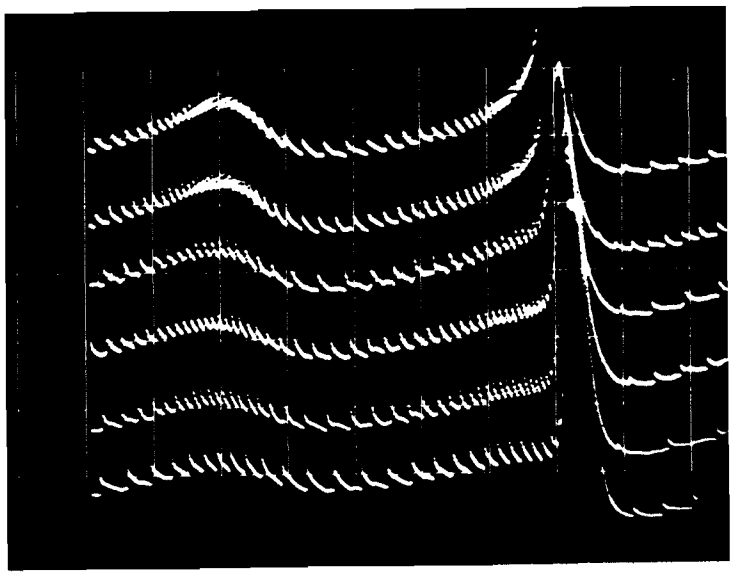

A

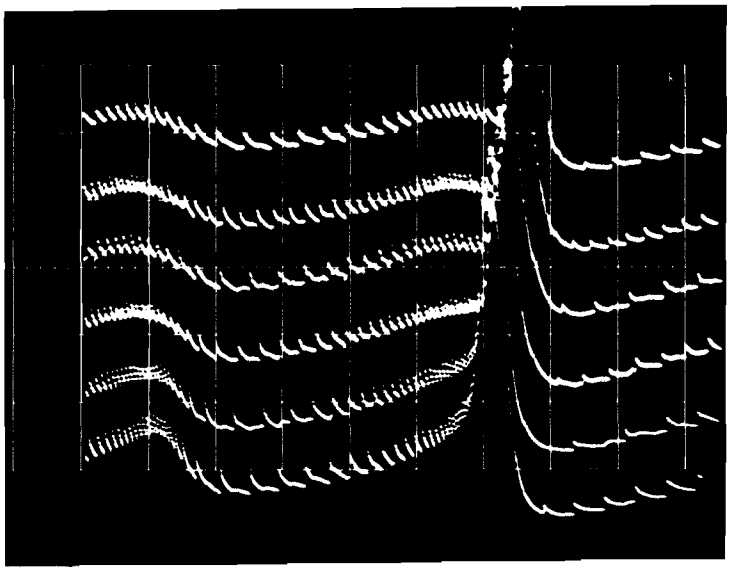

B

Figure 41. Detail of Conducted Subthreshold Potentials.

The origin of the potential was node 1 in the upper photograph, node 6 in the lower photograph. The major vertical divisions represent 20 mv; the major horizontal divisions represent 5 ms.

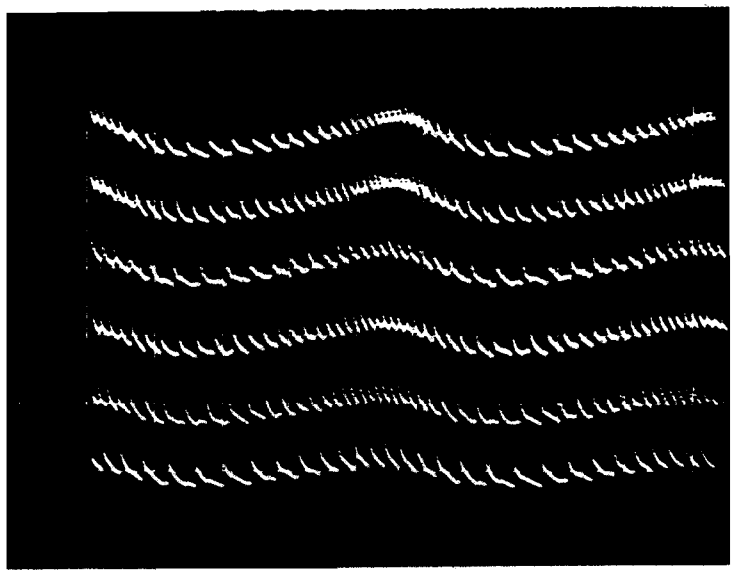

A

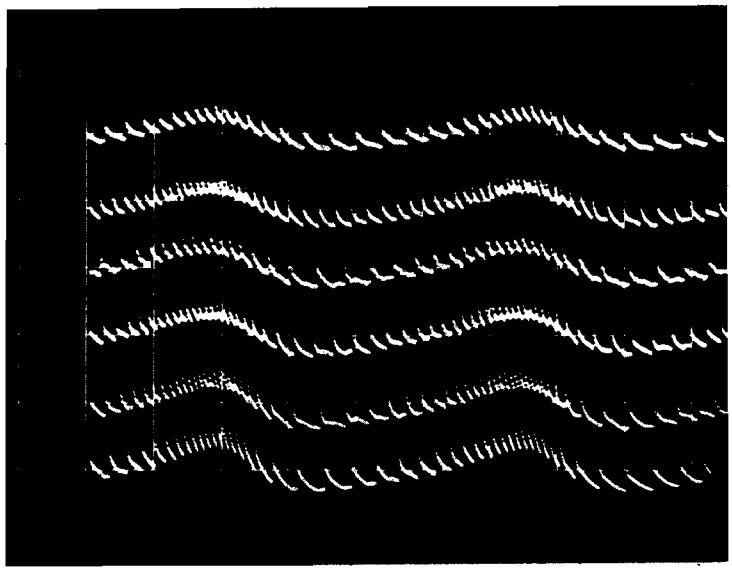

B

Figure 42. Conducted Subthreshold Potentials in the Absence of Spikes.

The potentials originated at node 1 in the top photograph, node 6 in the bottom photograph.

The shunt elements in the axon model are all essentially identical, and they all tend to oscillate in the presence of a steady depolarizing current. In terms of the Hodgkin-Huxley Model, the oscillations are due to the dynamic opposition of potassium ion and sodium ion currents across the membrane. A small depolarization produces an almost immediate increase in the sodium conductance and a delayed increase in the potassium conductance. The increased sodium conductance leads to further depolarization of the membrane, leading to a further increase in the sodium conductance, etc.; and the process becomes regenerative. When the initial depolarization is suprathreshold, the regenerative process produces a spike. On the other hand, when the initial depolarization is subthreshold, the acceleration of the regenerative process is sufficiently slow to allow the delayed potassium current and the sodium inactivation to catch up and reverse the process before a full spike develops.

If the initial subthreshold depolarization is produced by a steady d-c current, the regenerative process can lead to subthreshold oscillations of the membrane potential (see Lewis, 1965). The period of these oscillations depends on their amplitude. The magnitude of the potassium conductance and the degree of sodium inactivation both increase with increasing depolarization. These factors will both be increasingly larger during the polarizing phase (i.e., the phase of negative slope) of an oscillation as the amplitude of the oscillation becomes larger. The polarizing phase of the oscillation becomes increasingly more rapid as the potassium conductance is increased; and large amplitude oscillations tend to exhibit a sawtooth form, while small amplitude oscillations are more nearly sinusoidal. While the increased potassium conductance thus tends to shorten the duration of the polarizing phase, its residue after the polarizing phase, along with the increased residual sodium inactivation, tends to lengthen the subsequent phase of depolarization.

Whether the phase of depolarization is prolonged more than the polarizing phase is reduced is determined by relative magnitudes of several parameters in the Hodgkin-Huxley formulation. Important among these parameters is the rate of recovery from sodium inactivation. In the simulations employed in the six-lump axon model, the rate of recovery from sodium inactivation was constant and equal to the value determined by Hodgkin and Huxley for recovery after a 44-mv step depolarization (Hodgkin and Huxley, 1952). Hodgkin and Huxley did not determine whether this rate was dependent on membrane potential, however, so the assumption that it is constant may lead to phenomena in the model which are not present in the squid axon.

In the model, the prolongation of the depolarizing phase was greater than the shortening of the polarizing phase, so the period of oscillatory potentials increased as their amplitude increased. This leads to the following explanation of phase lead in conduction of subthreshold oscillations from a pacemaker node; oscillations at the driving node of the axon model induced sympathetic oscillations at the adjacent nodes; these oscillations were reduced in amplitude and therefore tended to have a shorter period; while the actual periods of

the sympathetic oscillations were identical to the period of oscillation at the driving node, they tended toward shorter periods and thus tended to lead in phase. In the case of figure 42B, as the oscillations were conducted past node 4, they apparently became sufficiently attenuated that they failed to excite the regenerative processes and sympathetic oscillations at succeeding nodes. Beginning at node 4, therefore, conduction became purely passive and decremental; and progressive phase lead gave way to progressive phase lag.

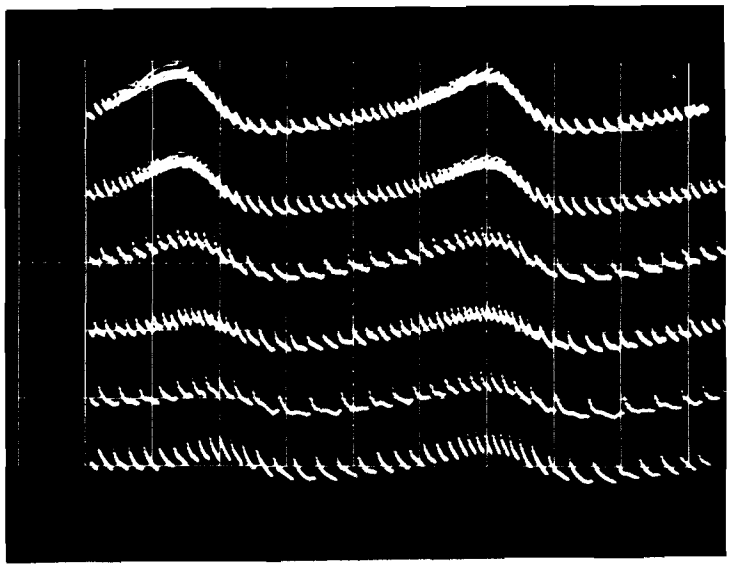

Figure 43. Transient Onset of Conducted Subthreshold Potentials.

The photograph in figure 43 shows the oscillatory potentials in the axon model immediately after the onset of the depolarizing current at node 1. The first wave is conducted from node to node in the normal decremental manner, with progressive delay. The second wave appears to be conducted without any delay at all. At nodes 3, 4, 5 and 6, the amplitude of the second wave is conspicuously larger than that of the first, corroborating the existence of regenerative buildup and sympathetic oscillations.

THE DEPENDENCE OF SPIKE VELOCITY ON AXON CORE RESISTANCE

Steady depolarizing current of magnitude sufficient to elicit periodic spikes was applied to node 1 of the axon model. These spikes propagated along the axon model from node 1 to node 6, and the interval of time between the peak of the depolarizing phase at node 1 and that at node 6 was measured and taken to be the spike conduction time for the axon model. The resistances between nodes were varied simultaneously;

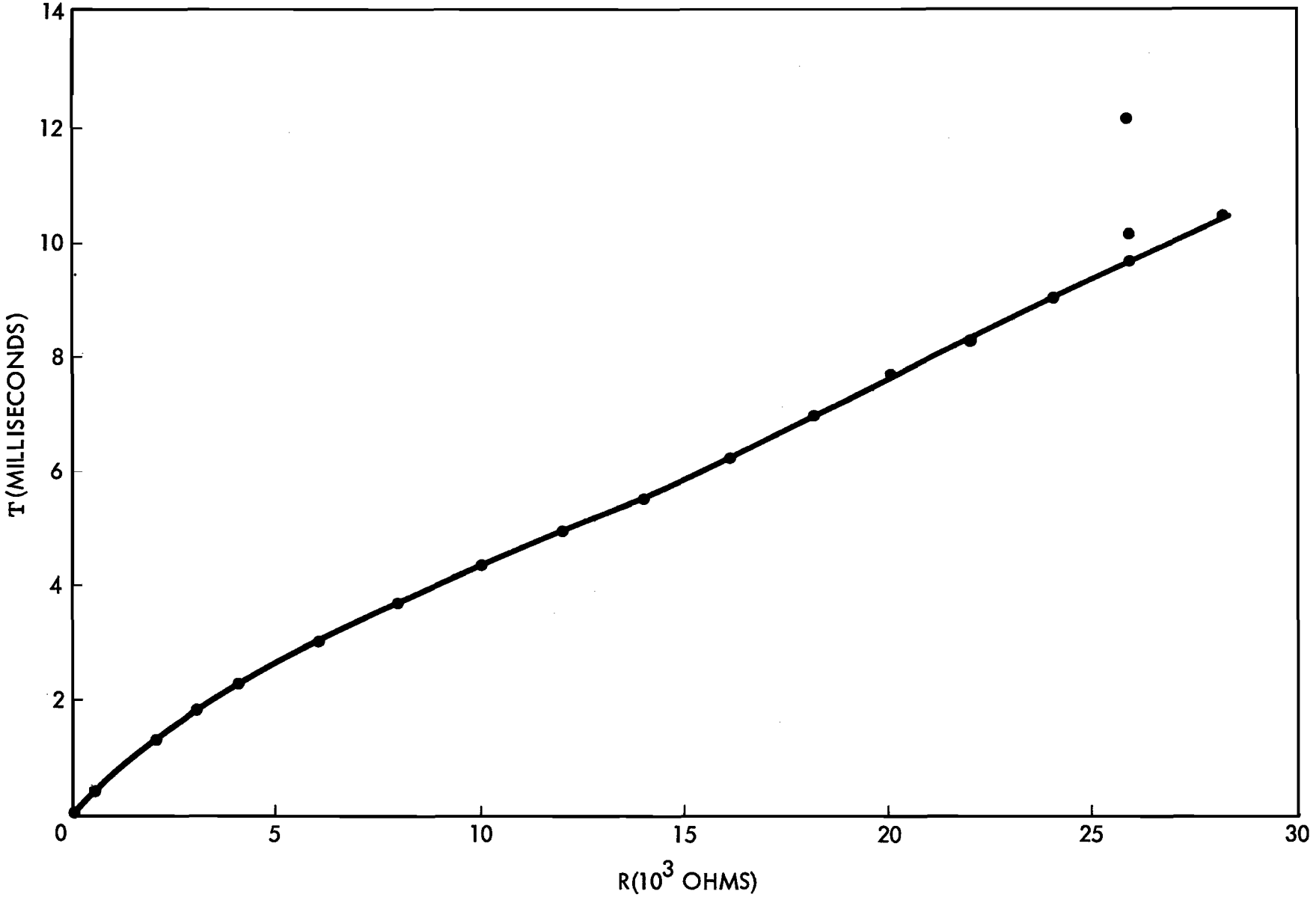

Figure 44. Propagation Time (T) Plotted against Core Resistance (R) for the Six-Lump Axon Model.

so that during a conduction time measurement, the internodal resistances were all equal, but the magnitude of those resistances was varied from one measurement to the next. Figure 44 shows the spike conduction time, T, plotted against the magnitude of the individual internodal resistance, R. The plot exhibits a rather steep initial rise of T(R) with some non-linearity; but over most of the range of the plot, T(R) is a straight line.

When the value of R was greater than 25KΩ, spike conduction began to be intermittent. At 26KΩ, only alternate spikes conducted and the intervening spikes were blocked (see figure 45). Finally, when R was slightly more than 28KΩ, conduction ceased altogether. The conduction time at 25KΩ was very close to five spike durations. In the

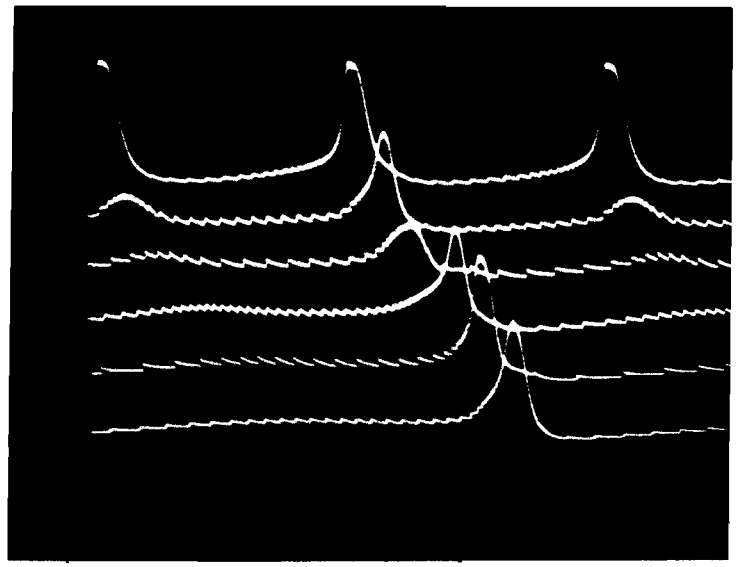

Figure 45. Propagation of Alternate Spikes in the Six-Lump Axon Model.

range of resistances between 25KΩ and 28KΩ, the behavior of the axon model was unusual in several respects. First, conduction of every spike was more likely to occur when the frequency of spike generation at node 1 was high rather than when it was low. This apparently indicates some sort of temporal summation of excitation. Second, node 1 often tended to produce spikes in distinct pairs (figure 46), but only one member of a pair would conduct. This pair production did not occur when the shunt element of node 1 was isolated, but only when it was connected to the rest of the axon model; so the pair-production mechanism appears to be associated with the quasi-distributed nature of the axon model. Finally, when R was close to 26KΩ, the conduction time was extremely unstable, varying between 10 ms and 12 ms. Over the rest of the resistance range, however, it appeared to be quite stable.

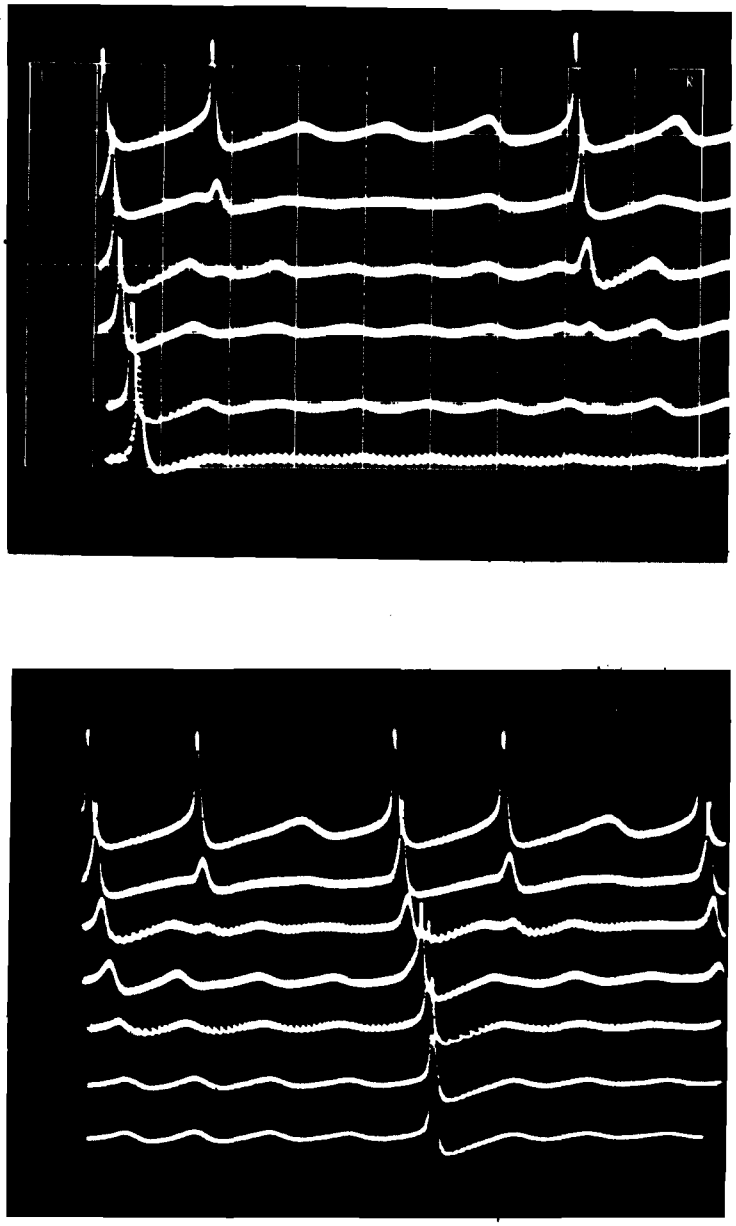

Figure 46. Spontaneous Spike Pairs in the Six-Lump Axon Model.

Spikes originated in node 1 (top trace).

SPIKE COLLISIONS AND THE RACETRACT EFFECT

An eight-lump axon model was constructed with 10KΩ internodal resistors. The shunt elements were identical to those used in the experiments described in the previous parts of this section. Figure 47 shows the potentials at all eight nodes when spikes were initiated by simultaneous stimuli at node 1 and node 8. The spikes collided at node 5 and were annihilated.

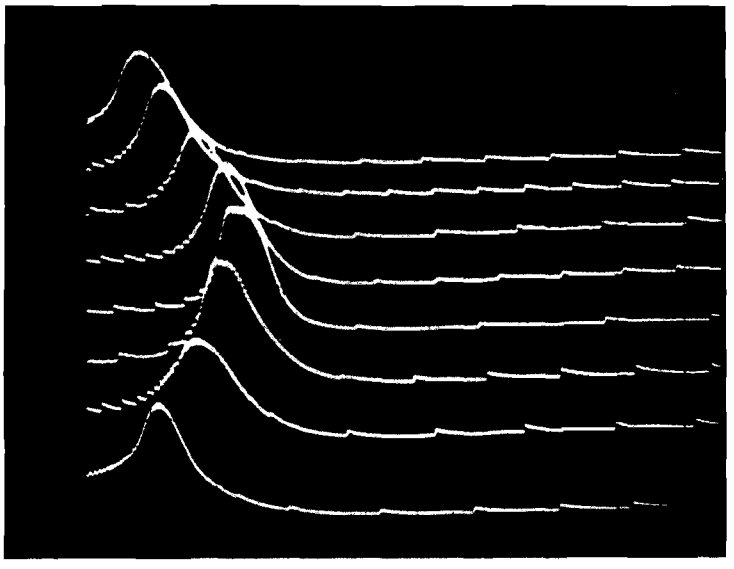

Figure 47. Collision of Two Spikes in an Eight-Lump Axon Model.

Figure 48 shows the potentials at five alternate nodes of a ten-lump axon model. In this case node 10 was connected back to node 1 through a resistor in series with a diode. The diode insured that a spike originated at node 1 would propagate in only one direction (i.e., to nodes 2, 3, 4, etc., not to nodes 9, 8, 7, etc.). In figure 48A, a spike initiated at node 1 propagated once around the loop, but failed to conduct past node 9 on the second time around. In figure 48B, the spike continued around the loop, periodically passing each of the ten nodes. This is the racetrack effect discussed by Crane (1962, 1964) in his neuristor studies. Crane has also discussed the possible logical power of mutual annihilation of spikes by collision.

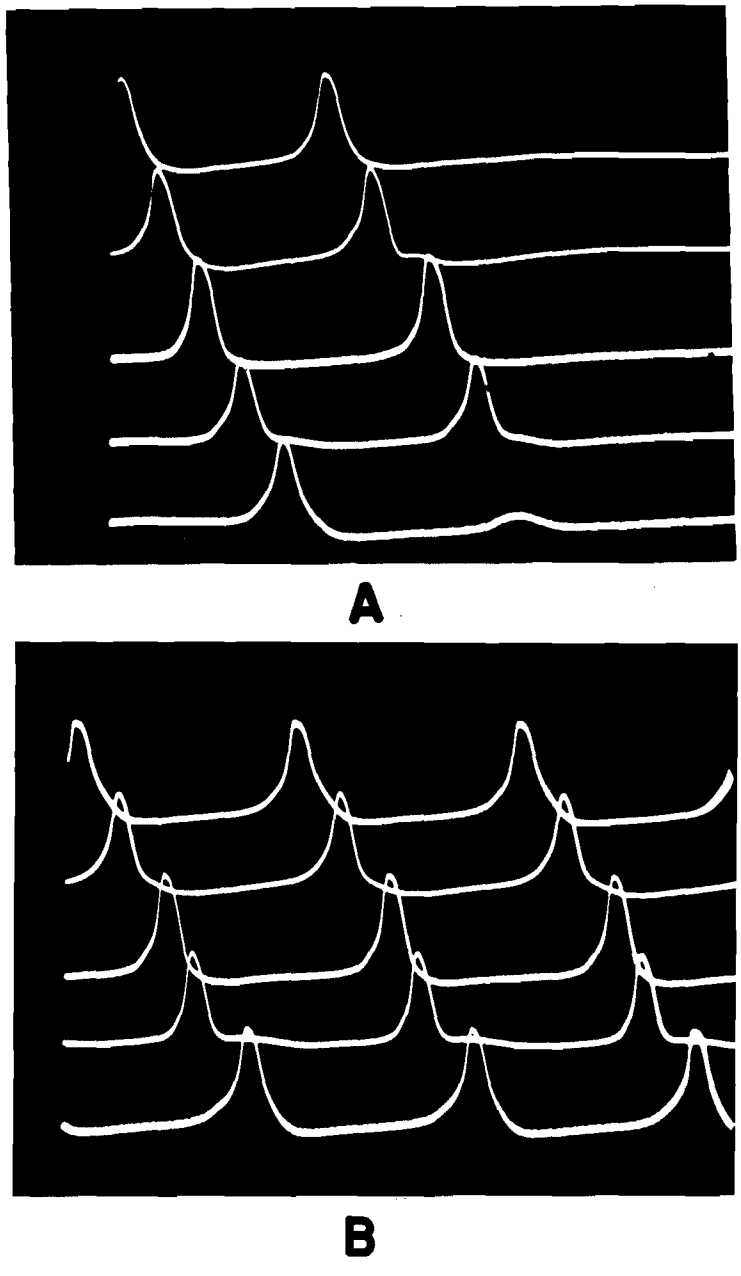

Figure 48. Spikes Propagating around a Continuous Ten-Lump Axon Model.

Traces show potentials at nodes 1, 3, 5, 7 and 9. Node 10 was connected back to node 1.

SECTION VI

SIMULATION OF THE LOBSTER CARDIAC GANGLION

INTRODUCTION

The cardiac ganglion of the lobster Panulirus has been selected as a subject for simulation studies for several important reasons. For example, this ganglion comprises only nine neurons, yet it has several important central properties: it is autonomous; its neural elements are coupled electrotonically as well as synaptically; and it makes afferent and efferent connections with a complete effector; and, perhaps most important, it is capable of integrative and patterned activity. It is a well known ganglion. Its topology has been studied; its overall system behavior has been examined in considerable detail; and the properties of its individual neurons have been studied in great detail with the aid of intracellular microlectrodes. No comprehensive theory has been formulated to explain its behavior, however, and present limitations of physiological techniques make it unlikely that any comprehensive theory will result from further gathering of purely physiological data. Such a theory could very well result, on the other hand, from coalition of physiological experimentation and studies with an analog facility where hypotheses can be tested quickly and efficiently.

STRUCTURE AND FUNCTION OF THE CARDIAC GANGLION OF THE LOBSTER PANULIRUS

The cardiac ganglion of Panulirus consists of nine neurons embedded in a common ganglionic trunk (Alexandrowicz, 1932). It produces spontaneous, periodic bursts of spikes at a rate of approximately one burst per second (Maynard, 1953 a, b). The five large anterior cells of the ganglion are motor neurons for the heart, which together elicit a contraction during a burst. The four small posterior cells act as interneurons and pacemakers (see figure 49). A burst normally begins with a spike originating in one of the small cells. This is followed by coordinated activity from all nine cells in the ganglion, each cell firing more than once during a given burst. While the bursts themselves are initiated from within a ganglion, the rate and intensity of bursts can be controlled through extrinsic innervation of the ganglion. It receives one pair of inhibitor axons and two pairs of accelerator axons (Florey, 1960, Maynard, 1953, Terzuolo, 1956). Each of these axons is thought to send branches to each of the nine cells in the ganglion. In addition to extrinsic regulatory innervation, each of the five large cells receives nearly synchronized synaptic inputs from the same sources, presumably small cell axons. No other synaptic interconnections are known to exist in the ganglion (Bullock and Terzuolo, 1957, Hagiwara and Bullock, 1957, Hagiwara, Watanabe and Saito, 1959). However, all nine cells are interconnected electrotonically, presumably by means of fine syncytial fibers (Hagiwara, Watanabe and Saito, 1959, Watanabe and Bullock, 1960). These electrotonic connections are effective only for slowly varying potentials; they are unable to transmit spikes.

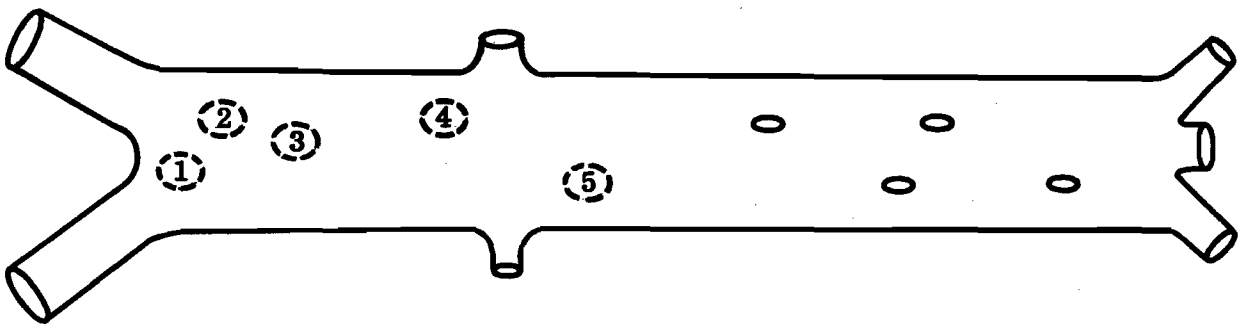

Figure 49. Disposition of the Somata of the Cardiac Ganglion of Panulirus (redrawn from Bullock and Terzuolo, 1957).

The dendrites of both the large and small cells extend into the muscle of the heart and are thought to be sensitive to stretch. This proprioceptive feedback is not necessary for the production of periodic bursts, however, since the ganglion continues to function in a normal manner even when completely isolated from the myocardium.

Many of the cells of the ganglion have a tendency toward spontaneity. If separated from the rest of the ganglion, for example, some individual large cells will produce periodic, single spikes at a frequency considerably higher than the burst frequency of the intact ganglion (Maynard, 1955 a, b). This pattern is suppressed, however, in the normally functioning ganglion; and nine cells, some of which as individuals tend to be independently free-running, are somehow coordinated to produce periodic bursts in which every cell takes part. Groups of as few as three large cells isolated from the rest of the ganglion can produce periodic bursts not qualitatively different from those of the intact ganglion.

The five large cells of the cardiac ganglion have been penetrated with microelectrodes and studied by several physiologists (see, for example, Bullock and Terzuolo, 1967, Hagiwara and Bullock, 1957, Otani and Bullock, 1959, Watanabe, 1958). These studies have not only contributed to the knowledge of the anatomy of the ganglion (e. g., the discovery of the electrotonic interconnections), but have also yielded considerable data on the subthreshold activity in the somata of the individual neurons. It has been shown, for example, that the somata of the large cells are electrically inexcitable, and that the action potential, or spike, does not propagate antidromically into the soma of any of these cells. The soma potential is not reset, therefore, after each spike; in fact a single excitatory postsynaptic potential (epsp) may result in as many as four orthodromic spikes. The triggering of a single orthodromic spike, on the other hand, may require an accumulation of several epsp's. The large cells thus are highly

integrative neurons. In response to presynaptic spikes from the small cells, the large cells exhibit antifacilitating epsp's which sum temporally and spatially. The synapses are all on or near the soma, and apparently originate from the same presynaptic fibers since the epsp's in the five large cells are synchronized. In addition to postsynaptic potentials, isolated large cells exhibit low frequency pacemaker potentials similar to those observed in most sensory cells (Bullock, 1962, Hagiwara and Bullock, 1957, Watanabe, 1958). These potentials usually elicit a single spike, but occasionally a single pacemaker potential results in a burst of two to four spikes.

In response to external stimulation of the accelerator fibers, both the intensity and frequency of the ganglion bursts increase (Florey, 1960). This acceleration exhibits facilitation and prolonged aftereffects. Individual epsp's have been observed in some large cells on stimulation of the accelerators, but more often the postsynaptic effect is a gradual depolarization with no distinguishable epsp's. The accelerator pairs appear to function as a single fiber. The net acceleration is dependent on the total frequency of accelerator spikes, but is independent of the manner in which these spikes are shared by the two fibers. Presynaptic spikes on the inhibitory fibers produce different effects in the various large cells. In some, facilitating inhibitory postsynaptic potentials (ipsp's) are observed; in others, facilitating depolarizations occur and are followed by rebound inhibition (Terzuolo and Bullock, 1958). The response to inhibitory stimuli is facilitated for a brief time, but this is followed by adaptation. A ganglion in which spontaneous activity has been inhibited completely will adapt and eventually recover its original activity, even though the inhibitory stimulus has been maintained (Florey, 1960). The inhibitor pair, like the accelerator pair, appears to function as a single fiber. The degree of inhibition is determined by the total number of spikes arriving over both fibers, and is independent of the manner in which they are shared. In addition, if stimuli are applied to one of the two fibers at a given rate until some degree of adaptation is observable, and if the stimuli are then switched to the other fiber, the degree of adaptation is unaffected by the change.

If some of the ganglion cells are effectively removed by anesthesia or dissection, the remainder of the ganglion will continue to provide coordinated bursts of pulses similar to those produced by the intact ganglion. If, for example, the four small cells are all eliminated, one of the five large cells will usually assume the role of a pacemaker. If the new pacemaker is eliminated, one of the remaining four cells will take over the pacemaker function; and, in fact, as few as three cells may produce coordinated periodic bursts. The cardiac ganglion appears thus to have a built-in safety factor insuring it against damage.

ELECTRICAL PROPERTIES OF THE LARGE-CELL SOMATA

The cell bodies, or somata of the five large cells are capable of completely graded electrical activity, exhibiting no threshold and no spike potential. One should not infer from this evidence, however, that the soma membranes do not have voltage-dependent equivalent conductances for

certain ion species, such as the conductances of the Hodgkin-Huxley Model. The equivalent sodium and potassium conductances in these membranes or in contiguous membranes apparently are in fact voltage dependent, and those dependencies will be discussed in this section.

In addition to their diminished electrical excitability, the somata of the five large cells apparently exhibit a membrane capacitance considerably larger than that specified by Hodgkin and Huxley for the squid giant axon. Hagiwara, Watanabe and Saito (1959) measured capacitances of 4 to 10 microfarad per sq cm in the ganglion cells. From the evidence presented in Section IV as well as that presented in previous papers on the neural analogs (Lewis, 1965) one might conclude that this increase in membrane capacitance alone might account for the electrical properties of the ganglion somata. Although an increase of capacitance to 10 microfarads per sq cm will considerably reduce the electrical excitability of the Hodgkin-Huxley Model, it cannot make the static or dc electrical properties of the Hodgkin-Huxley Model correspond to those of the ganglion soma membrane. This point is examined in considerable detail in the following discussion. Hagiwara, Watanabe, and Saito (1959) found that the current-voltage relations (figure 50) in the large ganglion-cell soma were qualitatively similar to the current-voltage relations (figure 51) observed by Hodgkin, Huxley and Katz (1952) in the squid, but the relations exhibited considerable quantitative differences. The data in both cases were obtained in approximately the same way. In both preparations the membrane potential was suddenly changed and held at a new value; and in both preparations the steady-state data was taken after the current reached a constant value. In the squid axon, the transient inward current was measured at a fixed interval (0.63 msec) after the onset of the voltage change. The transient inward current passed through a maximum and declined toward zero in the squid axon preparation. In the ganglion soma, on the other hand, the transient peaks of inward current were recurrent. Hagiwara took these recurrent peaks to be the result of spikes generated at a remote spike initiator region in the axon. The transient inward current in the soma was measured at the first of the recurrent peaks after the onset of the voltage change. The transient inward current data from the two preparations are therefore not comparable.

The steady-state data, on the other hand, may be comparable, if consideration is given to the fact that in one preparation (the squid axon) the system was not spatially distributed, while in the other preparation, the soma was connected to an axon.

AN ATTEMPT TO EXPLAIN THE D-C CURRENT-VOLTAGE RELATION IN THE SOMA IN TERMS OF THE HODGKIN-HUXLEY DATA

In the range of membrane potentials greater than the resting potential (i.e., negative potentials in figures 50 and 51), the current-voltage relations were linear in both the squid axon and the ganglion soma. Both membranes were alike, therefore, in exhibiting constant conductance in this range. In the range of membrane potentials less than the resting potential, the current-voltage relations were nonlinear in both preparations; and both membranes were alike in exhibiting conductances that increased

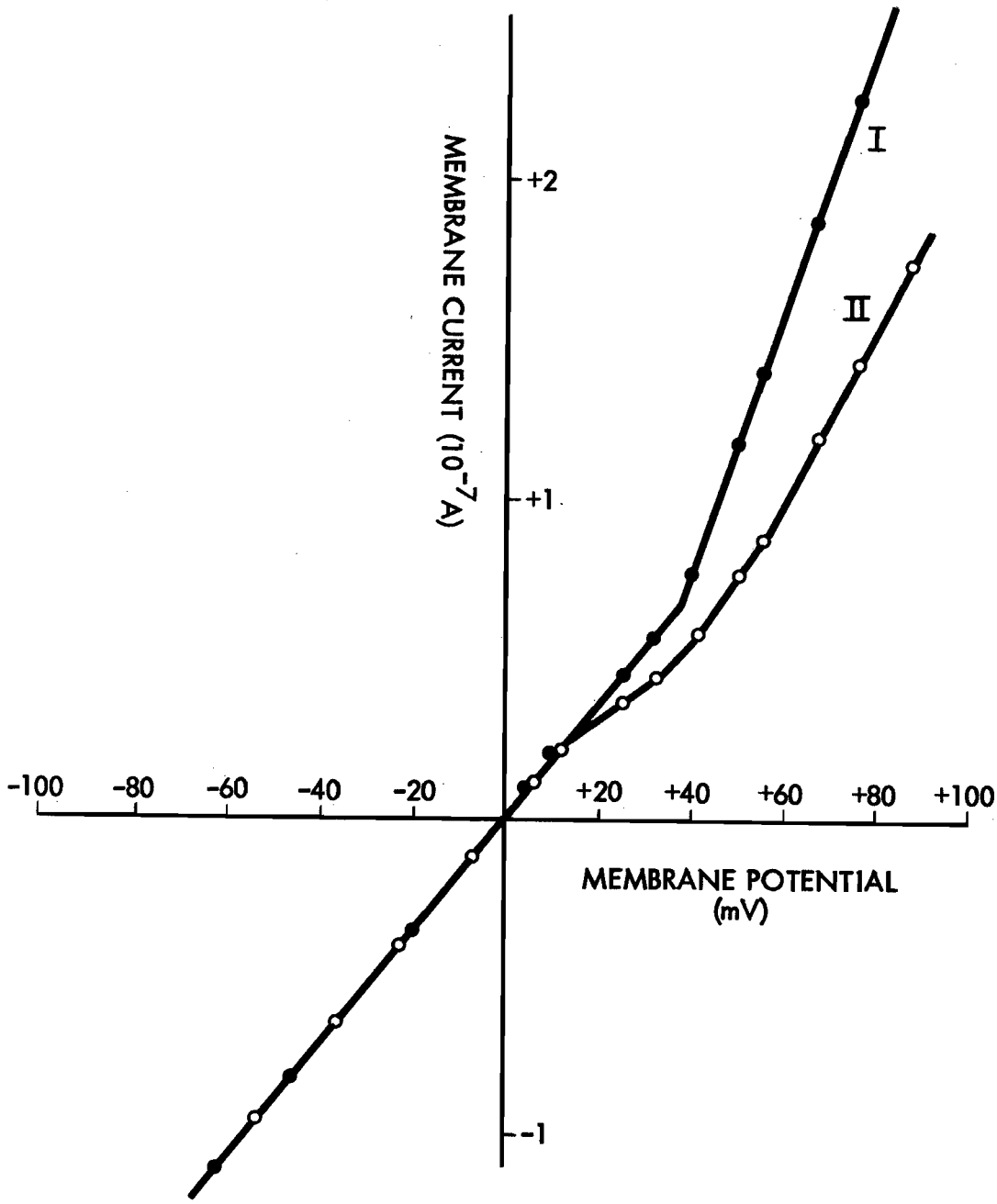

Figure 50. Voltage-Current Relations in a Soma of the Lobster Cardiac Ganglion (redrawn from Hagiwara, et al, 1959).

Open circles are data for peak inward current; solid circles are steady-state data.

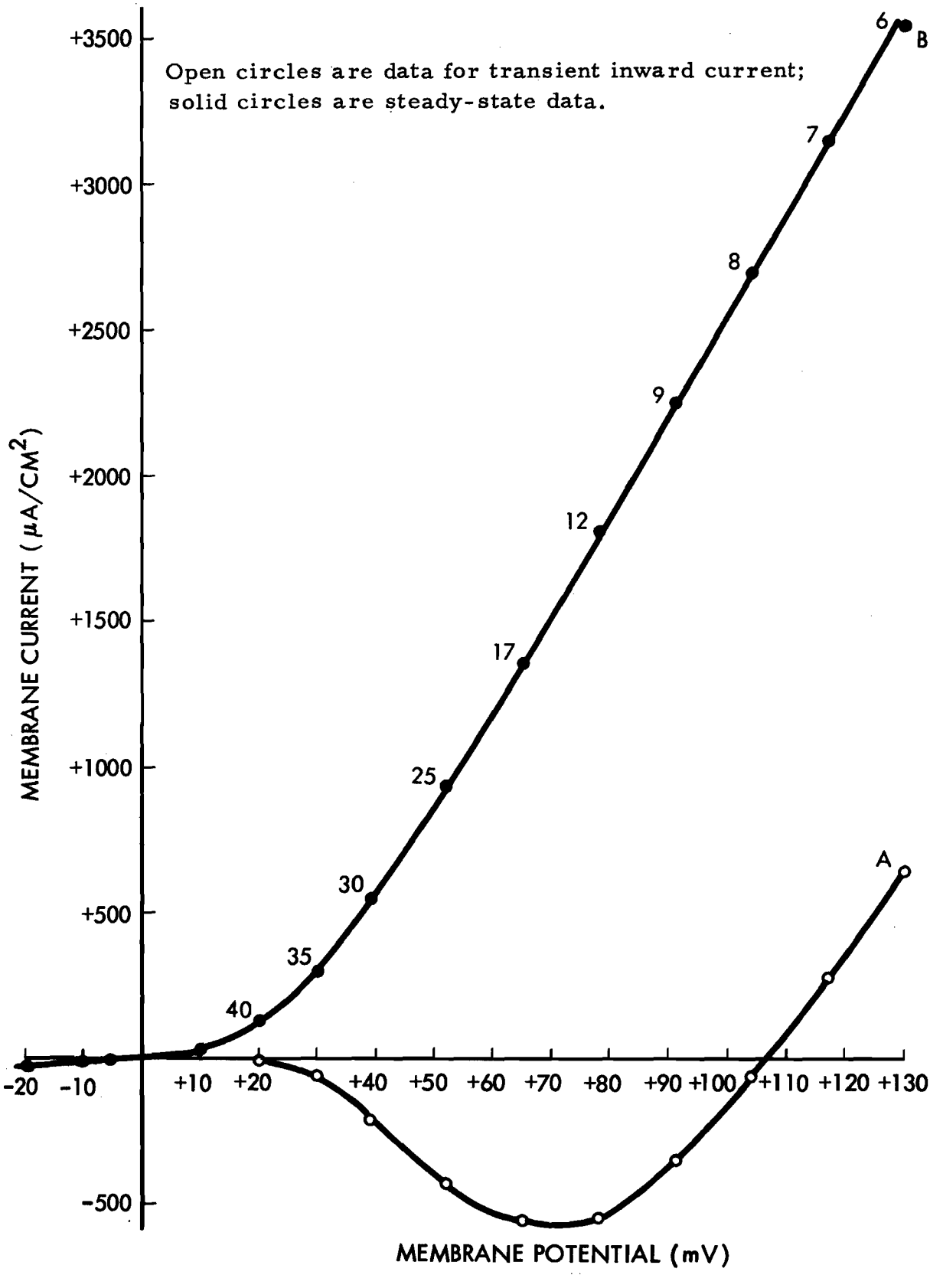

Figure 51. Voltage-Current Relations in the Squid Giant Axon (redrawn from Hodgkin, Huxley and Katz, 1952).

with increasing depolarization. In the squid axon, the membrane conductance began to increase immediately as the membrane potential was reduced from the resting level. In the soma, on the other hand, the conductance apparently did not begin to increase until the potential was nearly 40 mv below the resting level. The ratio of maximum conductance to minimum conductance in the squid axon was nearly 70:1; while in the soma the same ratio was less than 3:1. The soma data thus is similar to the squid axon data, but with the threshold for conductance increase shifted to the right and with a much smaller ratio of maximum to minimum conductances. These differences appear to be at least partially reconcilable. The difference in conductance ratios can be explained under the assumption the soma exhibits a large voltage-independent conductance effectively in parallel with an electrically excitable membrane similar to that of the squid axon. The shift in threshold for the conductance increase, on the other hand, might be explained under the assumption that the electrically excitable membrane in the ganglion cell is remote from the soma, so that voltages applied at the soma are attenuated by the time they reach the region with voltage dependent conductance. These assumptions suggest a soma and axon hillock, each with voltage-independent membrane conductance, connected to an electrically excitable axon but partially isolated from it by the resistance of the axoplasm in the hillock.

A Square-Law Approximation to the Steady-State Current in the Squid Axon

In order to determine the properties of the system of three conductances and a capacitance that they had proposed, Hodgkin and Huxley transformed their data into explicit mathematical descriptions. In the present case, time variations and complicated interactions of state variables are not being considered. Nonetheless, an explicit mathematical statement of the data certainly would facilitate calculations. One possibility in the case of the steady-state conductance of the squid-axon membrane is a square-law approximation. In Table 2, three sets of numbers are given. One is a set of values computed by interpolation on a smooth curve drawn by Hodgkin and Huxley through their squid axon data. The other two sets are square-law approximations to the first.

TABLE 2

Square Law Approximations to the Steady-State Current-Voltage Relation in the Squid Axon

V Membrane Depolarization (Millivolts)	I Membrane Current Interpolated from the Hodgkin-Huxley data (Microamps/cm^2)	$0.3V^2$	$0.33V^2$
10	30	30	33
20	130	120	132
30	325	270	297
40	550	480	528
50	840	750	825
60	1180	1080	1188
70	1500	1470	1617
80	1840	1920	2112

All of the approximations in the third column are within 17 percent of the interpolated current values in the second column, but the greatest errors occur for intermediate magnitudes of depolarization. The approximations in the fourth column are all within 15 percent of the data, but the absolute magnitudes of the errors are large for depolarizations greater than 60 mv. In the range of depolarizations from 0 to 60 mv, however, the figures in the fourth column are within 10% of those in the second column, so $0.33\ V^2$ is a better approximation in that range. The accuracy of the square law approximation is particularly impressive in view of range of current magnitudes involved. Figure 52 illustrates the accuracy of the two approximations.

Calculation of the Steady-State Current-Voltage Characteristics of an Infinite Uniform Axon

For the case of a uniform axon whose potentials and currents do not vary with time, the following equations are applicable:

$$8) \quad \frac{dV}{dx} = -rI$$

$$9) \quad \frac{dI}{dx} = -cJ_m$$

where V is the internal potential of the axon; I is the axial current; r is the axoplasm resistance per unit length in the axial direction; x is distance in the axial direction; c is the axon circumfrence; and J_m is the radial current density at the membrane (i.e., the membrane current);

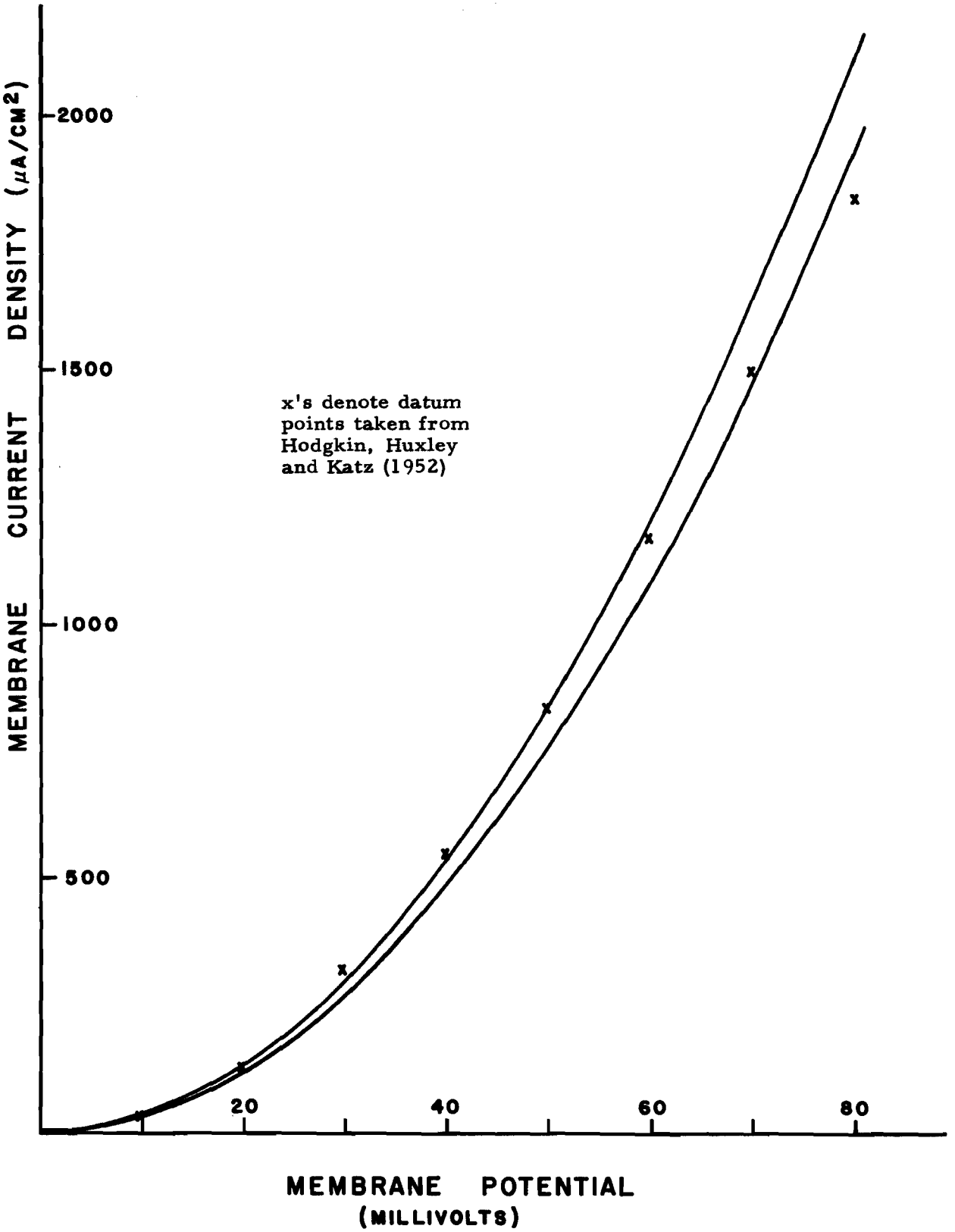

Figure 52. Square-Law Approximations to the Squid-Axon Voltage Current Relations.

the external potential is taken to be independent of x. Assuming the membrane current is proportional to V^2, we obtain

$$10) \qquad J_m = \beta V^2$$

where β is an arbitrary constant.

Differentiating both sides of Equation 8 and substituting Equations 9 and 10, one obtains the following differential equation:

$$11) \qquad \frac{d^2V}{dx^2} = r\, c\beta V^2$$

A solution to Equation 11 is

$$12) \qquad V = \frac{6}{r\, c\beta\, (x + k)^2}$$

where k is a constant. Taking the point x = 0 to be the input terminal of the axon and V_{in} to be the input voltage, one obtains

$$V_{in} = \frac{6}{rc\beta k^2}$$

or

$$k = \sqrt{\frac{6}{rc\beta V_{in}}}$$

Differentiating both sides of Equation 12, and substituting the result in Equation 8, one obtains the following equation for axial current:

$$I = \frac{12}{r^2\, c\beta\, (x + k)^3}$$

The axial current at the input terminal is simply I(x=0) or $12/r^2 c\beta k^3$. Substituting the expression for k, one obtains

$$13) \qquad I_{in} = \sqrt{\frac{2\, c\beta}{3\, r}}\; V_{in}^{3/2}$$

The square-law approximation for membrane current thus leads to a 3/2-power law for the dependence of input current on input voltage for an infinite, uniform axon. Since steady depolarizations usually are not sustained over more than a very short segment of an axon, equation 6 should be valid even for reasonably short axons.

Two-Lump Representations of a Cardiac-Ganglion Soma for D-C Potentials

The d-c current-voltage relationship found by Hagiwara in the cardiac-ganglion soma is shown once more in figure 53. The smooth curve drawn through the data points exhibits two apparently linear segments joined by a sharp knee. The plotted data extends slightly beyond 80 mv on the horizontal axis. When the abscissa is 80 mx, the ordinate of the extrapolated data is almost exactly 2.5×10^{-7} amp, while that of the extended initial linear segment (dashed line in figure 53) is 1.43×10^{-7} amps. In the following discussion, the nearly piecewise linear relationship illustrated in figure 53 is compared with the current-voltage relationships calculated for circuits that include square-law representations of axon membrane.

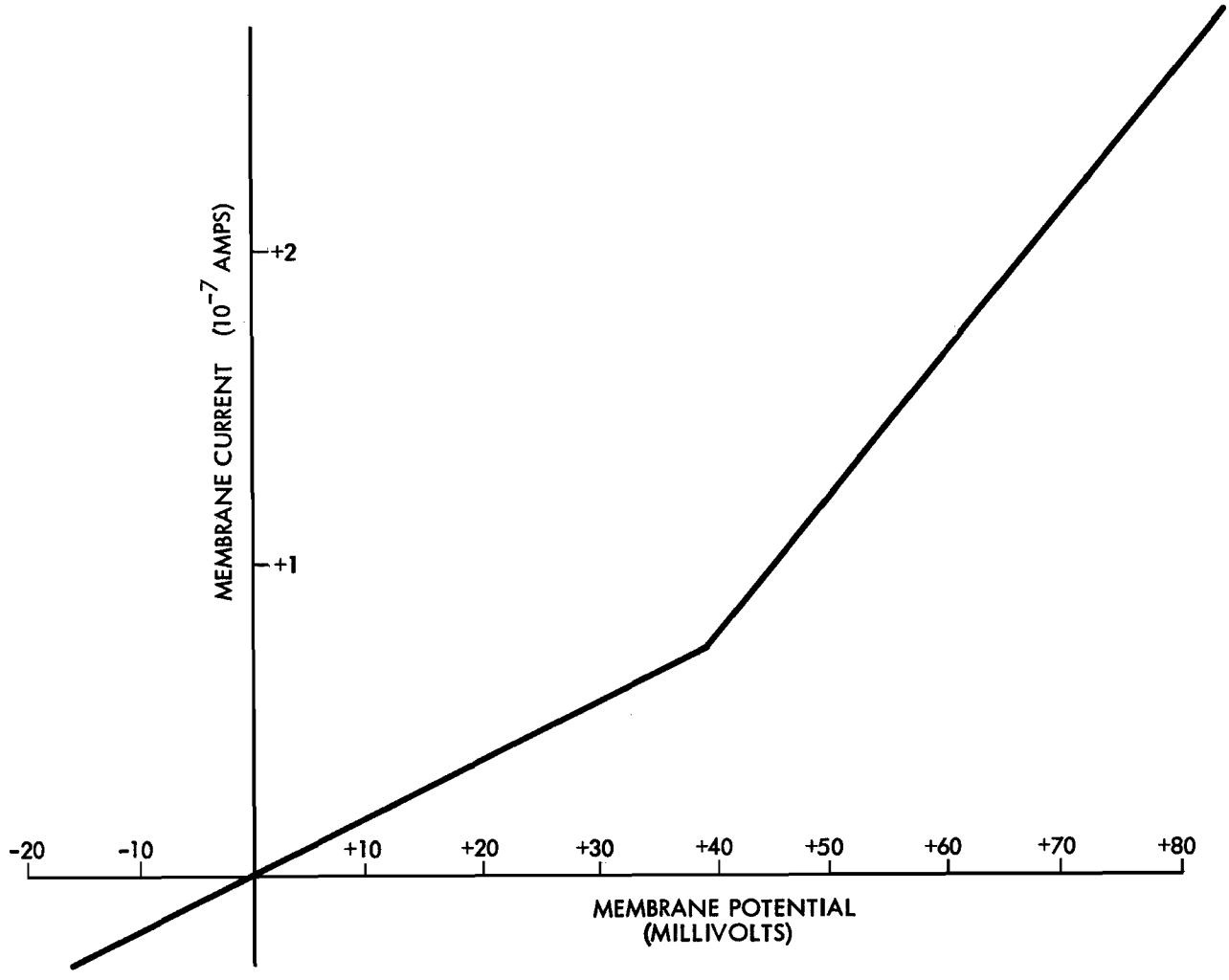

Figure 53. Steady-State Voltage-Current Relations in the Cardiac Ganglion Soma.

Figure 54 shows two electrical circuit equivalents of a soma and axon hillick with a fixed membrane conductance (G) connected through the axoplasm resistance (R) of the hillock to the voltage-dependent conductance of the axon. In figure 54A the axon is represented by a shunt element whose current is proportional to the three-halves power of voltage. This element represents a spatially distributed axon with a square-law and represents a nondistributed patch of axon membrane. The input currents (I) and input voltages (V) of the two circuits can be computed from the following equations:

$$V = V' + I'R$$

$$\frac{I}{G} = V' + (R + \frac{1}{G})\, I'$$

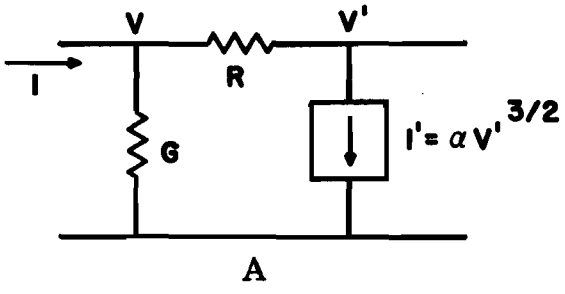

A

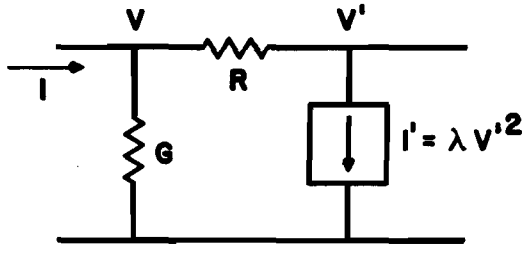

B

Figure 54. D-C Equivalent Circuits for a Passive Circuit Connected to a Square-Law Axon.

In the top circuit, the axon is assumed to be distributed; in the bottom circuit, it is treated as a non-distributed membrane patch.

In the case of the circuit in figure 54A, these equations become

$$14) \qquad V = V' + K\beta V'^{3/2}, \text{ and}$$

$$15) \qquad \frac{I}{G} = V' + \beta V'^{3/2};$$

where $\beta = \alpha (R + 1/G)$, and $K = RG/(1 + RG)$. The ranges of the parameters (K and β) in Equations 14 and 15 can be established from the properties of the data in figure 53. The criterion selected for this discussion is matching the data at its extremities. To meet this criterion simultaneous solutions of Equations 14 and 15 (i.e., the solutions for I(V)) will be forced to intersect the data at the origin and at the extremity of positive abscissas, 80 mv; and the slopes of the solutions will be forced to match the slope of the data at the origin.

The plotted data in figure 53 passes through the origin; and the simultaneous solutions of Equations 14 and 15 meet this criterion for all values of K and β. From Equations 14 and 15, the slope of I(V) at the origin is G. The slope of the plotted data at the origin is approximately 1.8×10^{-6} amp/volt, so $G = 1.8 \times 10^{-6}$ mho.

Finally, the solutions to 14 and 15 must pass through the point (80 mv, 2.5×10^{-7} amp), so

$$(V =)\ 80 \text{ mv} = V' + K\beta V'^{3/2}$$

when

$$(\frac{I}{G} = \frac{2.5 \times 10^{-7}}{1.8 \times 10^{-6}} \text{ volts} =)\ 140 \text{ mv} = V' + \beta V'^{3/2}.$$

These equations can be solved simultaneously to yield

$$16) \qquad \beta = 60/(1 - K) V_1^{3/2}$$

and

$$17) \qquad V_1 = \frac{140K - 80}{K - 1} \text{ mv}$$

where V_1 is the magnitude of V' when V = 80 mv.

Since V cannot be greater than I/G, K must be less than unity. In addition, V_1 cannot be negative; the maximum value of K which is less than one and for which V_1 is positive can be obtained from Equation 14:

$$K_{max} = \frac{80}{140} = 0.57$$

or, since $K = RG/(1 + RG)$ and $G = 1.8 \times 10^{-6}$ mho,

$$R_{max} = 0.74 \times 10^{6} \text{ ohms.}$$

R_{max} is the largest value of R that allows I(V) to pass through (80 mv, 2.5×10^{-7} amp).

The range of K is given by $0 \leq K \leq 0.57$.

In this range, V_1 decreases monotonically and β increases monotonically as K increases. The minimum allowed value of β occurs, therefore, when K = 0. From Equation 17, V_1 (K = 0) = 80 mv; substituting this value into Equation 16 yields

$$\beta\ (K = 0) = 0.0842 \text{ mv}^{-1/2}$$

As the value of K approaches 0.57, on the other hand, V_1 approaches zero, and β approaches infinity. The range of β, therefore, is given by

$$0.842 \text{ mv}^{-1/2} \leq \beta \leq \infty$$

Figure 55 shows three solutions of Equations 14 and 15 for I(V), along with a continuous line representing the data from the cardiac-ganglion soma. Of the three solutions, the bottom line represents that for $\beta = 0.0842$ and K = 0 (i.e., the solution for R = 0), and the top line represents that for values of approaching 0.57 and values of K approaching infinity. All other solutions that meet the established criteria fall between those two lines. Obviously none of the solutions will be a very good approximation to the cardiac-ganglion data; so a lumped, passive membrane loaded by a distributed squid axon is apparently not a good model for the soma in the lobster cardiac ganglion.

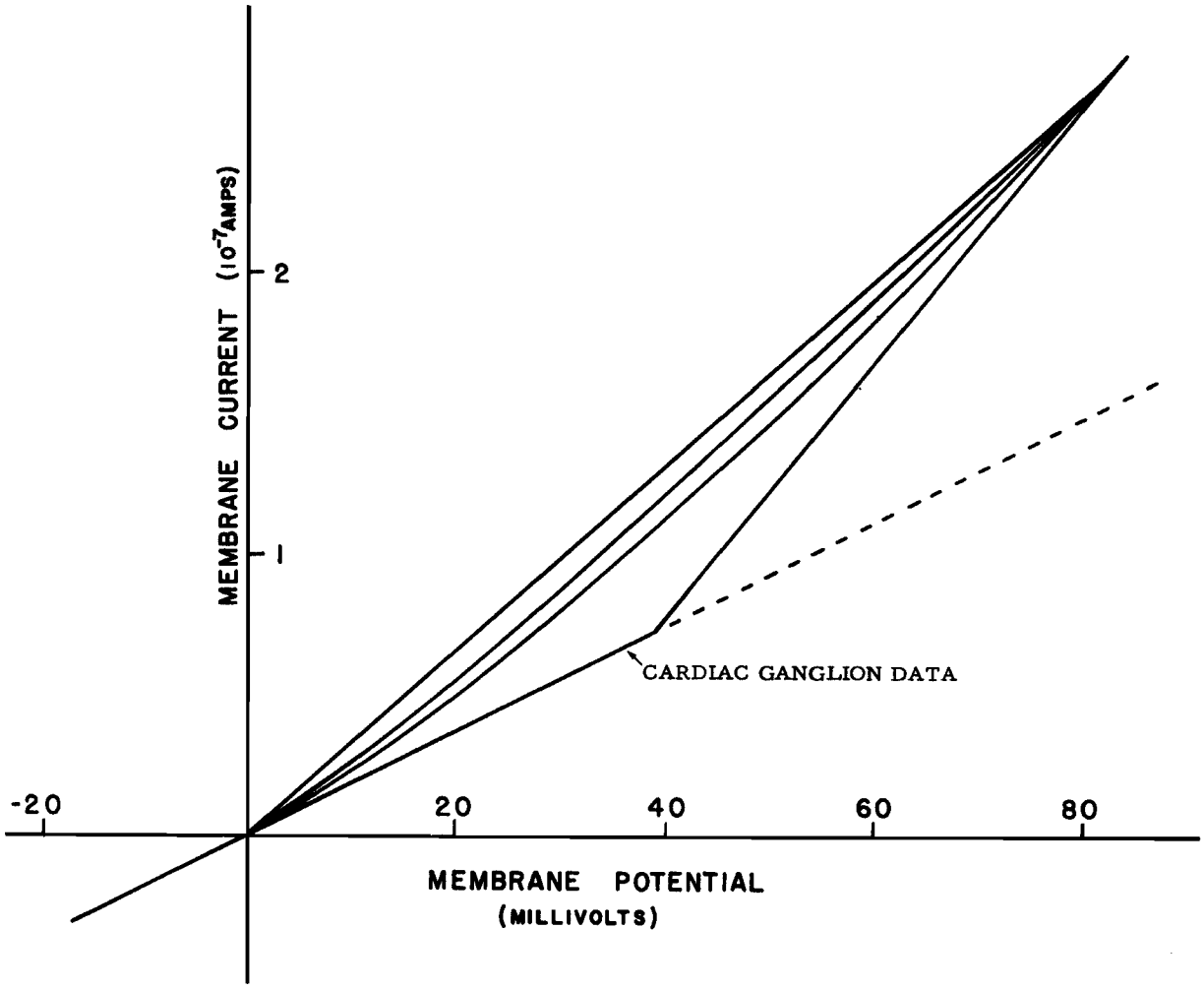

Figure 55. D-C Voltage-Current Relations of a Passive Soma Connected to a Distributed Square-Law Axon, Compared to the Voltage-Current Relations in the Lobster Soma.

The second proposed model (see figure 54B) is a lumped, passive membrane loaded by a patch of squid-axon membrane (according to the square-law approximation). Equations 14 and 15 in this case become

$$18) \qquad V = V' + K'\sigma V'^2$$

$$19) \qquad \frac{I}{G} = V' + \sigma V'^2$$

Once again matching the data at its extremities, one can determine the limits of K' and γ. Equations 15 and 16 become identical to Equations 9 and 10 as V' approaches zero, so the magnitude of G must be the same in both cases: $G = 1.8 \times 10^{-6}$ mmho.

Since the solutions to Equations 18 and 19 must pass through (80 mv 2.5×10^{-7} amp), the following equations must be valid:

$$20) \qquad \gamma = 60/(1 - K')V'^2$$

$$21) \qquad V' = \frac{140K' - 80}{K' - 1} \text{ mv}$$

As in the case of K in Equations 14 and 15, K' in Equations 18 and 19 cannot be greater than unity and therefore is limited by Equation 21 to the following range: $0 \leq K' \leq 0.57$.

Based on considerations analogous to those applied to Equations 16 and 17, the range of is limited to $0.0094 \leq \gamma \leq \infty$.

All solutions of Equations 19 and 20 that conform to this parameter range will lie between the top and bottom curves in figure 56. While none of these solutions will be a good approximation to the data, the bottom curve is considerably closer to the data than any of the solutions to Equations 14 and 15.

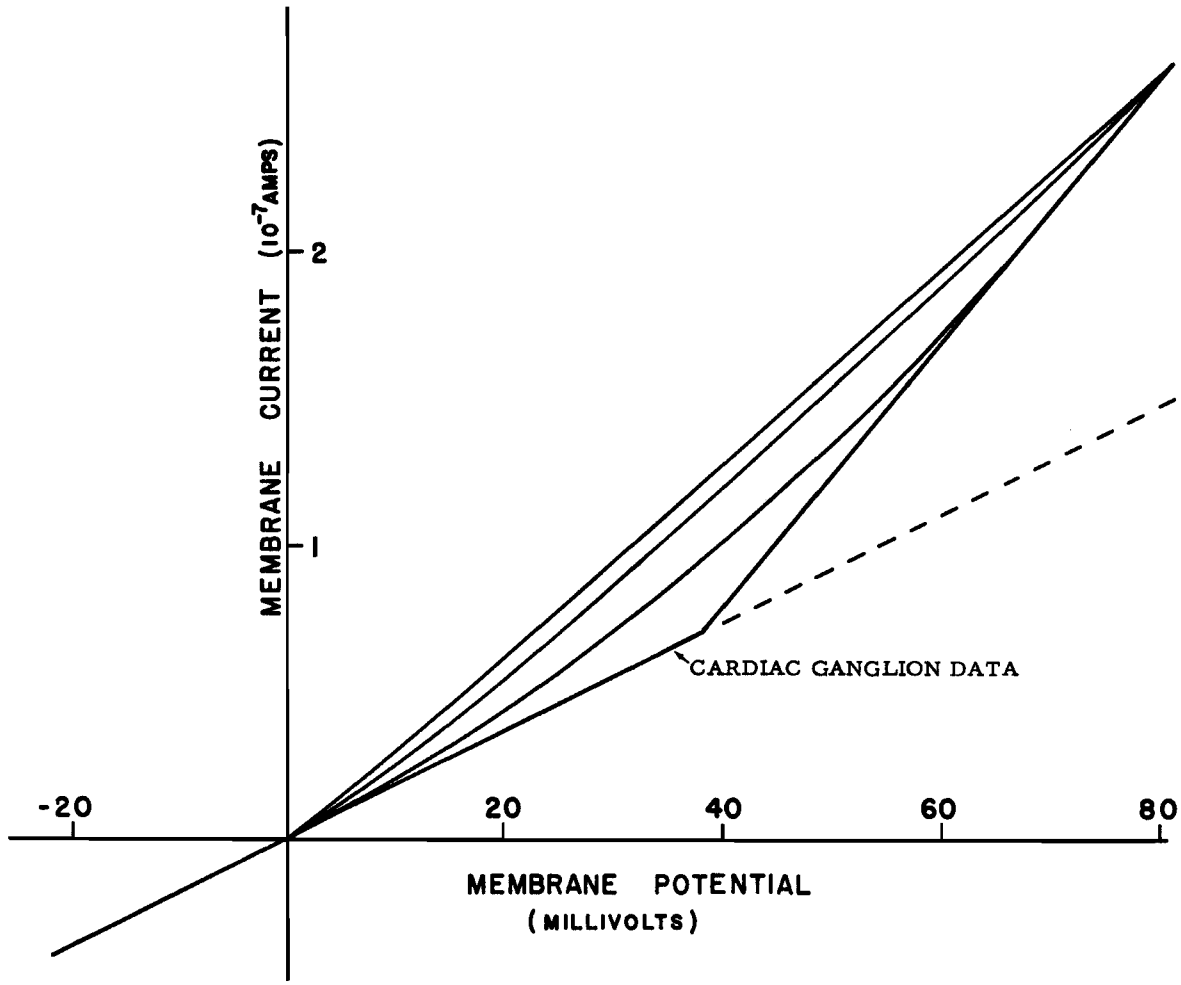

Figure 56. D-C Voltage-Current Relations of a Passive Soma Connected to a Patch of Square-Law Membrane, Compared to the Voltage-Current Relations in the Lobster Soma.

Summary and Discussion

The dc current-voltage relations in a patch of squid-axon membrane were shown to be approximated quite well by a square-law dependence of current on voltage. This square-law relation for a membrane patch leads to a three-halves power law for the distributed axon viewed from one end. In an attempt to reconcile the dc current-voltage relations in a cardiac-ganglion soma with those of a squid giant axon, two models were tested.

In one model, the soma membrane was assumed to exhibit a fixed conductance which was connected electrically through the axon-hillock core resistance to a distributed axon with properties similar to those of the squid axon (i. e., an axon obeying a three-halves power law). In the other model, the assumed configuration was the same except that the axon was taken to be lumped rather than distributed (i. e., the axon was represented by a square law). Neither of these models provided current-voltage relations with the sharp knee exhibited by the cardiac-ganglion data.

Several perturbations of these models (e. g., a distributed combination of fixed shunt conductances and series core resistances representing the axon hillock) were explored. None of these exhibited current-voltage relations that were closer to the data than those for the lumped axon with a large, fixed conductance in parallel with it (bottom curve in figure 56).

It seems unlikely, in fact, that any justifiable combination of passive elements and d-c squid axon models will provide the piecewise-linear relation found by Hagiwara. At least two other explanations are possible. The electrical properties of excitable membrane in the lobster may be completely different from those in the squid; or the occurrence of spikes at the axon during the application of the test voltage at the soma obscurred the dc characteristics of the system, even in the interspike interval. Two things are clear from Hagiwara's data, however. The increased capacitance of the soma membrane is not the only difference between it and the squid-axon membrane. The soma membrane exhibits a voltage-independent conductance that is very large compared to its voltage-dependent conductance; and, unlike the squid-axon membrane, the soma membrane exhibits no transient negative resistance.

SPONTANEITY IN THE CARDIAC GANGLION

Normal Spontaneity

Since the lobster cardiac ganglion is the pacemaker for the lobster heart, perhaps its most salient property is its spontaneity. The normal burst rate for the ganglion, as indicated by the frequency of heart beats, is from 1/2 to 2 bursts per second. All nine neurons of the ganglion apparently participate in a burst, each contributing several spikes. The maximum spike frequency of any single neuron during a burst is approximately 100 spikes per second (Maynard, 1955 b). Most of the neurons operate at a considerably lower frequency, however.

The sequency of spike initiation by the various neurons at the beginning of a burst is often constant for long periods of time. Maynard (1955 b), for example, observed the same pattern of several spikes from several neurons repeated at the beginning of more than 3500 successive bursts. Under normal conditions, the first few spikes in a burst apparently are initiated by small cells. After several spikes from the small cells, the large cells begin producing spikes. Toward the end of the

burst, the frequency of spikes from the large cells decreases until only the small cells are firing again; so the last few spikes in the burst are also from the small cells (Maynard, 1955 b).

Intracellular Recordings from the large cells during burst activity indicate that the five large cells do not all behave in the same way during a burst (Bullock and Terzuolo, 1957, Hagiwara and Bullock, 1957). All five cells have a resting potential of 50 mv and all five cells exhibit rapid depolarizations of about 20 mv at the beginning of each burst. Following this initial depolarization, cells 1, 2 and 5 (see figure 49) exhibit a sustained depolarization of 10 to 15 mv which lasts for several tenths of a second during a burst. Superimposed on the sustained depolarization are a large number of large and small excitatory post-synaptic potentials (epsp's) and, in cells 1 and 2, several miniature spikes presumably reflected from the axon. Usually miniature spikes also were seen in cell 5. The amplitudes of the reflected spikes vary from less than 10 mv to more than 20 mv. The frequency of miniature spikes usually decreases monotonically during a burst. The large depolarization in cells 1, 2 and 5 at the beginning of a burst usually is preceded by only one spike, suggesting that the depolarization is a single epsp (Bullock and Terzuolo, 1957). Hagiwara and Bullock (1957) observed that single epsp's in the large cells can be as large as 20 to 30 mv. Some presynaptic pathways to cells 1 and 2 are not that effective, however; and spikes in these pathways induce epsp's that are extremely small (e. g., 1 or 2 mv). The large epsp's usually end abruptly during a burst, and cells 1 and 2 exhibit only small epsp's for the final few tenths of a second.

Cell 4 of the cardiac ganglion usually exhibits transient potentials similar to cells 1 and 2, but without the sustained depolarization. Cell 3, on the other hand, exhibits potentials very similar to those in cells 1 and 2, including the sustained depolarization; but it also usually exhibits spontaneous spikes in the interburst interval. These spikes apparently result from a tendency toward spontaneous depolarization in cell 3. Occasionally this depolarization is reset before a spike can occur, and in general the waveform has the appearance of a subthreshold oscillation with a single spike occuring randomly on the rather broad peak of its depolarizing phase (see Bullock and Terzuolo, 1957, fig. 6, p. 350). Maynard (1955) proposed that either cell 5 or one of the small cells is responsible for initiation of a normal burst; but Hagiwara and Bullock (1957) attributed burst initiation to two of the small cells.

Anomolous Spontaneity

Although the burst activity in the cardiac ganglion normally is initiated by one of the posterior cells - probably one of the small cells, Maynard (1955) observed that complete removal of these cells did not alter significantly the burst activity in the remaining cells (i. e., in cells 1, 2, 3 and 4). In fact, preparations with as few as three large cells often continued to produce bursts. In some apparently damaged preparations, two independent bursts were seen, one including only spikes from small

cells, the other including spikes from both small and large cells. Occasionally single neurons produced long independent runs of periodic spikes, particularly when other cells were silent. When isolated, some of the large cells tended to produce spikes at a constant frequency of as much as 15 spikes per second.

Bullock and Terzuolo (1957) also found evidence of independent runs in the intracellular potentials of the large cells. Occasionally periodic, small epsp's appeared in the interburst interval. It was not clear whether these epsp's were the result of spikes in the small cells or in a spontaneous large cell such as cell 3. The fact that cell 3 usually was producing spontaneous spikes, while the small interburst epsp's were rare, indicates that cell 3 probably was not responsible for the epsp's. Another large cell may have been responsible, however.

Watanabe (1958) applied anaesthetics to the posterior pool of cells, which includes the four small cells and cell 5. In some preparations this permanently blocked all further electrical activity in the ganglion. In other preparations, however, a slow oscillatory potential appeared in the large cells, spreading among them through their electrotonic connections. The frequency of oscillation was approximately one cycle per second; and in the case presented by Watanabe (1958, p. 314), the oscillations appear to have originated in cell 3. This is consistent with the results of Bullock and Terzuolo (1957) who observed two-cycle-per-second oscillations in cell 3. It does not explain completely Maynard's observation, on the other hand, of continuous independent runs at frequencies from 2 to 15 spikes per second.

Conclusion

The cardiac ganglion seems to comprise two types of cells, those that are innately spontaneous and those that are innately quiescent. Burst of spikes in the ganglion apparently are initiated by one of the former and sustained with the help of the latter. The spontaneous cells include two or more of the small cells and probably cell 3. The quiescent cells may include cells 1, 2, 4 and 5. When isolated, the spontaneous cells tend to produce runs of periodic spikes at frequencies from 1/2 to 15 spikes per second. The spike frequency of individual cells during a burst is usually higher than 15 spikes per second, however; so some acceleration must be present during the early phases of a burst.

One important question about the operation of the cardiac ganglion is how the tendency toward periodic spike production in a few cells is transformed into coordinated bursts of spikes from all nine cells. The following discussion includes an examination of this question.

SPONTANEITY IN THE NEURAL ANALOG

The parameters of the SOMA MODEL were adjusted to the values specified in Table 1, so that it represented a patch of squid-axon membrane for large excursions of membrane potential. A steady depolarizing current was applied across the simulated membrane. As this current was increased, oscillations appeared at the node representing the inside of the membrane. With further increase of the current, the oscillations became spikes whose frequency increased monotonically with increasing current. When the spike frequency was approximately 100 spikes per second, it no longer increased. Instead, the spike amplitude diminished and the response reverted to small oscillations. With further increase in the current, the oscillations disappeared. At this point the simulated membrane potential was the equivalent of approximately 30 mv below the resting potential. This sequence of events is shown in the photographs of figure 57.

Periodic activity of the type shown in figure 57 can be induced in the SOMA MODEL by any mechanism that tends to depolarize the membrane and prevent maintenance of the resting potential. The system described by the Hodgkin-Huxley data is inherently unstable and includes several possible oscillatory modes. Many of these have been described in considerable detail in an earlier publication (Lewis, 1965). When the parameters of the SOMA MODEL are adjusted to match the Hodgkin-Huxley data, the minimum frequency of the subthreshold oscillations is approximately 50 Hz. Since a spike does not necessarily occur on every cycle of the oscillation, the minimum spike frequency is considerably less than 50 spikes per second. The minimum frequency with stable operation, however, is approximately 16 spikes per second. All of these frequencies are higher than those observed in the cardiac ganglion of the lobster.

The following discussion concerns parametric changes of the SOMA MODEL that make its spontaneous operation conform to that of cardiac ganglion cells.

Variations of the Time Constants of Potassium Conductance

The parameter settings listed in Table 1 for the SOMA MODEL are intended to make it correspond to a patch of squid-axon membrane for large excursions of the membrane potential, such as spikes. For depolarizations of less than 30 mv, the time constant, τ_n, for the increase of of the potassium conductance variable (n) is too small by a factor of five. The time constant is correct for small depolarizations when R5, R6 and R7 in the potassium circuit are equal to 1000 Ω, 2000 Ω and 3000 Ω, respectively.

With τ_n in the SOMA MODEL increased from 1 ms to 5 ms, the spike duration is approximately doubled and slope of the repolarizing phase is considerably reduced (see figure 58). The minimum frequency for subthreshold oscillations is reduced from 50 Hz to approximately 25 hz, but these oscillations are much less stable and are more likely to develop

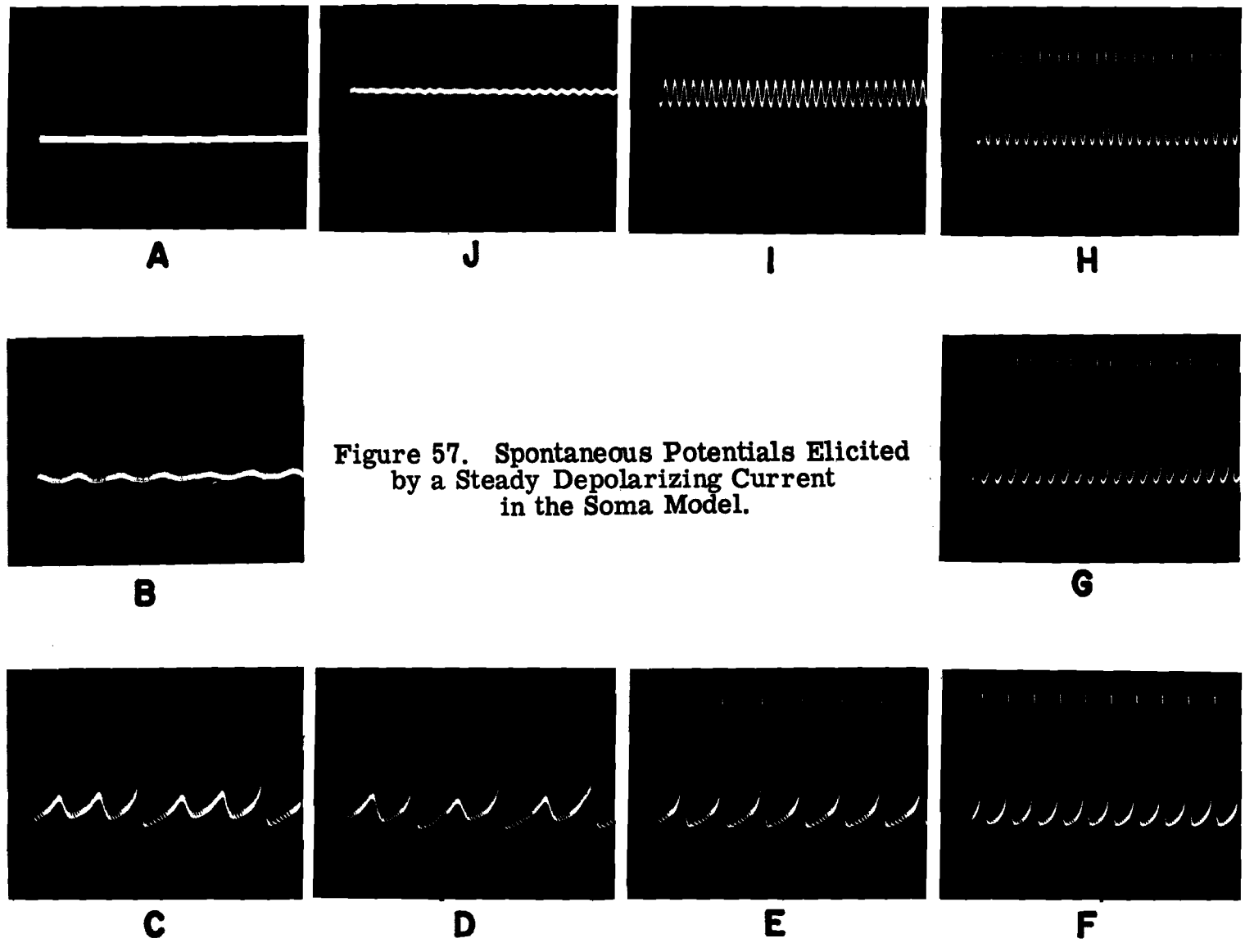

Figure 57. Spontaneous Potentials Elicited by a Steady Depolarizing Current in the Soma Model.

into full spikes. This instability is due to the inability of the slow potassium conductance to overtake and arrest the regenerative action of the sodium conductance before the occurrence of a spike. Since with τ_n equal to 5 ms the parameters of the SOMA MODEL are very closely to those specified by Hodgkin and Huxley for small excursions of potential across the squid-axon membrane, subthreshold oscillations in that system also should be unstable.

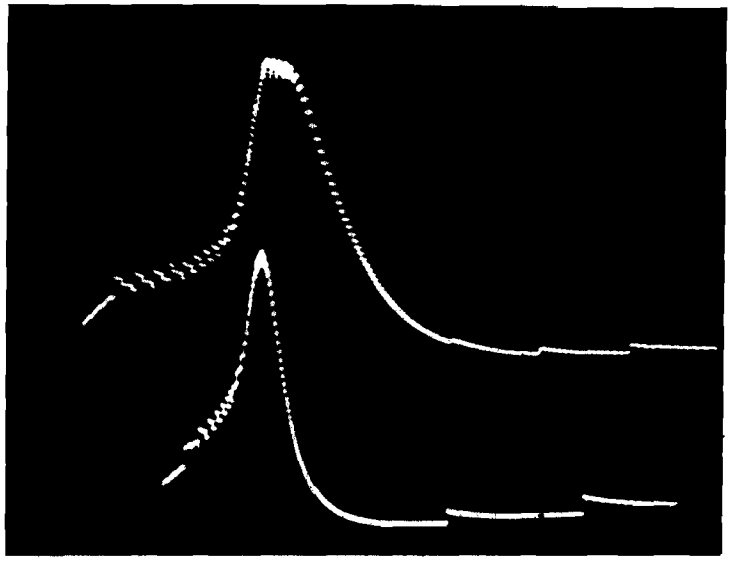

Figure 58. Spike with τ_n Equal to Five Milliseconds (upper trace) Compared to Spike with τ_n Equal to One Millisecond (lower trace).

In the squid axon, the rate of decline of the potassium conductance was nearly constant at approximately 0.20 ms^{-1} both for excursions of membrane potential less than 30 mv and for rapid repolarization to potentials within 30 mv of the resting potential (Hodgkin and Huxley, 1952 b, p. 492). In the SOMA MODEL, this rate constant is treated in terms of its reciprocal, the time constant τ_n* in Table 1. The value of τ_n* according to the Hodgkin-Huxley data is 5 ms. With τ_n (the time constant for the increase of potassium conductance) set equal to 5 ms, τ_n* (the time constant for decline of the potassium conductance) was varied from 5 ms to 80 ms. The effects of this variation on spontaneous spikes are shown in figure 59. The spike frequency decreased with increasing magnitudes of τ_n*, from 50 spikes per second when τ_n* = 5 ms to 7 spikes per second when τ_n* = 80 ms. The spike frequency was not linearly related to τ_n* since a 16 fold increase in τ_n* brought a 7-fold reduction in frequency.

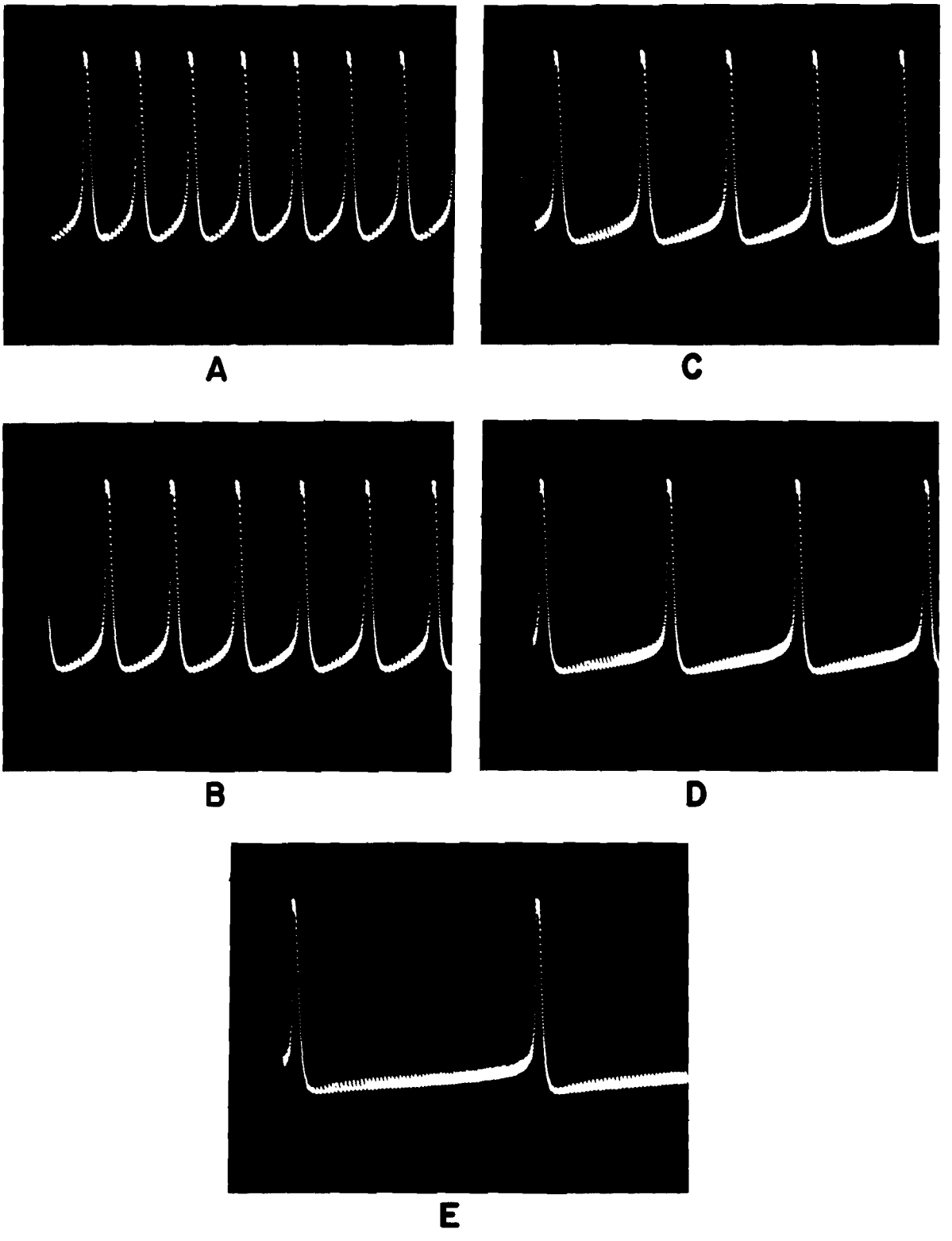

Figure 59. Spontaneous Spikes for Various Magnitudes of τ_n*.

The magnitudes of τ_n* were as follows: A. - 5 ms; B. - 10 ms; C. - 20 ms; E. - 40 ms; E. - 80 ms.

With τ_n and τ_n^* both equal to 5 ms, the simulated membrane capacitance in the SOMA MODEL was increased to 1.0 microfarad (the equivalent of 4 microfarads per sq cm in the squid axon). A steady depolarizing current applied to the model produced the oscillatory potentials shown in figure 60A. These potentials could be described as attenuated spikes, since they exhibited an all-or-nothing characteristic. In other words, this periodic waveform was stable in form and amplitude, and changed only in frequency as the magnitude of the depolarizing current was varied. Once again τ_n^* was varied from 5 ms to 80 ms, and the effects are shown in the remaining photographs of figure 60. The amplitude of the waveform was constant and its all-or-nothing nature persisted until τ_n^* was increased beyond 20 ms. When τ_n^* was 40 ms, the amplitude of the oscillations was reduced to the equivalent of approximately 20 mv in the squid axon, and their frequency was approximately 8Hz.

With τ_n and τ_n^* both equal to 5 ms, the simulated membrane capacitance was increased again, this time to 2 microfarads (8 microfarads per sq cm in the squid). The amplitude of the oscillations was completely graded, depending on the magnitude of the depolarizing current. The frequency of these oscillations increased monotonically with increasing current. Their amplitude, on the other hand, was a nonmonotonic function of depolarizing current, increasing as the current was increased from low magnitudes, passing through a maximum equivalent to approximately 30 mv, then decreasing as the current was increased further. The amplitude of these oscillations is plotted against their frequency in figure 61.

The depolarizing current was fixed at a magnitude that induced a 8-Hz oscillation with an amplitude equivalent to approximately 20 ms, as shown in figure 62A. Then τ_n^* was increased from 5 ms to 80 ms, and the results also are shown in figure 62. As τ_n^* was increased, the amplitude of the oscillation increased, and the frequency decreased. When τ_n^* was equal to 80 ms, the amplitude was equivalent to approximately 30 mv and the frequency was approximately 4 Hz.

In their mathematical formulation of the squid-axon data, Hodgkin and Huxley (1952 d) assumed that the rate of rise and the rate of fall of the potassium conductance were related. The solution of their equation for the potassium conductance variable, n, in response to a sudden change in membrane potential is

$$22) \qquad n = n_\infty - (n_\infty - n_o)\, e^{-t/\tau_n}$$

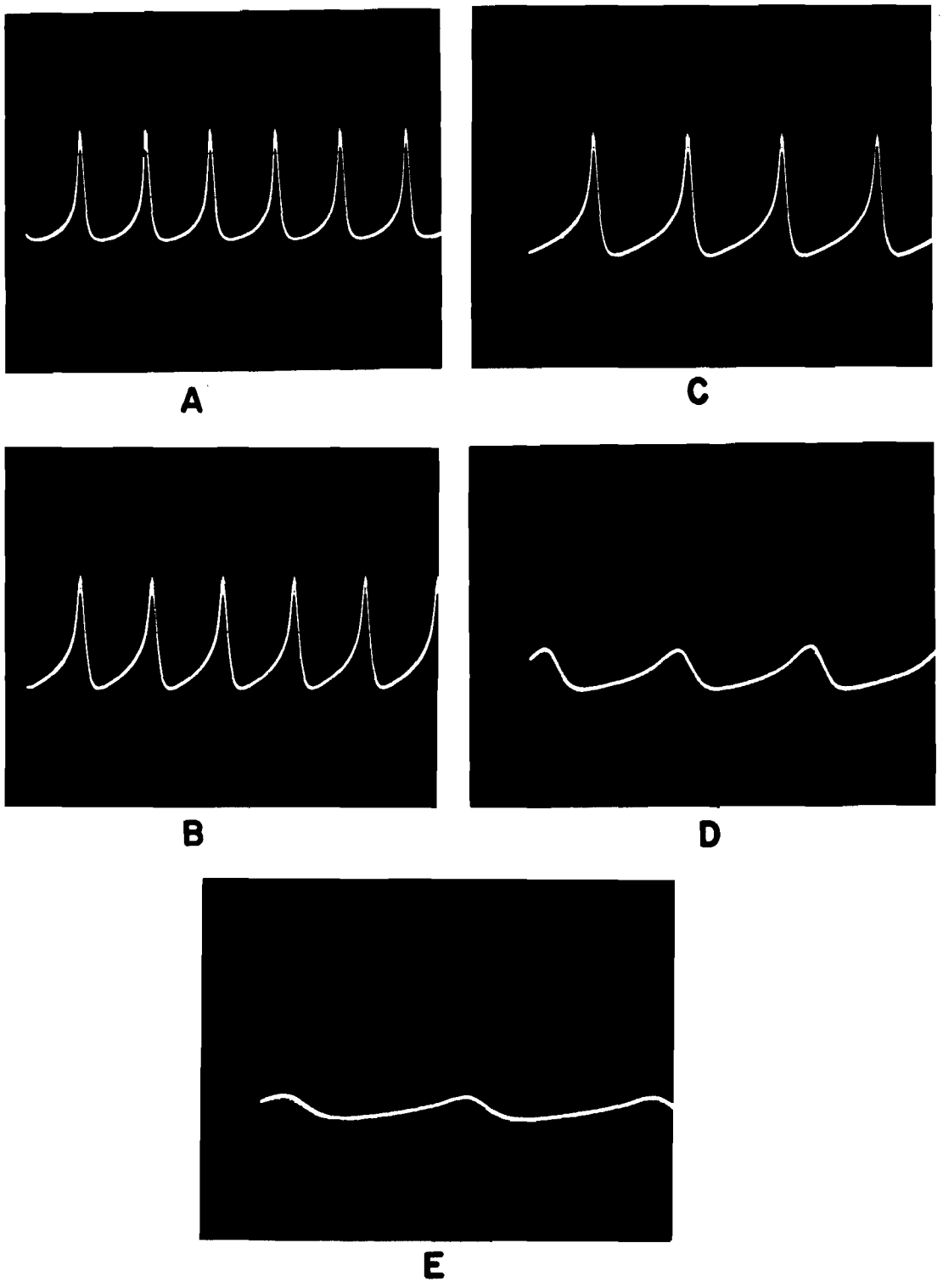

Figure 60. Spontaneous Spikes for Various Magnitudes of τ_n* with C_m Equal to Four Microfarads per Square Centimeter.

The magnitudes of τ_n* were as follows: A. - 5 ms; B. - 10 ms; C. - 20 ms; D. - 40 ms; E. - 80 ms.

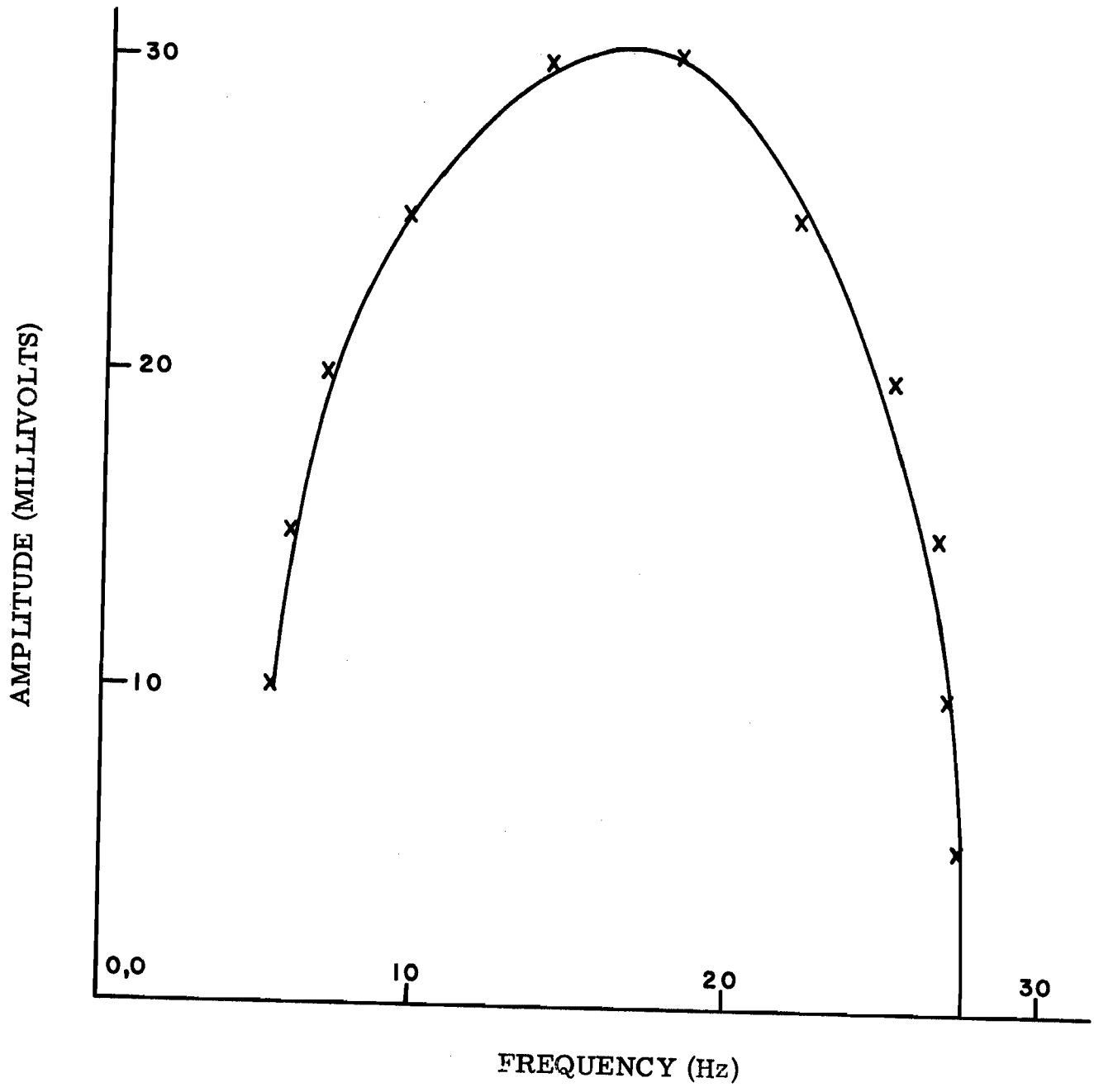

Figure 61. Amplitude of Subthreshold Oscillations in the Soma Model as a Function of Frequency.

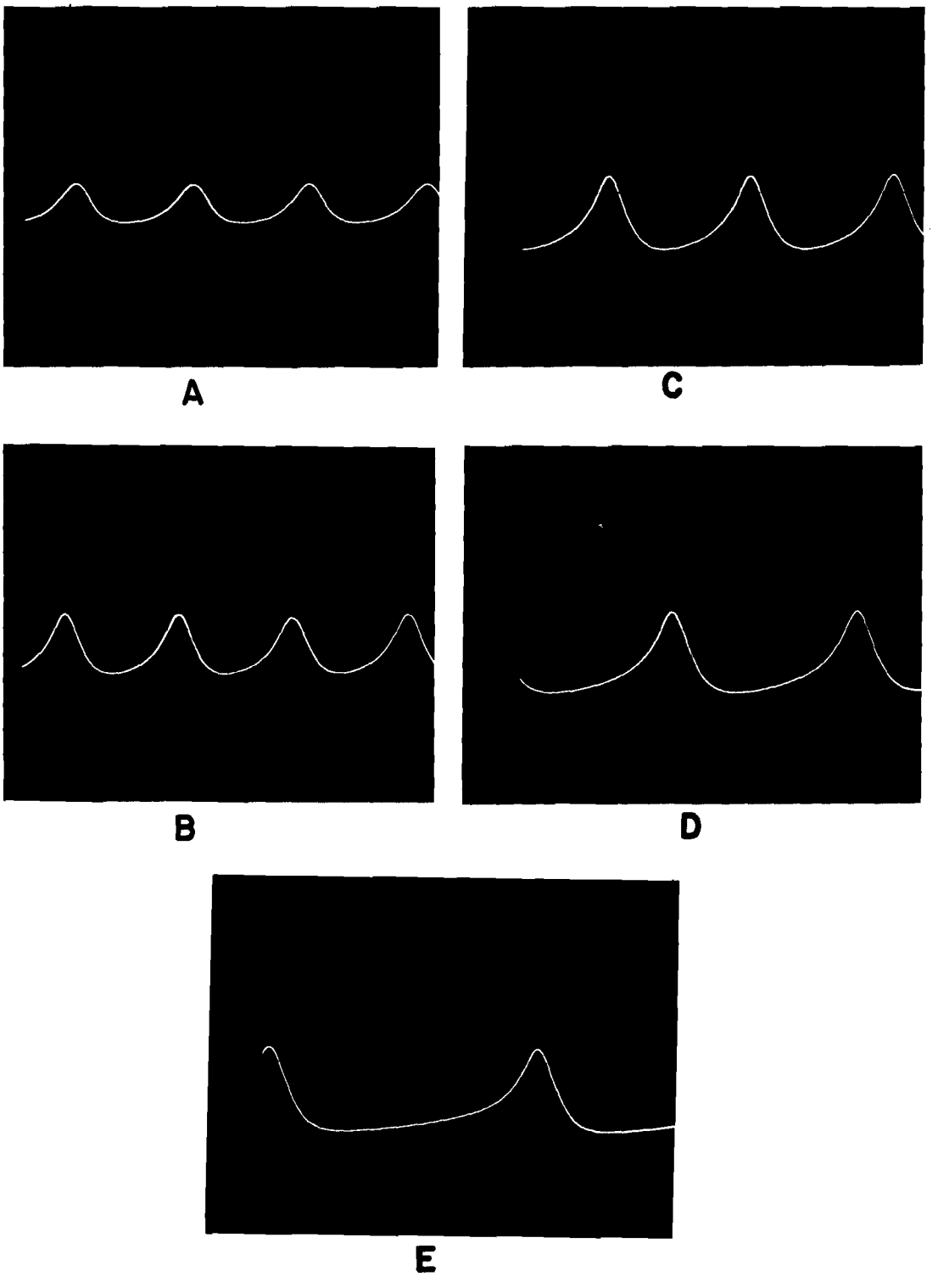

Figure 62. Subthreshold Oscillations in the Soma Model: Dependence on τ_n* when C_m Equals Eight Microfarads per Square Centimeter.

The magnitudes of τ_n* were as follows: A. - 5 ms; B. - 10 ms; C. - 20 ms; D. - 40 ms; E. - 80 ms.

where n_o is the initial value of n, and n_∞ is its final value. They related the potassium conductance to n by

$$23) \qquad G_K = \bar{g}_K n^4$$

where $\bar{g}_K$ is a constant. In the case of depolarizations, n_∞ is greater than n_o, so the potassium conductance has the same form as $(1 - e^{-t/\tau_n})^4$, which is an inflected rise to a constant value, 1.0. In the case of repolarization, n_o is greater than n_∞, so the potassium conductance has the same form as $(a + be^{-t/\tau_n} + ce^{-2t/\tau_n} + de^{-3t/\tau_n} + ge^{-4t/\tau_n})$, which is a noninflected fall to a constant value, a. For repolarization from a highly depolarized state, all terms but the last one become vanishingly small; and the fall is described by a simple exponential, ge^{-4t/τ_n}. In this case the time constant for decreasing potassium conductance is $\tau_n/4$. The relationship between the rate of rise and the rate of fall of the potassium conductance in the Hodgkin-Huxley equations thus depends on the exponent in Equation 23. Larger exponents actually provide a better match for the data on the inflected rise of potassium (Hodgkin and Huxley, 1952 d). The relationship between rates is therefore doubtful, and independent variation of τ_n and τ_n* in the SOMA MODEL is at least partially justified.

Independent variation of τ_n* did not provide the behavior that was sought in the SOMA MODEL, however. The minimum frequency of subthreshold oscillation in the cardiac ganglion was approximately 1 Hz; the minimum frequency observed in the experiment described in this section was approximately 4Hz, and that occurred with τ_n* equal to sixteen times the value specified by Hodgkin and Huxley.

Variations of the Sodium Inactivation Time Constants

All of the parameters of the SOMA MODEL except τ_n were adjusted to the values specified by Hodgkin and Huxley for the squid axon and outlined in Table 1; τ_n was adjusted to 5 ms, the value specified by Hodgkin and Huxley for small excursions of membrane potential. A steady depolarizing current was applied across the simulated membrane, inducing periodic spikes at a frequency of approximately 40 spikes per sec. The individual spikes were slightly more prolonged than those generated by the model when τ_n was adjusted to its value for large excursions of membrane potential. The time constant (τ_r) of recovery from inactivation of the sodium conductance was increased in three steps from 12 ms (see Table 1) to 100 ms; the effects are shown in figure 63. Although the duration of the individual spike was decreased very slightly as τ_r was increased, the

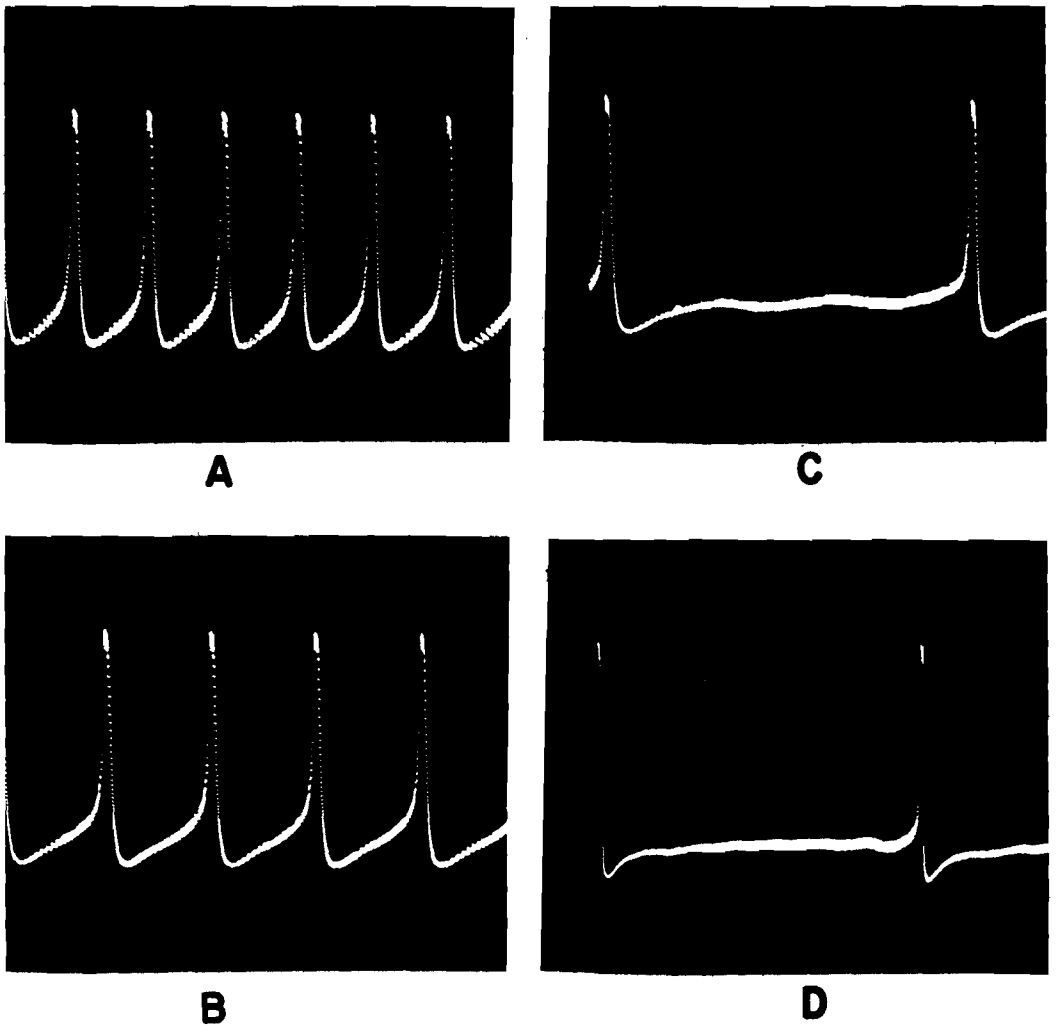

Figure 63. Spontaneous Spikes in the Soma Model: Dependence on τ_r.

The magnitudes of τ_r were as follows: A. - 12 ms; B. - 24 ms; C. - 50 ms; D. 100 ms.

over-all appearance of the spike virtually was unchanged. The spike frequency, on the other hand, was changed considerably, decreasing monotonically 40 spikes per sec to 4 spikes per sec as τ_r was increased from 12 ms to 100 ms.

With τ_r readjusted to 12 ms, the simulated membrane capacitance was increased to 2 microfarads, which corresponded to 8 microfarads per sq cm in the squid axon. In this case, the depolarizing current produced periodic subthreshold oscillations instead of spikes. τ_r was increased again from 12 ms to 100 ms, and the effects are shown in figure 64. The frequency of oscillation decreased monotonically with increasing values of τ_r, but the relationship was not linear. The frequency decreased from 10 Hz to 4 Hz, while τ_r was increased from 12 ms to 100 ms.

Finally, both time constants of sodium inactivation were varied simultaneously. Before each measurement, the voltage-dependent time constant of inactivation (τ_i in Table 1) and the time constant of recovery from inactivation (τ_r) both were increased or decreased by the same factor from their values specified by Hodgkin and Huxley. The factor was varied from measurement to measurement, and the results are shown in figure 65. In the case of figure 65A, both time constants were one-fourth the magnitudes determined for the squid axon (see Table 1). A steady depolarizing current applied to the model elicited periodic spikes whose amplitudes were approximately 60% that of a full spike in this sytem. The spike frequency in this case was approximately 40 spikes per sec. In the case of 65B, the time constants were one-half their squid-axon values. The spikes now were nearly full size, but their frequency was still approximately 40 spikes per sec. Figure 65C shows the periodic spikes when both time constants were equal to their squid-axon values; and 65D through G shows the effects of increasing these time constants to 2-, 5-, 10- and 20- times the squid-axon values. As these time constants were increased, the spikes became prolonged, exhibiting plateaus, and the spike frequency was diminished. In the case of figure 65G, for example, the spike duration was nearly 10 ms and the frequency was approximately three spikes per sec.

The principal effect of increasing the time constant of inactivation was to prolong the spike. This effect is certainly not unexpected, since sodium inactivation is an important part of the recovery processes that terminate a spike. When this time constant was decreased to values considerably below its value in the squid axon, on the other hand, the spikes failed to reach their full amplitude. This is simply because the sodium conductance was effectively inactivated before the regenerative depolarization was completed. Increasing the time constant of recovery from inactivation had the opposite effect. The residual inactivation at the time of a spike tended to increase as τ_r was increased. This residue shortened the time required for inactivation and thus tended to shorten the spike duration. The residue also was increased as the spike frequency increased. This effect is evident in the photographs of figure 66. In this case the spikes

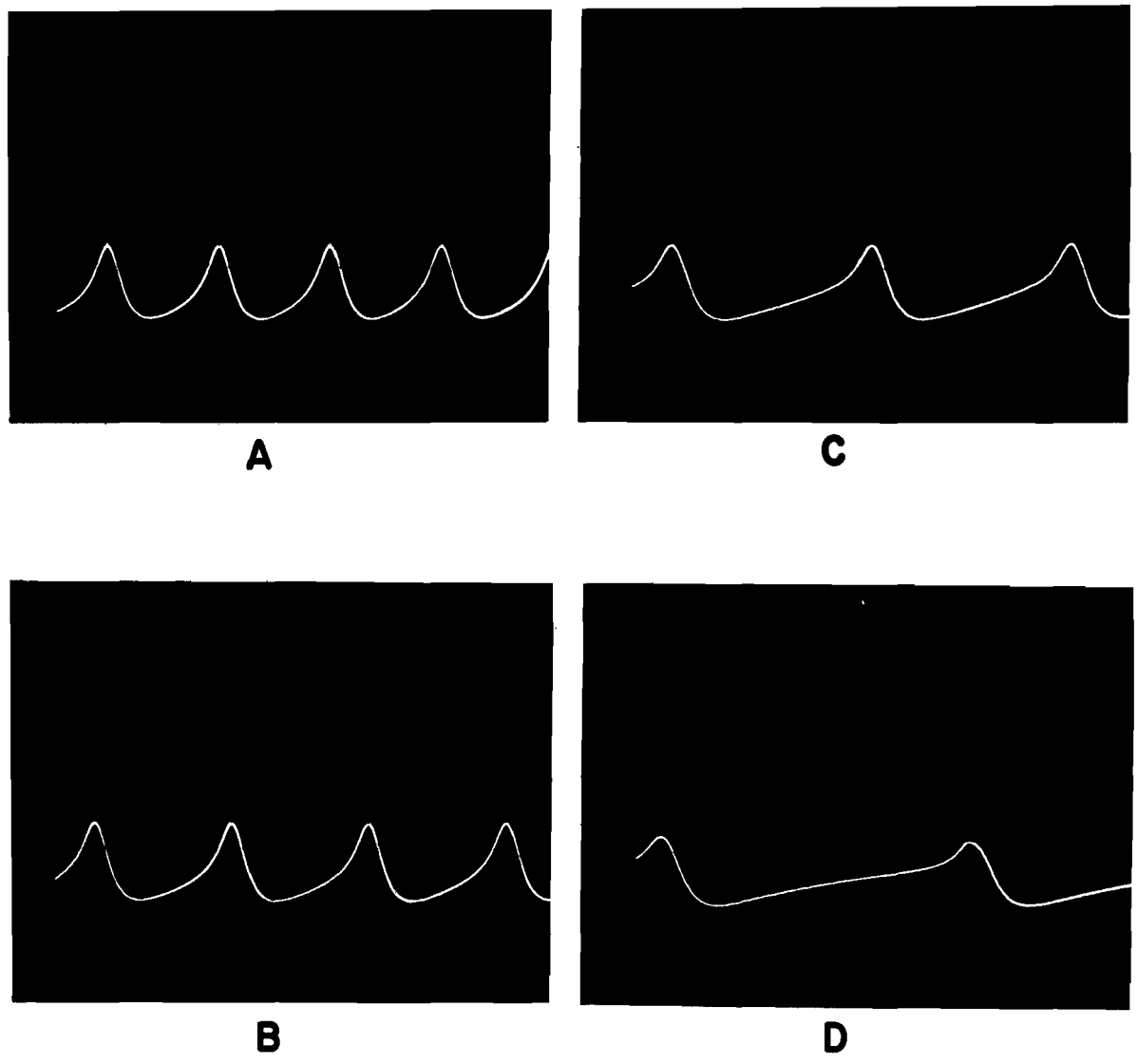

Figure 64. Spontaneous Oscillations in the Soma Model: Dependence on τ_r when C_m Equals Eight Microfarads per Square Centimeter.

The magnitudes of τ_r were as follows:

A. - 12 ms; B. - 24 ms; C. - 50 ms;
D. - 100 ms.

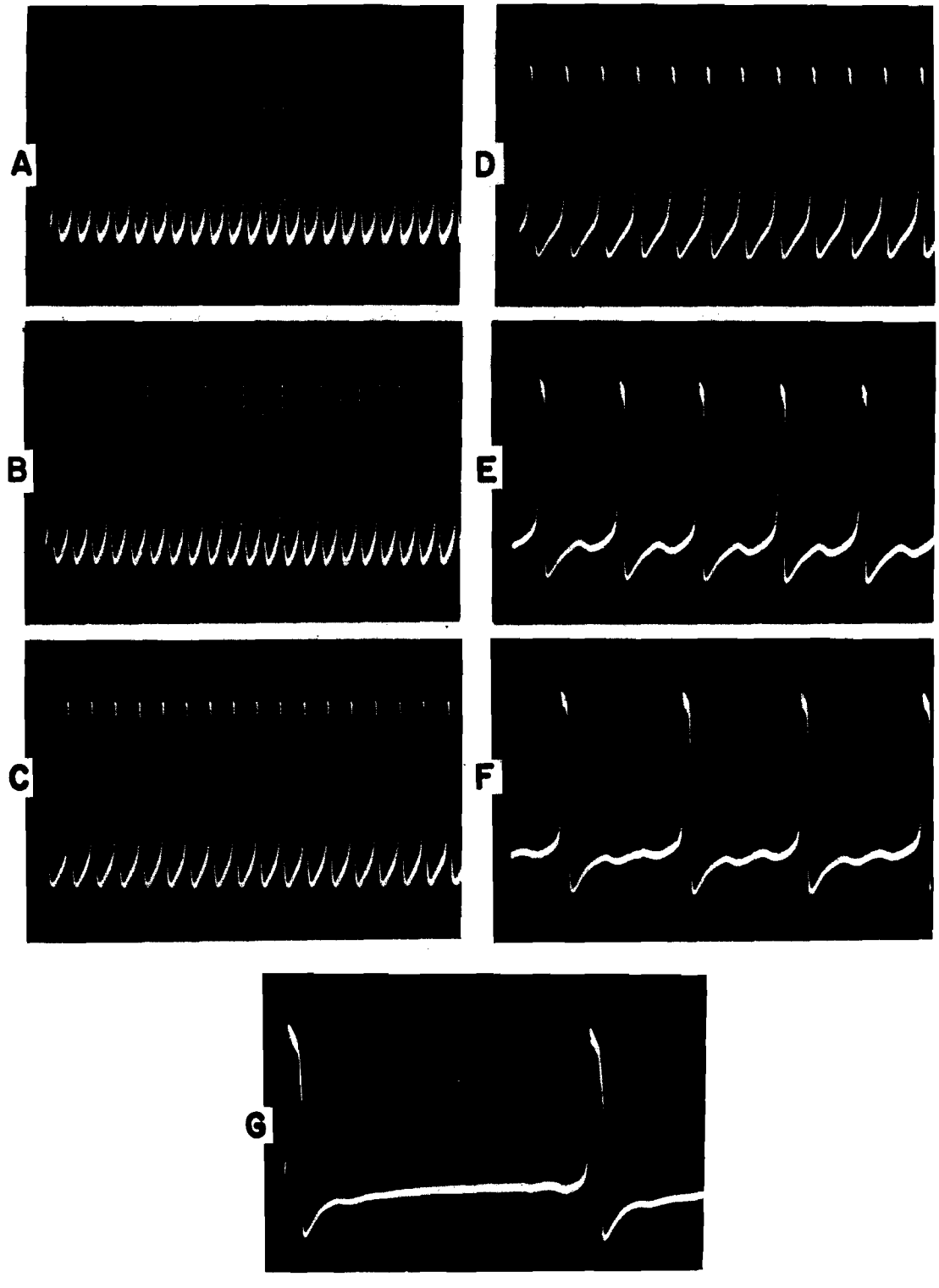

Figure 65. Spontaneous Spikes in the Soma Model: Dependence on Both Time Constants of Sodium Inactivation.

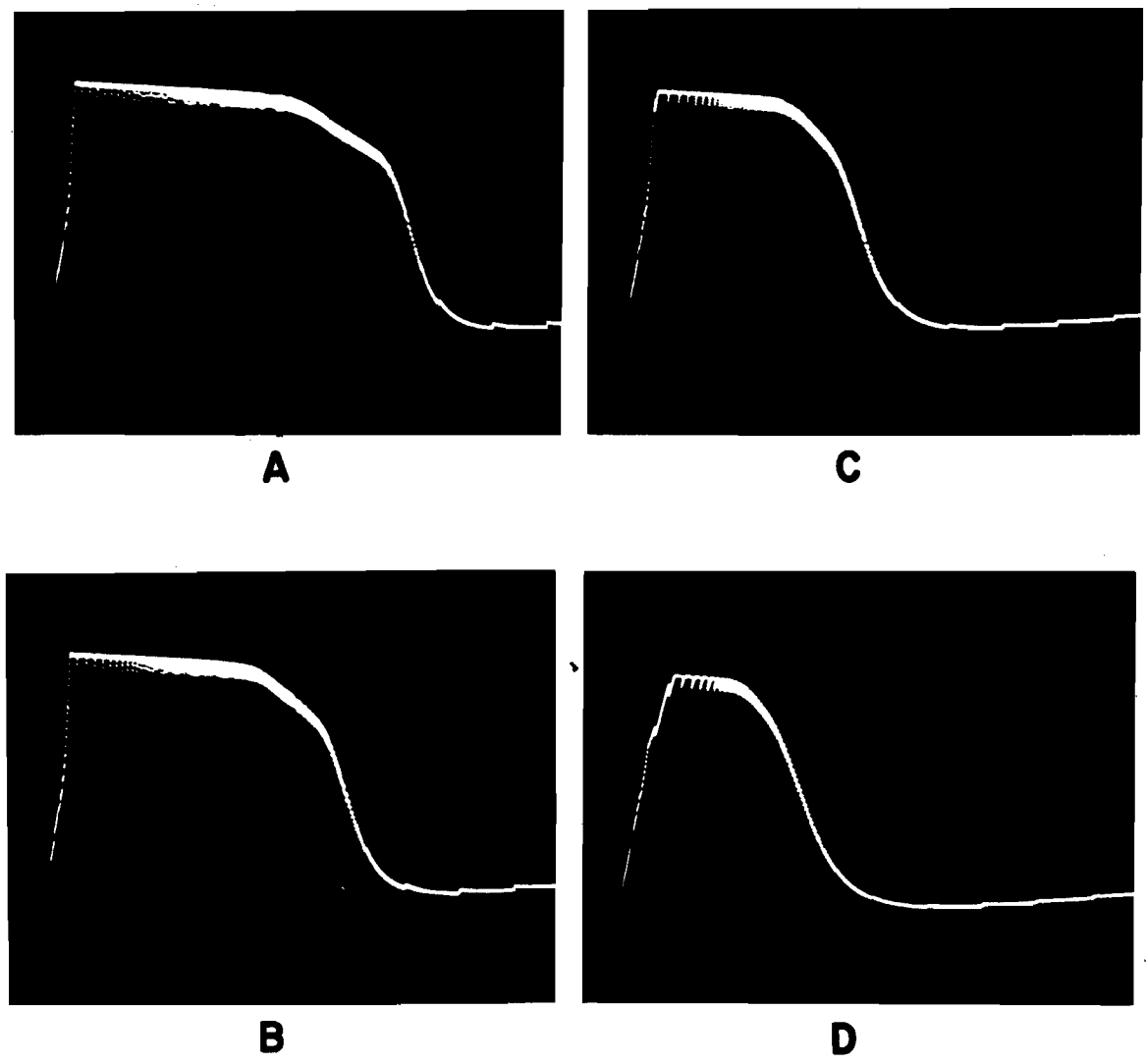

Figure 66. Plateau Potentials in the Soma Model: Dependence on Frequency.

Frequencies were as follows: A. - 1 Hz; B. - 10 Hz; C. - 20 Hz; D. - 40 Hz.

were elicited by a pulse source with controllable frequency rather than by a steady depolarizing current. As the spike frequency was increased, the spike width decreased from approximately 12 ms to approximately 5 ms.

Once again reasonable variation of the parameters did not provide the low frequency oscillations that were observed in the cardiac ganglion. Increasing τ_r to eight times its magnitude in the squid axon decreased the frequency of oscillation to 4Hz in the SOMA MODEL; but the frequency of oscillations in the cardiac ganglion is as low as 1 Hz.

Combined Parameter Variations

For oscillations in the SOMA MODEL that can be classified as subthreshold and graded, the parameters most effective in determing frequency are τ_r and τ_n*. These parameters have been increased to magnitudes many times the values specified in the Hodgkin-Huxley data, but the resulting frequencies of oscillation still have been considerably higher than the minimum frequencies in the cardiac ganglion. Now we shall describe some rather drastic measures that were taken in attempts to force the SOMA MODEL to oscillate at frequencies close to 1 Hz.

When τ_n* and τ_r are adjusted to the values specified by Hodgkin and Huxley, the SOMA MODEL is unable to sustain oscillations when the simulated membrane capacitance is equivalent to 20 microfarads or more per sq cm. With increased magnitudes of τ_n* or τ_r, on the other hand, oscillacan be sustained with higher capacitance values. Figure 67 shows photographs of oscillations that occurred in the SOMA MODEL with τ_n* equal to 100 ms and C_M equal to 5 microfarads (equivalent to 20 microfarads per sq cm in the squid axon); all other parameters were adjusted to the values specified in Table 1. The sequence of photographs shows the effects of increasing the steady depolarizing current that elicited the oscillations. The frequency of oscillation increased monotonically with increasing current, but the amplitude was a nonmonotonic function of current. This particular configuration of the SOMA MODEL provided the most stable, low amplitude oscillations that were observed in all of the experiments described up to this point. The minimum amplitude of stable oscillation in this case was equivalent to less than 5 mv in the squid axon. The minimum frequency, on the other hand, still was greater than the 1-Hz objective. Further increase of the membrane capacitance alone did not reduce the frequency significantly.

With the simulated membrane capacitance equal to 20 microfarads per sq cm and τ_n* equal to 100 ms, τ_r was increased to 100 ms. Stable low amplitude oscillations again were observed, and the minimum frequency was reduced to 2 Hz. Figure 68 shows the oscillations in this system and the effects of increasing the steady depolarizing current.

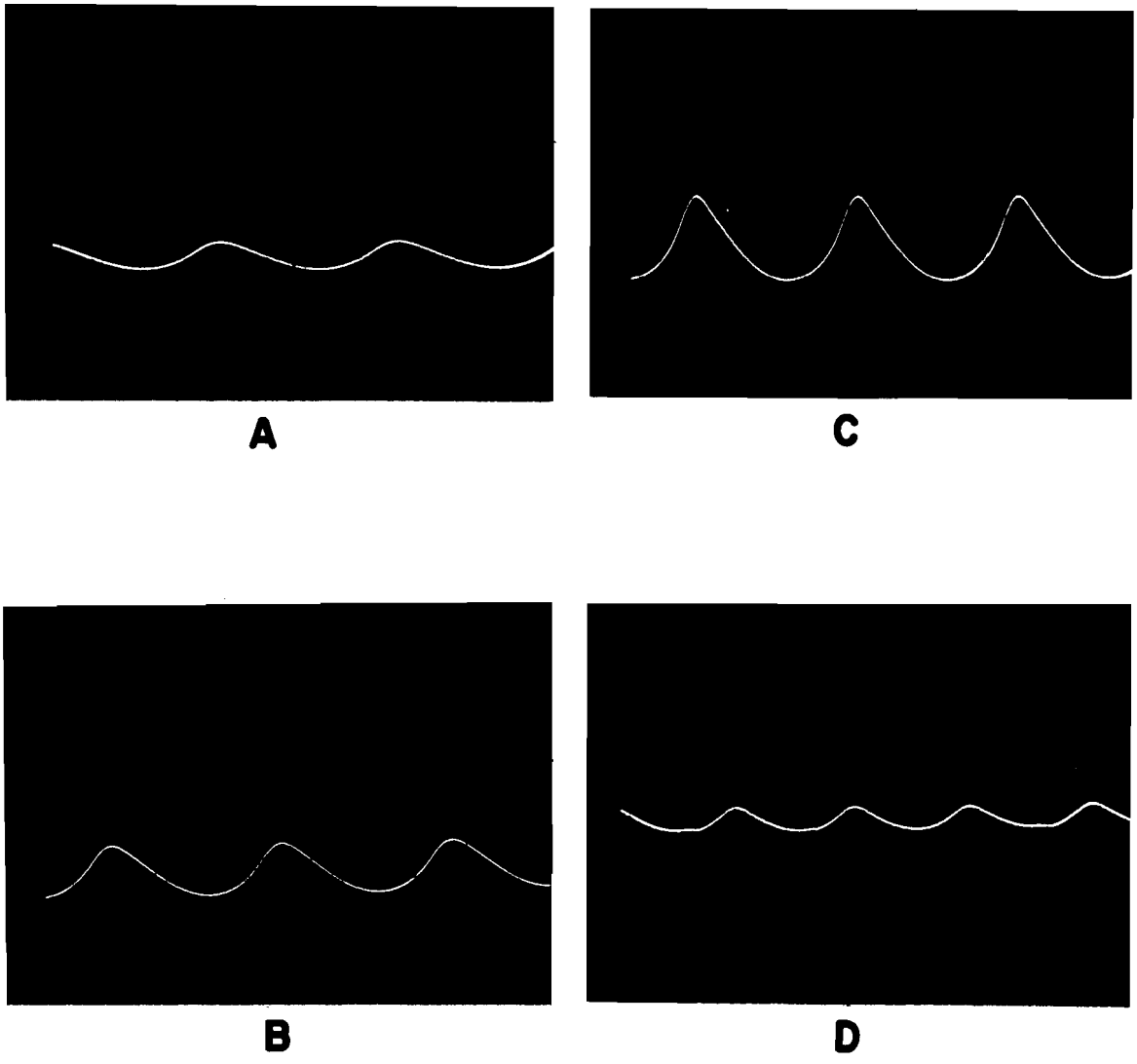

Figure 67. Spontaneous Subthreshold Oscillations in the Soma Model with τ_n* Equal to 100 Milliseconds and C_m Equal to 20 Microfarads per Square Centimeter.

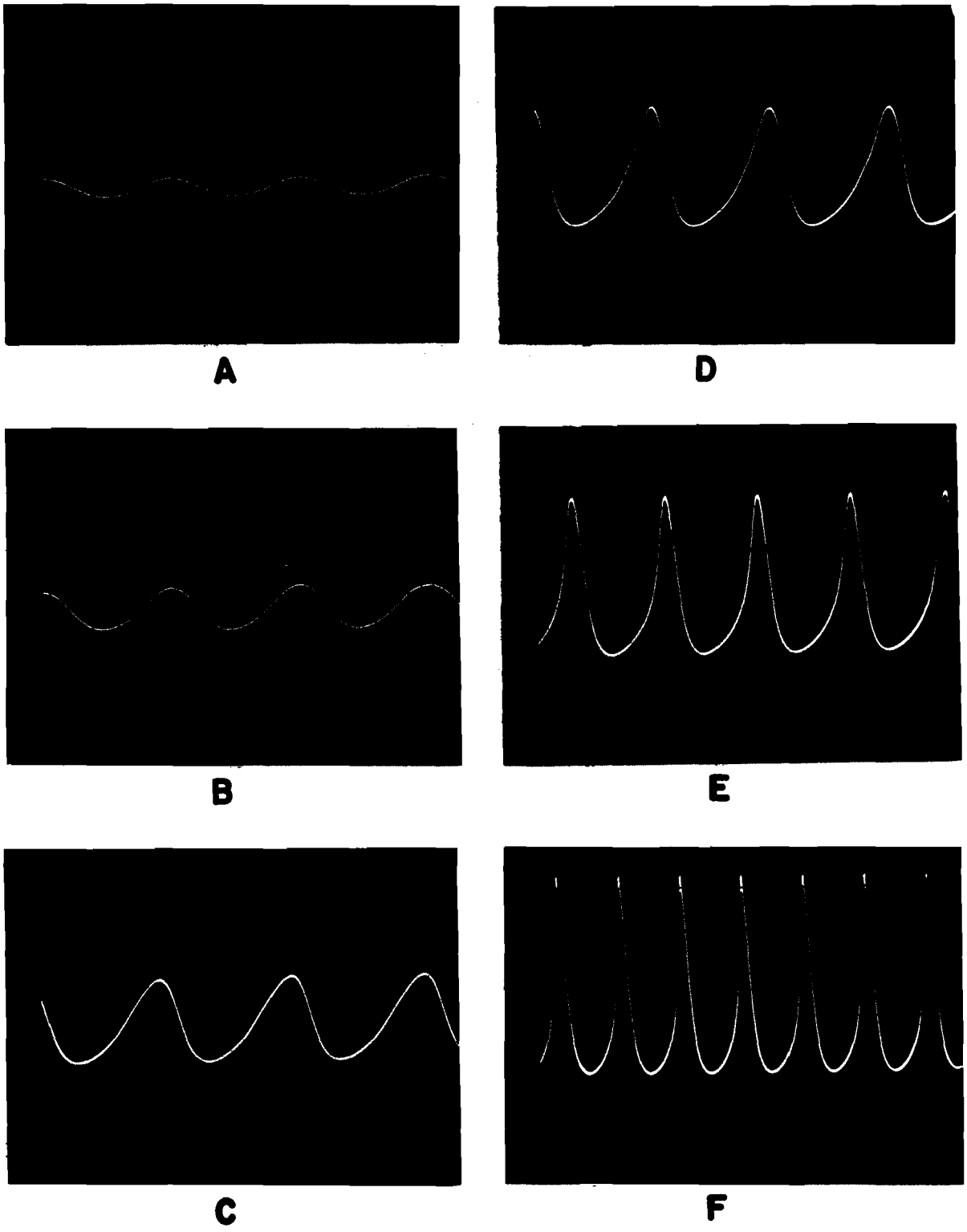

Figure 68. Spontaneous Oscillations in the Soma Model with both τ_n* and τ_r equal to 100 ms and C_m equal to 20 Microfarads per Square Centimeter.

Finally, with the simulated membrane capacitance equal to 20 microfarads per sq cm and τ_n* equal to 100 ms, τ_r and τ_i were both scaled up by the same factors - but with τ_r beginning at 100 ms. Figure 69A shows the oscillations obtained with τ_i equal to the voltage-dependent values specified by Hodgkin and Huxley and τ_r equal to 100 ms. In 69B, τ_i was equal to twice the values specified by Hodgkin and Huxley; τ_r was 200 ms. In 69C through E, τ_r was scaled to values 5-, 10- and 20- times those in the squid axon, and τ_r was equal to 500 ms, 1 sec and 2 sec respectively. In 69E, the frequency of oscillation finally approaches the 1-Hz objective; but the SOMA MODEL no longer bears much resemblance to the squid axon. Its capacitance is twenty times the squid-axon capacitance, and its time constants are 10 to 100 times those of the squid axon.

A resonable conclusion seems to be that the electrically excitable membrane of the squid giant axon would require extensive modifications in order to produce the stable 1-Hz oscillations observed in the lobster neurons. Oscillations at frequencies as low as 4Hz, on the other hand, apparently would require large but defensible changes in single parameters.

LOCATION OF THE PACEMAKER

Location of the Pacemaker in the Cardiac Ganglion

The physiologists who have examined intracellular potentials in the cardiac ganglion generally agree that the point of origin of the spike is not at the soma, but some distance from it - presumably along the axon (see Bullock and Terzuolo, 1957, Hagiwara and Bullock, 1957, Watanabe, 1958). The evidence supporting this contention is convincing; the current-voltage relations of the soma certainly are not conducive to spike generation, and spikes that do appear in the soma are highly attenuated and are not always concurrent with peaks of depolarization. The point of origin of the slow oscillations or pacemaker potentials, on the other hand, is not so easily assessed. Bullock (1958, 1959, 1962) suspected that the processes underlying these oscillations might be completely separate from those involved in spike initiation, and he postulated a separate "pacemaker locus" in or near the soma. The evidence for a pacemaker locus spatially separate from the spike initiator includes the fact that spikes do not occur in a fixed position on the depolarizing peak of the oscillations and, occasionally, the oscillation proceeds through a complete cycle without eliciting a spike.

Location of the Pacemaker in a Two-Patch Model

Two SOMA MODELS were connected together to form a two-patch simulation of a cardiac ganglion cell. One model represented the spike initiator site and all but one of its parameters were adjusted to the values listed in Table 1 for the Hodgkin-Huzley Model. The remaining parameter, τ_n, was adjusted to 5 ms; so the model represented a patch of squid-axon

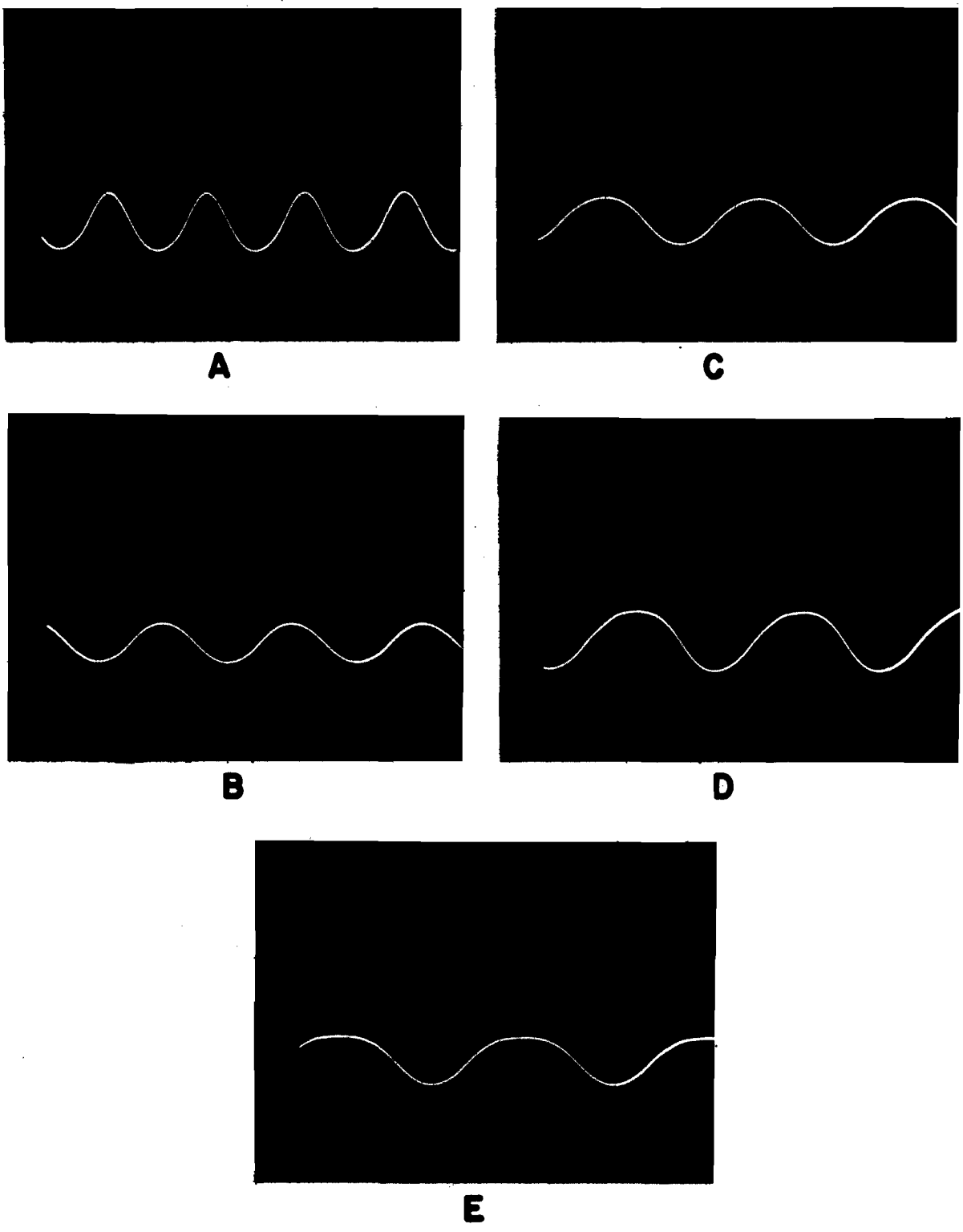

Figure 69. Spontaneous Subthreshold Oscillations in the Soma Model: Dependence on Both Time Constants of Sodium Inactivation.

membrane for small excursions of membrane potential. The other SOMA MODEL represented a cardiac-ganglion soma. The simulated membrane capacitance was set to be equivalent to 8 microfarads per sq cm, a value close to halfway between the limits determined by Hagiwara, Watanabe and Saito (1959) for the soma.

The leakage conductance was doubled and corresponded to the maximum value measured by Hagiwara, et al. τ_n* was adjusted to 100 ms to provide the capability of reasonably low frequency oscillations, and τ_n was adjusted to 5 ms. The remaining parameters of the model were adjusted to the values in Table 1. The configuration of the two models was identical to that shown in figure 22. The nodes representing the outsides of both membrane patches were grounded; the nodes representing the insides were connected together through a resistor, R. In this configuration, the resistances of extracellular current paths are taken to be negligible.

Spontaneous oscillations were induced in the two-patch model by a steady depolarizing current applied either to the spike-initiator patch or to the soma patch. Figure 70 shows typical simulated soma potentials during the oscillations. In the cases of 70A and B, the connecting resistance, R, was 10,000 ohms. 70A shows the soma potential in response to a steady depolarizing current applied to the soma itself. The waveform is nearly sawtoothed, with a frequency of approximately 6 Hz. Attenuated reflections of single spikes can be seen in various positions on the peak of the sawtooth. The spike on each cycle appears to have initiated the resetting of the potential. Figure 70B shows the simulated soma potential in response to a steady depolarizing current applied to the spike initiator. The waveform is noticeably different from that of Figure 70A. Small undamped oscillations precede the spike. The frequency of these oscillations is characteristic of the simulated axon membrane with its short time constants. The simulated soma cannot sustain such high-frequency oscillations.

Figures 70C and D show the simulated soma potential after the connecting resistance was reduced to 5000 ohms. In 70C the depolarizing current was applied to the soma; in 70D it was applied to the spike initiator. The waveforms in these photographs lack the distinctions apparent between those in 70A and 70B. As the resistance was reduced further, the distinctions became even less obvious. In figures 71 and 72, the soma potentials for a 5000-ohm connecting resistance are shown with an expanded time scale. In figure 71, the depolarizing current was applied to the soma. The attenuated spikes appear in various positions on the peaks of the oscillations; and in one case, the oscillation completed a cycle without eliciting a spike. In figure 72, the depolarizing current was applied to the spike initiator. Again the attenuated spikes appear in various position on the peak of the oscillation; in fact in two cases (the third and ninth peaks) the spikes appear after the peak, on the repolarizing phase. Occasionally in this mode, the oscillation completed a cycle without eliciting a spike (see figure 73).

In figure 71, the negative phase following the aborted spike (i. e., the third negative phase) is noticeably smaller in amplitude than the other negative phases; and the interval between the aborted spike and the subsequent spike is shorter than the other interspike intervals. Both of

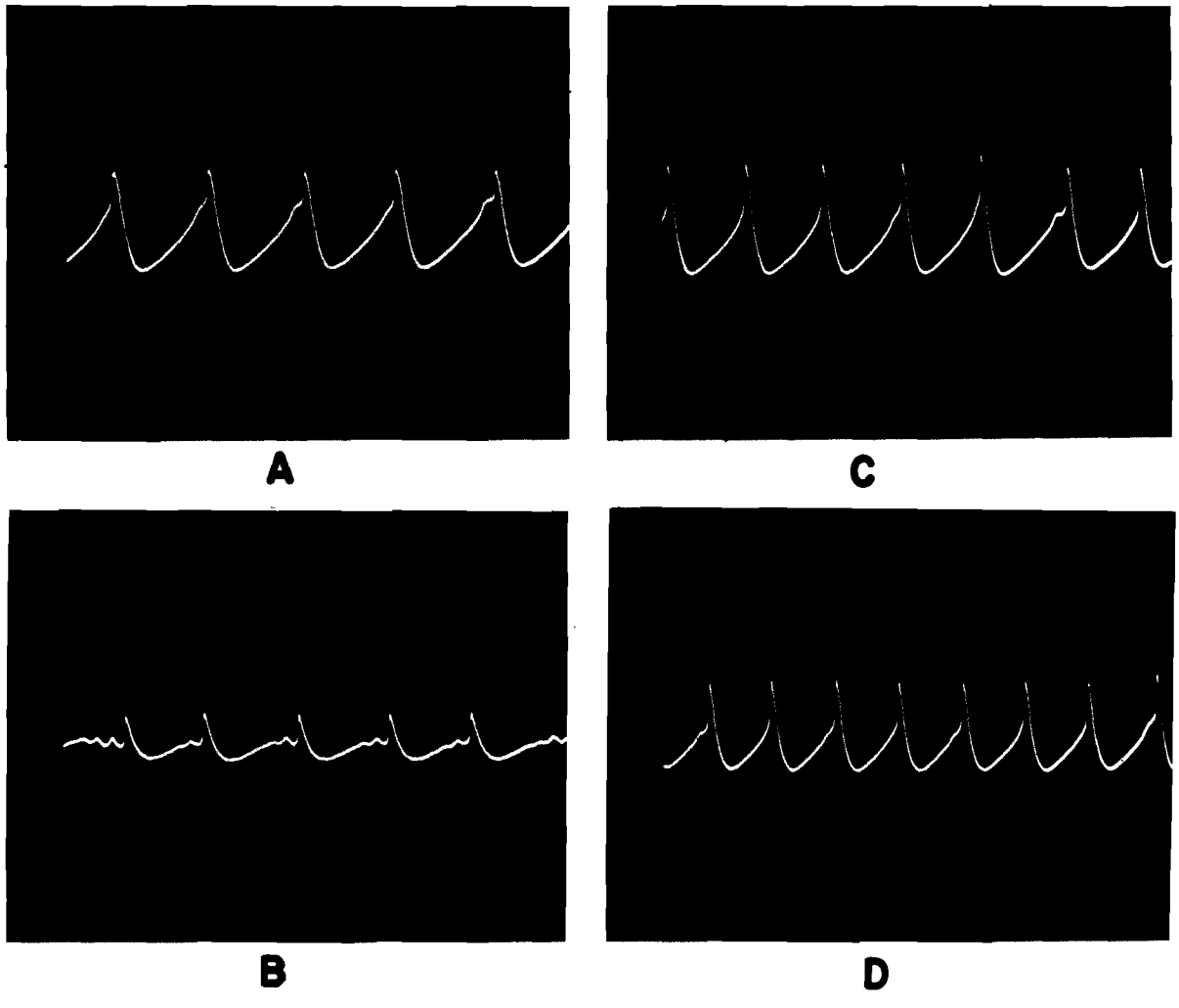

Figure 70. Soma Potentials in a Spontaneously Active Two-Patch Model.

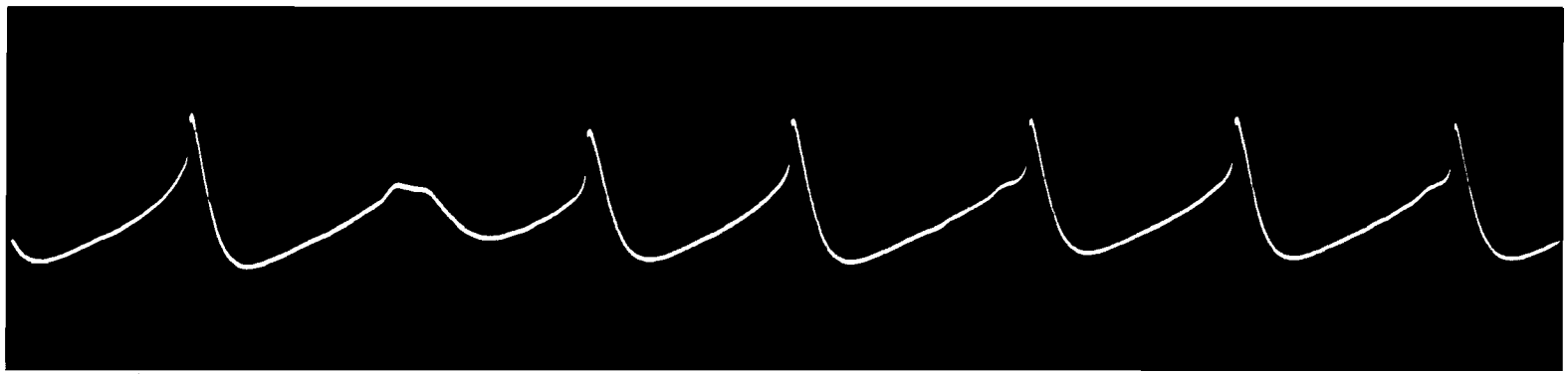

Figure 71. Soma Potentials in a Spontaneously Active Two-Patch Model: Depolarizing Current Applied to Soma.

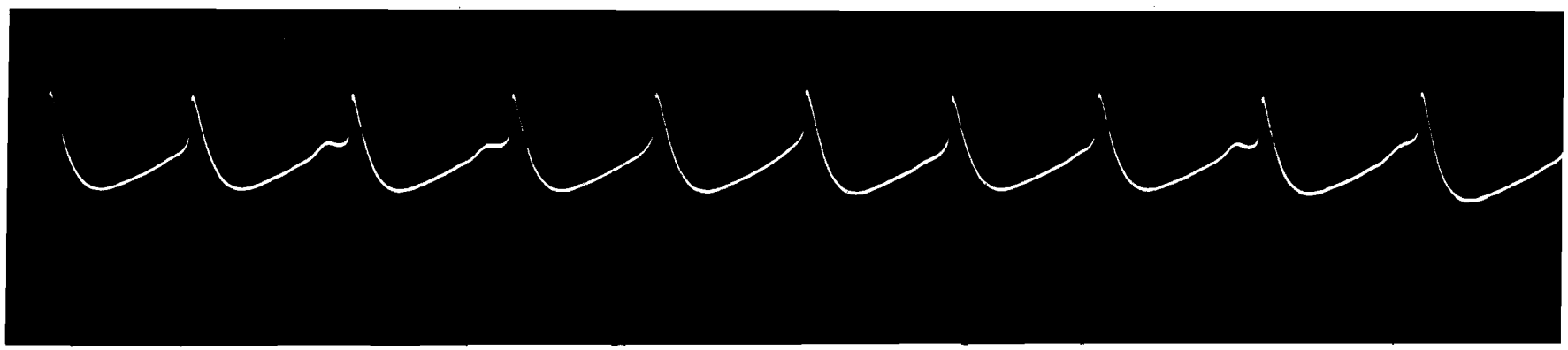

Figure 72. Soma Potentials in a Spontaneously Active Two-Patch Model: Depolarizing Current Applied to Spike Initiator.

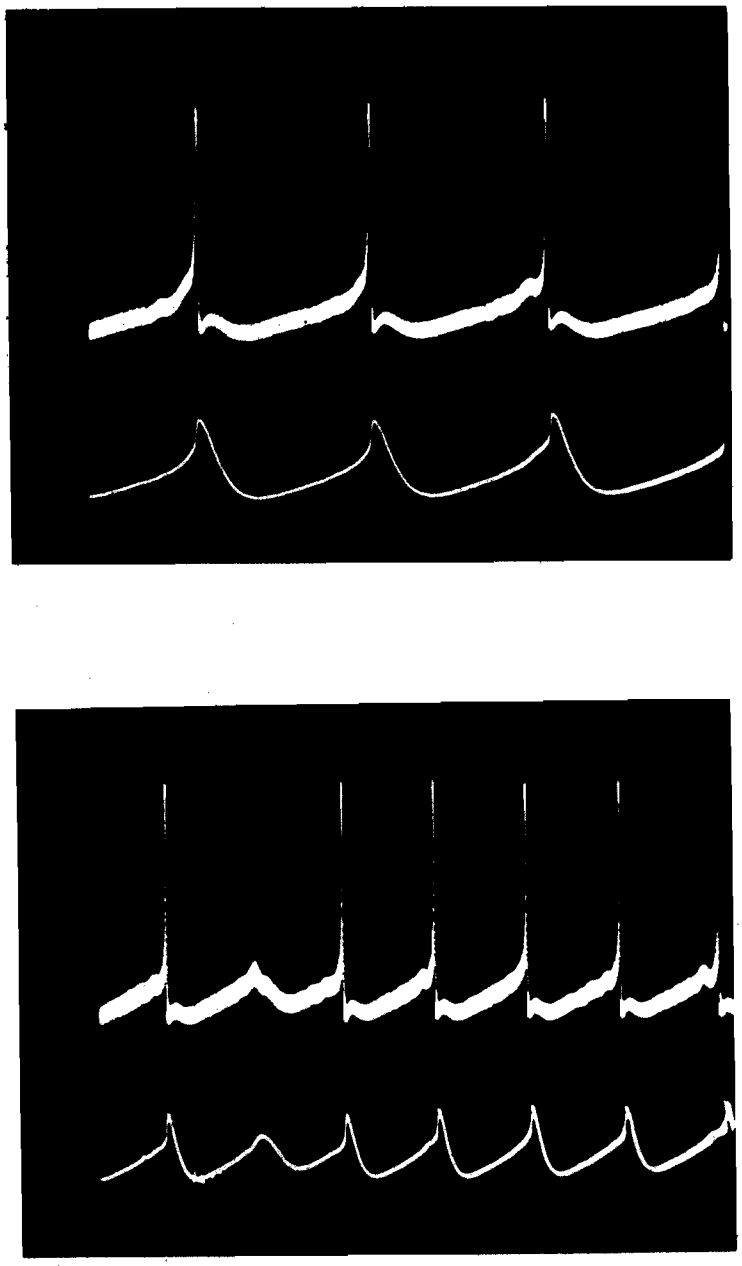

Figure 73. Spontaneous Potentials at the Spike Initiator (upper trace) and Soma (lower trace) of a Two-Patch Model: Depolarizing Current Applied to Spike Initiator.

these phenomena also occur in the cardiac ganglion following an aborted spike (see Bullock and Terzuolo, 1957, p. 350); and both are explained easily in terms of the Hodgkin-Huxley Model. The positive excursion of membrane potential in the case of the aborted spike is much smaller than the other postive excursions. The response of the potassium conductance to the reduced positive excursion is less than it is to the normal excursions. In addition, the degree of sodium inactivation in response to the reduced excursion is less. The reduced potassium conductance leads to the smaller negative phase, and both the reduced potassium conductance and the reduced inactivation lead to the shorter interval.

Figure 73 shows the potentials as they occurred simultaneously at the spike initiator and soma when the depolarizing current was applied to the spike initiator. The connecting resistance in this case was 5,000 ohms. The potential at the spike initiator following each spike is considerably modified from its usual form by the slow potential induced at the soma. Figure 74A shows periodic spikes induced at the spike initiator by the same current that was applied in the case of figure 73, but in this case the simulated soma was disconnected. The loading effect of the soma on the axon is quite apparent; loading reduced the spike frequency on the axon by a factor of ten. Figure 74B shows oscillations in the simulated soma under the same conditions as in figure 71, but with the axon disconnected. These oscillations are reduced in both amplitude and frequency and exhibit no attenuated spikes.

Discussion

When the coupling between soma and spike initiator in the two-patch model was weak, the location of the depolarizing current was apparent from the form of the soma potential. When the coupling was strong, however, the location of the depolarizing current made very little difference in the soma potential. If the pacemaker locus is defined as the region that has a spontaneous, depolarizing transmembrane current, the location of the locus could be very difficult to assess from intracellular recordings.

In the case of strong coupling in the model, both simulated patches strongly influenced the form of the potential at the soma, and one cannot reasonably attribute the potential to the properties of a particular patch.

THE CONSEQUENCES OF ELECTROTONIC INTERCONNECTION

Strong evidence indicates that electrotonic as well as synaptic connections exist among the cells of the lobster cardiac ganglion (Hagiwara, Watanabe, and Saito, 1959, Watanabe, 1958, Watanabe and Bullock, 1960). In general, the electrotonic connections are capable of transmitting only slowly varying or dc potentials and incapable of transmitting spikes. The connections appear to be passive and linear, describable in terms of a series resistance (R_i) between the sending cell and the receiving cell and the membrane resistance (R_m) and capacitance (C_m) of the receiving cell. Hagiwara, et al (1959)

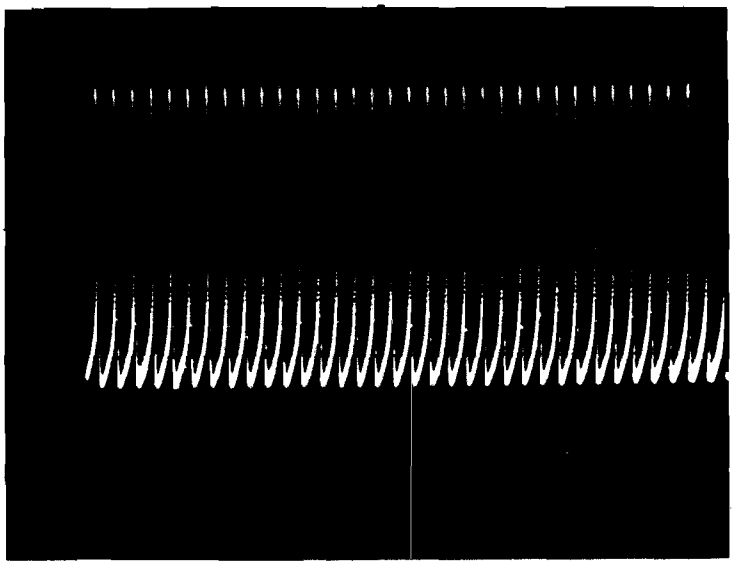

A

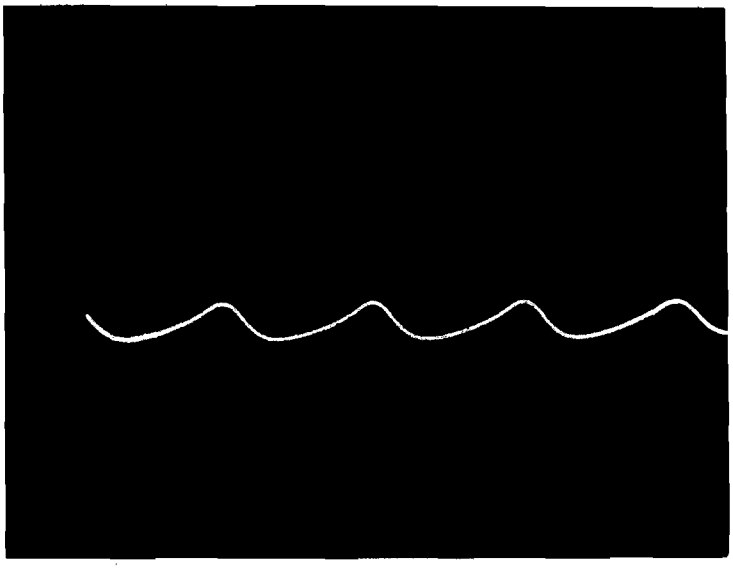

B

Figure 74. Spontaneous Potentials in the Isolated Spike-Initiator Patch (upper trace) and in the Isolated Soma Patch (lower trace).

determined the apparent values of these parameters for several of the electrotonic connections among the cardiac ganglion cells (see Table 3). Since all nine cells presumably are interconnected electrotonically, the values in Table 3 may reflect the effects of both direct and indirect paths between cells as well as the loading effects of several cells connected to the receiving cell. The data gathered by Hagiwara, et al, do not include the effects of size differences among the somata, since the voltage at the sending cell was clamped; and results were independent, therefore, of the size of the sending cell. The photographs published by Watanabe, on the other hand, are indicative of the total effects of one cell on another, including the effects of size; but, clearly, much more data is needed in order to specify quantitatively the electrotonic connections.

TABLE 3

Apparent Parametric Values of Electronic Connections Between Cells of Lobster Cardiac Ganglion.

	1	2	3	4
Distance between two cells	0.3 mm.	0.6 mm	2.0 mm.	1.6 mm.
Ri/Rm	1.27	3.46	4.00	3.25
RiCm	23.1 msec.	83.3 msec.	71.5 msec.	58.1 msec.
RmCm	18.2 msec.	24.0 msec.	17.9 msec.	17.9 msec.

All of the data concerning the electrotonic connections indicate that conduction through these paths is accompanied by considerable attenuation and distributed delay. In the case of oscillatory potentials, the delay is manifest in phase lag (Watanabe, 1958). The oscillatory potentials observed, however, were of very low amplitude (less than 10 mv) and presumably could not elicit sympathetic oscillations in the receiving cell. If sympathetic oscillations were induced, the apparent attenuation and phase lag would have been diminished considerably.

The effects of electrotonic coupling among models in the neural analog facility have been examined in considerable detail. The pertinent results can be summarized in three statements:

1. Electrotonic conduction of low-frequency or d-c potentials is degenerative, generally imposing attenuation and phase lag.

2. The attenuation is reduced, but not eliminated, when sympathetic oscillations are induced at the receiving model. Phase lag on the other hand, may give way to phase lead in the case of sympathetic oscillations.

3. Electrotonic conduction between simulated spontaneously firing spike initiators can produce synchrony of spike generation but cannot produce mutual acceleration of the spike initiators. [1]

CONCLUSIONS: MECHANISMS OF BURST FORMATION

Perhaps the most interesting questions concerning the cardiac ganglion of the lobster are those related to burst formation. The individual neurons, when disconnected from the ganglion, either are completely quiescent or are spontaneously active and produce periodic spikes at a frequency greater than the normal frequency of bursts but less than the frequency of spikes from any one neuron during a burst. Somehow, by virtue of being connected to the other cells in the ganglion, the individual spontaneous cell loses its tendency toward periodic spike production and cooperates instead in the production of bursts. The spike production of the cell is accelerated considerably during a burst and usually is completely quenched during the interburst interval. One should look, therefore, for two types of mechanisms to account for burst formation: an accelerating mechanism and a quenching mechanism.

Since the cardiac ganglion cells apparently are interconnected electrotonically, one might begin by asking whether electrotonic connections can provide acceleration. The experiments conducted with electrotonic connections between models in the analog facility have indicated that in general the answer must be no, electrotonic interconnections cannot provide acceleration. Electrotonic interconnections are basically degenerative, strongly attenuating conducted signals. Acceleration generally requires interconnections that are regenerative and can supply some amplification. Although the conclusion that electrotonic connections are insufficient for acceleration generally should be valid, there is at least one obvious exception: a loop of electrotonically coupled spike initiators. Consider a spike initiator that by itself produces spontaneous spikes at a low frequency. If this were coupled into the racetrack network described in Section V, the first spike from the spontaneous spike initiator could propagate around the loop and initiate a second spike long before the spike initiator normally would have generated the second spontaneous spike. Extending this notion, one might envision a small network of electrotonically interconnected spike initiators in which spikes are conducted continuously back and forth between various nodes in a more or less random fashion. A burst could be initiated in such a network by a single spontaneous spike initiator, and it could terminate when the paths of all spikes in the network were blocked by refractory nodes.

---

[1] A study of electrotonically coupled spike initiators was reported previously under this contract:

Lewis, E. R., "Synchronization in Small Groups of Neurons: a Study with Electronic Models". Presented at the 1966 Bionics Symposium and to be published in Cybernetic Problems in Bionics, New York: Gordon and Breach, (in press).

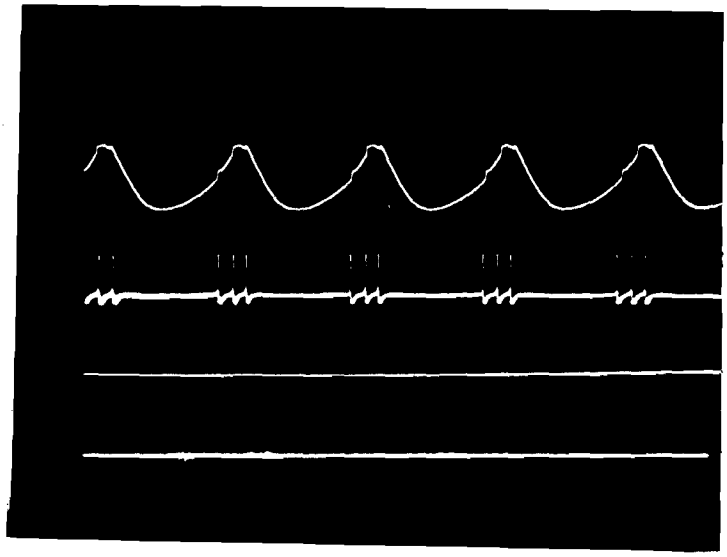

A

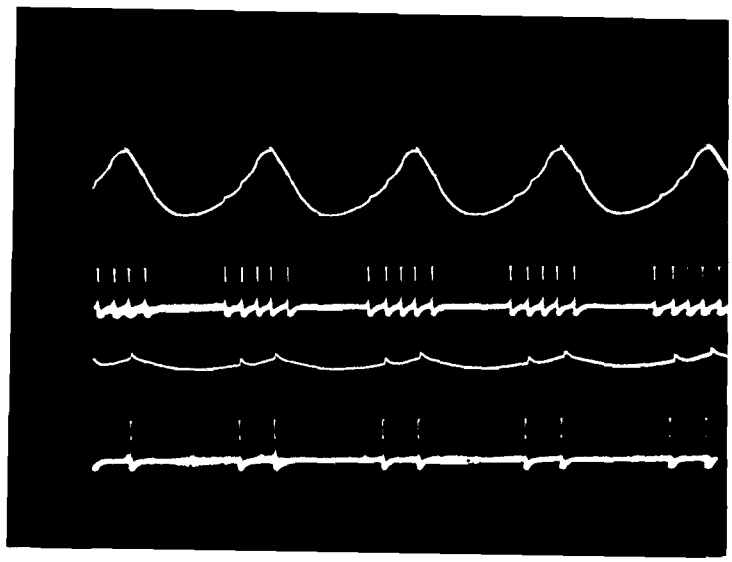

B

Figure 75. Spontaneous Potentials in Electrotonically Connected Three-Patch Models.

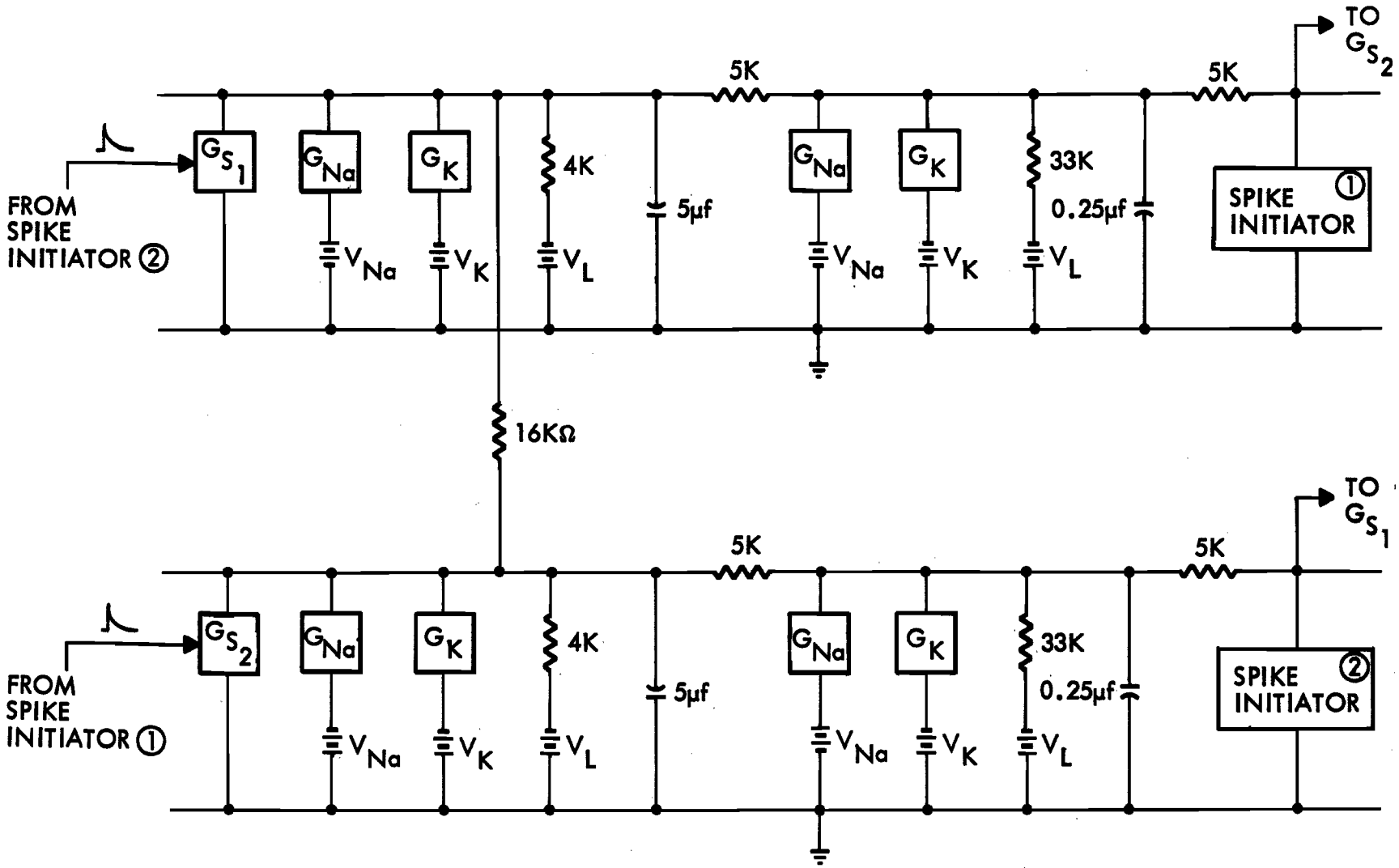

Figure 76. Three Patch Neural Models Connected Electrotonically and Snyaptically.

In the lobster cardiac ganglion, however, the electrotonic connections do not appear to be directly between spike initiators, otherwise production of individual spikes among the various cells would exhibit a tendency toward synchrony. The connections appear to be between the nonspiking somata, providing extremely indirect connections between the spike initiators. Some acceleration is possible in such a network, but its occurence in model studies was extremely rate. One example is shown in figure 75. The top photograph shows the potentials at the simulated soma (top trace) and spike initiator (second from top) of a spontaneously active, three-patch model (see figure 76). The two remaining traces in the photograph show the potentials from the same locations in a second three-patch model not connected to the first. The bottom photograph shows the potentials when the simulated somata were connected by a resistor. The oscillatoions of the spontaneous model are conducted with considerable attenuation and delay to the other model. After connection, the slope of the polarizing phase of the spontaneous soma (top trace) apparently is reduced sufficiently (either by the added capacitance of the second soma or by the delayed reflection of the oscillation) to allow the generation of two extra spikes by the spontaneous model.

The electrical parameters of the connection in this case were identical in both directions $R_i/R_m = 4$, $R_iC_m = 80$ ms, $R_mC_m = 20$ ms. These values are comparable to those in columns 2 and 3 of Table 3. With the same parameter values for the electrotonic connection, the spontaneous model was adjusted to produce one spike for each cycle of oscillation. The spike initiator of the spontaneous model then was connected synaptically to the soma of the second model, and the amplitude of the synaptic conductance adjusted to produce one spike for each epsp in the second model. Then the spike initiator of the second model was coupled synaptically back to the soma of the first, completing the loop. As in the case of mutual excitation described in Section IV, the two models now produced bursts of spikes. This series of events in shown in figure 77.

While acceleration by means of electrotonic connection in the models was difficult to obtain, even in the form shown in figure 75, acceleration was almost invariably the result in the case of excitatory synaptic interconnection. Excitatory synaptic coupling thus emerged in these studies as the most reliable and effective means of acceleration. We suggest, therefore, that the cardiac ganglion be examined for this type of connection.

For quenching mechanisms, one does not have to look beyond the Hodgkin-Huxley Model. The cumulative potassium conductance and sodium inactivation are completely adequate mechanisms for quenching. The system described by this model not only can become progressively more refractory from repetitive activity, such as spike production during a burst, but it also can become refractory by overdriving or excessive depolarization. The effects of overdriving are apparent in figure 57. As the quenching mechanisms in the cardiac ganglion, therefore, we suggest the voltage dependent potassium conductance and the inactivation of the sodium conductance.

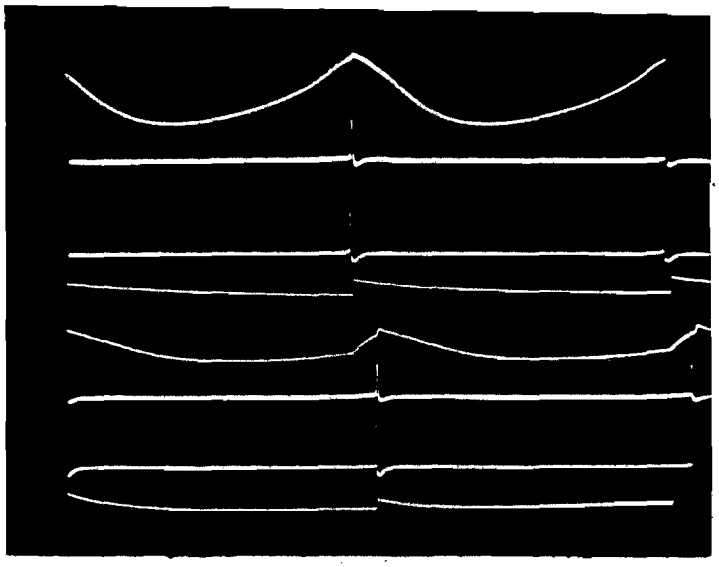

A

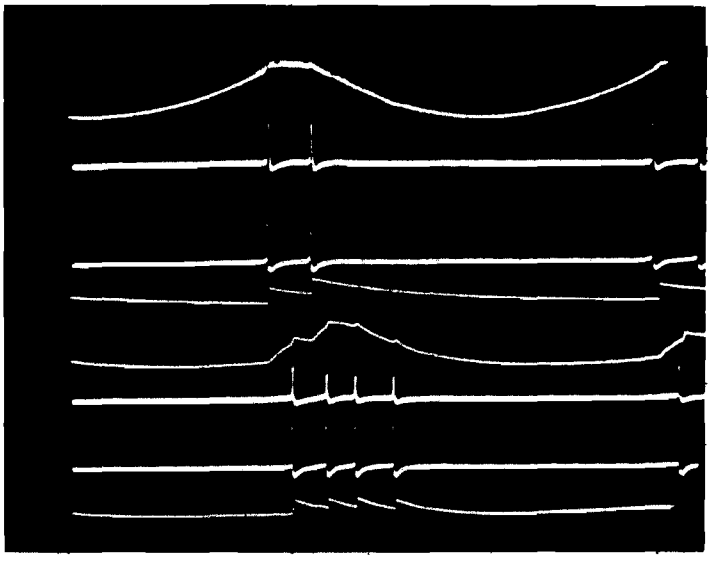

B

Figure 77. Potentials in a Pair of Mutually Exciting Three-Patch Models.

The upper photograph shows the potentials before the excitatory loop was closed. The lower photo shows spike bursts after the loop was closed. (Top trace: soma of spontaneous model; 2nd trace: axon hillock of spontaneous model; 3rd trace: axon of spontaneous model; 4th trace: synaptic conductance at soma of driven model; 5th trace: soma of driven model; 6th trace: axon hillock of driven model; 7th trace: axon of driven model; Bottom trace: synaptic conductance at soma of spontaneous model).

SECTION VII

REFERENCES

Alexandrowicz, J. S., 1932. "The innervation of the heart of Crustacea. I. Decapoda", Quat. J. Micro. Sci., vol. 75, pp. 182-250.

Bullock, T. H., 1957. "Neuronal integrative mechanisms", In: Recent Advances in Invertebrate Physiology, edited by B. T. Scheer. University of Oregon Pubs., Eugene, pp. 1-20.

Bullock, T. H., 1958. "Parameters of integrative action of the nervous system at the neuronal level", Exptl. Cell. Res. Suppl., vol. 5 pp. 323-337.

Bullock, T. H., 1959. "Neuron doctrine and electrophysiology", Science, vol. 129, pp. 997-1002.

Bullock, T. H., 1962, "Integration and rhymicity in neural systems", Am. Zool., vol 2, pp. 97-104.

Bullock, T. H., M. J. Cohen, and D. M. Maynard, 1954, "Integration and central synaptic properties of some receptors", Fed. Proc., vol. 13, p. 20.

Bullock, T. H., and C.A. Terzuolo, 1957, "Diverse forms of activity in the somata of spontaneous and integrating ganglion cells", J. Physiol. vol. 138, pp. 341-364.

Cole, W. H., 1941. "The perfusing solution for the lobster (Homarus) heart and the effects of its constituent ions on the heart", J. Gen. Physiol. vol. 25, pp. 1-6.

Cooley, J. W., and F. A. Dodge, Jr., 1966. "Digital Computer solutions for excitation and propagation of the nerve impulse", Biophys. J., vol 6, pp. 583-599.

Crane, H. D., 1962. "Neuristor - a noval device and system concept", Proc. IRE (Inst. Radio Engrs.), vol. 50, pp. 2048-2060.

Crane, H. D., 1964. "Possibilities for signal processing in axon systems". In: Neural Theory and Modeling, edited by R. F. Reiss. Stanford University Press: Stanford, pp. 138-153.

Eccles, J. C., 1964. The Physiology of Synapses. Academic Press; New York.

Fitzhugh, R., and H. A. Antosiewicz, 1959. "Automatic computation of nerve excitation - detailed corrections and additions", J. Soc. Ind. Appl. Math., vol. 7, pp. 447-458.

Florey, E., 1960. "Studies on the nervous regulation of the heartbeat in decapod crustacea", J. Gen. Physiol., vol. 43, pp. 1061-1081.

Frankenhaeuser, B., and A. L. Hodgkin, 1956. "The after-effects of impulses in the giant nerve fiber of Loligo", J. Physiol., vol. 131, pp. 341-376.

Hagiwara, S., and T. H. Bullock, 1955. "Study of intracellular potentials in pacemaker and integrative neurons of the lobster cardiac ganglion", Biol. Bull., vol. 109, p. 341.

Hagiwara, S., and T. H. Bullock,1957. "Intracellular potentionals in pacemaker and integrative neurons of the lobster cardiac ganglion", J. Cell, Comp. Physiol., vol. 50, pp. 25-47.

Hagiwara, S., A. Watanabe, and N. Saito, 1959. "Potential changes in syncitial neurons of lobster cardiac ganglion:, J. Neurophysiol., vol 22, pp. 554-572.

Harmon, L. D., 1964. "Neuromines: action of a reciprocally inhibitory pair", Science, vol. 146. pp. 1323-1325.

Hodgkin, A. L., and A. F. Huxley, 1952a. "Currents carried by sodium and potassium ions through the membrane of the giant axon of Loligo", J. Physiol., vol. 116, pp. 449-472.

Hodgkin, A. L. and A. F. Huxley, 1952b. "The components of membrane conductance in the giant axon of Loligo", J. Physiol. vol. 116, pp. 473-496.

Hodgkin, A. L. and A. F. Huxley, 1952c. "The dual effect of membrane potential on sodium conductance in the giant axon of Loligo", J. Physiol., vol. 116, pp. 497-506.

Hodgkin, A. L. and A. F. Huxley, 1952d. "A quantitative description of membrane current and its application to conduction and excitation in nerve", J. Physiol., vol. 117, pp. 500-544.

Hodgkin, A. L., A. F. Huxley, and B. Katz, 1952. "Measurement of current-voltage relations in the membrane of the giant axon of Loligo", J. Physiol., vol. 116 , pp. 424-448.

Huxley, A. F., 1959. "Can a nerve propagate a subthreshold disturbance", J. Physiol., vol. 148, pp. 80P-81P.

Lewis, E. R., 1965. "Neuroelectric potentials derived from an extended version of the Hodgkin-Huxley model", J. Theoret. Biol., vol. 10, pp. 125-158.

Lieberstein, H. M., 1967. "On the Hodgkin-Huxley partial differential equations", Math. Biosciences., vol. 1. pp. 45-69.

Matsui, K., "Spontaneous discharges of the isolated ganglionic trunk of the lobster heart (Panulirus japonicus)", Sci. Rept. Tokyo Kyoiku Daigaku, Sect. B, vol. 7, pp. 257-268. 1955.

Maynard, D. M., 1953a. "Activity in a crustacean ganglion. I. cardio-inhibition and acceleration in Panulirus Argus", Biol, Bull., vol. 104, pp. 156-170.

Maynard, D. M., 1953b. "Integration in the cardiac ganglion of Homarus", Biol. Bull., vol. 105, p. 367.

Maynard, D. M., 1953c. "Inhibition in a simple ganglion", Fed. Proc., vol. 12, p. 95.

Maynard, D.M., 1955a. "Direct inhibition in the lobster cardiac ganglion", Ph.D. Dissertation, Department of Zoology. University of California at Los Angeles: Los Angeles.

Maynard, D. M., 1955b. "Activity in a crustacean ganglion. II. Pattern and interaction in burst formation", Biol. Bull., vol. 109, pp. 420-436.

Maynard, D. M., 1958. "Action of drugs on Lobster cardiac ganglion", Fed. Proc., vol. 17, p. 106.

Maynard, D. M., 1960. "Heart rate and body size in the spiny lobster", Physiol. Zool., vol. 23, pp. 241-251.

Maynard, D. M., 1961. "Cardiac inhibition in decapod crustacea". In: Nervous Inhibition, edited by E. Florey. Macmillan: New York, pp 144-178.

Otani, T., and T. H. Bullock, 1957. "Responses to depolarizing currents across the membrane of some invertebrate ganglion cells", Anat. Rec., vol. 128, p. 599.

Otani, T., and T. H. Bullock, 1959. "Effects of presetting the membrane potential of the soma of spontaneous and integrating ganglion cells", Physiol. Zool., vol. 32, pp. 104-114.

Reiss, R. F., 1962. "A theory and simulation of rhythmic behavior due to reciprocal inhibition in small nerve nets". In: Proceedings of the 1962 A.F.I.P.S. Spring Joint Computer Conference. National Press: Palo Alto. vol. 21, p. 171-194.

Smith, O. J. M., 1958. Feedback Control Systems. McGraw-Hill: New York.

Terzuolo, C. A., and T. H. Bullock, 1956. "Measurement of imposed voltage gradient adequate to modulate neuronal firing", Proc. Nat. Acad. Sci., vol. 42, pp. 687-694.

Terzuolo, C. A., and T. H. Bullock, 1958. "Acceleration and inhibition in crustacean ganglion cells", Arch. Ital. Biol., vol. 96, pp. 117-134.

Watanabe, A., 1958. "The interaction of electrical activity among neurons of the lobster cardiac ganglion", Jap. J. Physiol., vol. 8, pp, 305-318.

Watanabe, A., and T. H. Bullock, 1960. "Modulation of activity of one neuron by subthreshold slow potentials in another in lobster cardiac ganglion", J. Gen. Physiol., vol. 43, pp. 1031-1045.

Welsh, J. H., 1939. "Chemical mediation in crustaceans, II. The Action of acetylcholine and adrenalin on the isolated heart of Panulirus Argus", Physiol. Zool., vol. 12, pp. 231-237.

Welsh, J. H., 1942. "Chemical mediation in crustaceans, IV. The action of acetylcholine on isolated hearts of Homarus and Carcinides", J. Cell, Comp. Physiol., vol. 19, pp. 271-279.

Welsh, J. H., and D. M. Maynard, 1951. "Electrical activity of a simple ganglion", Fed. Proc., vol. 10, p. 145.

Wilson, D.M., 1966. "Central nervous mechanisms for the generation of rhythmic behavior in arthropods", Symp. Soc. Exptl. Biol., vol. 20, pp. 199-228.

Security Classification

DOCUMENT CONTROL DATA - R & D

(Security classification of title, body of abstract and indexing annotation must be entered when the overall report is classified)

1. ORIGINATING ACTIVITY *(Corporate author)* General Precision Systems Inc., Librascope Group 808 Western Avenue Glendale, Calif. 91201	2a. REPORT SECURITY CLASSIFICATION UNCLASSIFIED 2b. GROUP N/A

3. REPORT TITLE

MODELS OF NEUROELECTRIC INTERACTIONS

4. DESCRIPTIVE NOTES *(Type of report and inclusive dates)*

Final Report, April 1965 - July 1967

5. AUTHOR(S) *(First name, middle initial, last name)*

Edwin R. Lewis, PhD

6. REPORT DATE	7a. TOTAL NO. OF PAGES	7b. NO. OF REFS
December 1967	136	48

8a. CONTRACT OR GRANT NO.	9a. ORIGINATOR'S REPORT NUMBER(S)
AF 33(615) - 2464	
b. PROJECT NO. 7233	
c. Task No. 723305	9b. OTHER REPORT NO(S) *(Any other numbers that may be assigned this report)*
d.	AMRL-TR-67-132

10. DISTRIBUTION STATEMENT

Distribution of this document is unlimited. It may be released to the Clearinghouse, Department of Commerce, for sale to the general public.

11. SUPPLEMENTARY NOTES	12. SPONSORING MILITARY ACTIVITY
	Aerospace Medical Research Laboratories Aerospace Medical Div., Air Force Systems Command, Wright-Patterson AFB, OH 45433

13. ABSTRACT

The Hodgkin-Huxley descriptions of electrically excitable conductances are combined with Eccles descriptions of synaptic conductances to provide the basis of an electronic analog of nerve cell membrane. A neural simulation facility is constructed, comprising ten pairs of these analogs with associated input and output equipment. A detailed description of the simulation facility is presented, including design philosophy, circuit, system and mechanical details. The simulation facility is used to model spatially distributed neuroelectric phenomena. Significant results include resetting of potentials in integrative regions by spikes generated at a remote site, stable spike synchrony in independently driven, mutually inhibiting distributed neural models, burst formation in mutually exciting neural models, and various nonuniformities of wave shape and velocity in conduction along a distributed axon. In addition, the facility is used in a simulation study of the lobster cardiac ganglion. As results of this study, mechanisms are proposed for ganglion operation and specific neuronal connectivities are predicted.

DD FORM 1 NOV 65 1473

Security Classification

14. KEY WORDS	LINK A		LINK B		LINK C	
	ROLE	WT	ROLE	WT	ROLE	WT
Neural Models						
Neuroelectric Interactions						
Models of Small Ganglia						
Electronic Neural Analogs						
Lumped Axon Models						
Reciprocal Inhibition						
Mutual Excitation						
Lobster Cardiac Ganglion						
Electrotonic Connections						